A series of photochemical based studies into the application of green chemistry principles to potentially industrially relevant chemical reactions

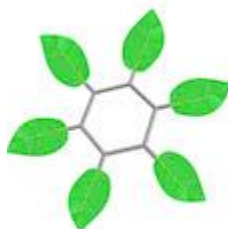**By Jonathan Hunter MSci**

Student number:4246469

Supervisors: Prof. Mike George and Prof. Sir Martyn Poliakoff

EPSRC Centre of Doctoral Training in Sustainable Chemistry

Thesis submitted to University of Nottingham for the degree of Doctor of Philosophy

August 2021

Declaration

I, Jonathan Hunter, hereby certify that this thesis has been written by me and that it is a record of my work over the period of October 2015 to September 2019. Where work has been carried out in collaboration, the relevant researcher or researchers have been acknowledged. This thesis has not been accepted in partial or complete fulfilment of any other degree or professional qualification.

Jonathan Hunter 2021

Summary

This Thesis details several research areas which attempt to address some of the issues associated with industrial scale photochemical reactions. In the first Chapter, an overview of industrial scale photochemistry is given, and these approaches have been critiqued from a green chemistry perspective. From this introduction, three main aims of the Thesis have been developed and are explored in the subsequent chapters. These are 1) to explore routes in improve the "green credentials" of a photoredox reaction, specifically for amide bond synthesis; 2) to develop a reactor which was capable of safely conducting photochlorination and use this system to try to solve several long-standing issues with this reaction; 3) to study the application of bio-derived solvents for use in photochemical reactions.

The efforts towards achieving these aims resulted in varying levels of success.

Regarding the first aim, it was possible to increase the scale of the photoredox reaction by ~500-fold and this was followed with the production of a chiral amide through the utilisation of a combined enzymatic and photochemical route. Additionally, a novel electrochemical process was identified to produce chiral amides.

With respect to aim two, a new photochemical reactor, based on a rotatory evaporator, was developed for the ease handling of chlorine gas, and conducting photochlorination reactions. This was used to production several chlorinated compounds including a key intermediate for the drug Plavix. Furthermore, it was shown that brine could be readily used for the *in-situ* production of chlorine gas for photochlorination reactions.

Finally, the progress made towards completing aim 3 resulted in the identification several bio-derived solvent alternatives for different types of photochemical reactions without affecting the yield or rate of those reactions.

Declaration

This is to certify that to the best of my knowledge; the content of this thesis is my own work. This thesis has not been submitted for any degree or other purposes. I certify that the intellectual content of this thesis is the product of my own work and that all the assistance received in preparing this thesis and sources have been acknowledged.

Jonathan Hunter – 31st August 2021

Acknowledgements

There are a great many people who I need to thank for their help in completion of the work documented in this thesis.

Firstly, to my supervisors Prof. Mike George and Prof. Sir Martyn Poliakoff, I thank you for our many interesting discussions and I also thank you for your help in making me become a better researcher.

Specific thanks need to attribute to people who aided in the work of each Chapter. Firstly, the work of Chapter 2 could not have been completed without the help of Clarissa Wilding and Drs. Darren Lee, Stephen Argent, Stephen Davis, James Ryan and Elaine O'Reilly.

For aid in the efforts discussed in Chapter 3, I would like to thank Neil Barnes and Dr. Rowena Howie. Furthermore, Chapter 4 would not have been possible without the developed of the solvent library thanks to Conor Forrest.

I would also like to thank the whole George/Poliakoff group who were able to brighten my day when things did not go well and were able to make my PhD experience much more bearable.

Finally, I would like to thank my wife Hannah Hunter who has been a constant support throughout all my studies and has given me the greatest gift of our son James.

James in the coming years, when you read this, remember that I tried to make the world a better place for you to live in.

Table of Contents

Chapter 1 – Introduction to industrial photochemistry

Background

The subject of this Thesis is photochemistry or, more specifically, the use of photochemistry to induce particular transformations of organic molecules. The use of photochemistry for the production of chemicals is not a new idea.[1–7] The ancient Egyptians recorded using sunlight to treat skin conditions over 3000 years ago, in a practise known as heliotherapy.[8] However, proposals to use light in the large-scale manufacture of chemicals began in earnest in the late 19th century, particularly with the Italian chemist Ciamician. He initially researched how plants produced chemicals using light and, as part of this work, began conducting photochemical reactions on the roof of his laboratory - **Figure 1**.[9–11]

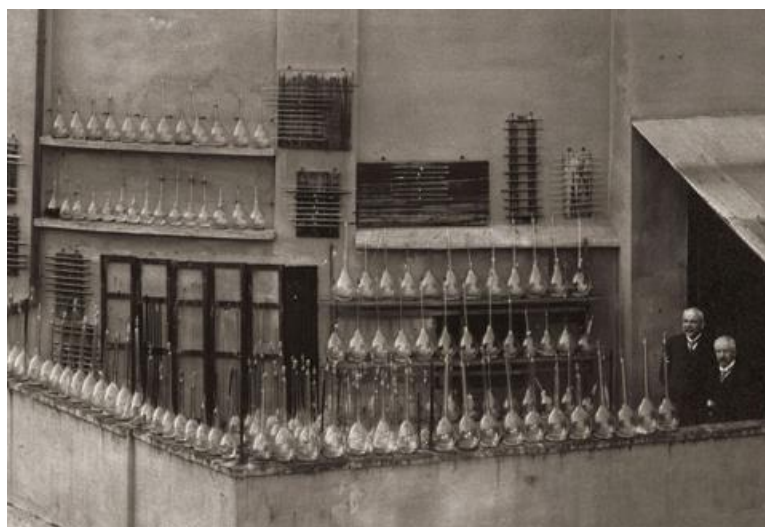**Figure 1: Ciamician conducting photochemical reactions on the roof of University of Bologna. Image taken from Ref [10].**

In 1912, Ciamician published a visionary paper in Science entitled *"The photochemistry of the future"*.[11] At that time, burning coal was the primary source of energy and the chemical industry was based almost entirely on coal tar, a by-product of the coal processing industry. There were real

worries that coal reserves would run out and Ciamician proposed that energy from coal should be replaced by solar radiation as a means of promoting chemical reactions.

He pointed out that, in only six hours, a square kilometre of land in the tropics receives a quantity of solar energy equivalent to the burning of 1000 tons of coal. From this he extrapolated that, over the course of a year, a small tropical area roughly the size of East Yorkshire (~3,000 km^2) receives the same amount of light energy as that released from burning coal by both America and Europe combined in 1909.

Therefore, to roughly paraphrase the message of his article, where the land is fertile, crops should be grown but where it is barren (e.g., in the Sahara Desert) glass factories should be built to manufacture chemicals via sunlight. Unfortunately, the First World War started only two years after Ciamician's paper was published and the switch to an oil-based chemical industry meant that his message was largely overlooked for many years. It was in the aftermath of the Second World War that industrial photochemistry began a slow revival. The Allied destruction of German cities caused terrible public health problems, including widespread infections of parasitic worms. With an urgent need for anthelmintic drugs (which expel the worms from the body) the German chemist Schenck responded to this need by manufacturing one such drug, ascaridole, using sunlight to generate singlet oxygen photochemically for the key stage in the process.[12] This reaction is discussed in more detail later. Since that time, a small number of photochemical processes have been successfully industrialized, usually in cases where more traditional approaches are either too expensive or too complex to make the desired product at an affordable price. Described below are some of these processes explaining in each case why photochemistry was chosen.

Over the years the widespread interest and application of photochemistry has fluctuated and since 2000 photochemistry has undergone a modern renaissance with chemists revisiting the power of Ciamician's vision - **Figure 2**.
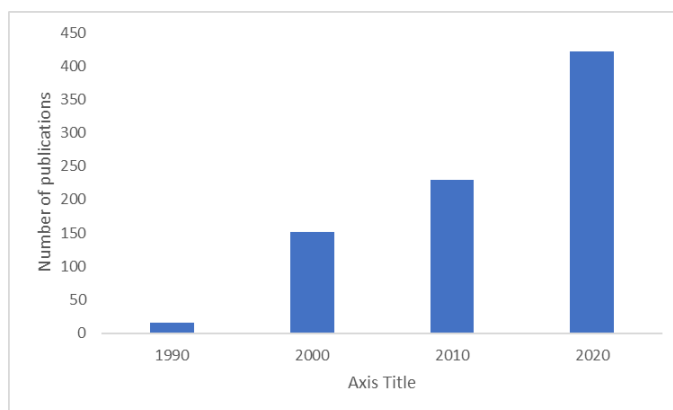
Figure 2: Web of Science results for number of publications with the topic of 'Organic Photochemistry' over the last 30 years.

There are multiple reasons for this renewed interest. These include: (a) the realisation that our once plentiful oil reserves are becoming depleted – an echo of Ciamician's original concerns about coal, (b) the rise of Green Chemistry and an increasing emphasis on more sustainable chemical manufacture, which is particularly relevant to personalised medicine - which is discussed later (c) an increase in the number and complexity of pharmaceutical compounds that need to be manufactured, (d) the rapid development of photoredox chemistry which is providing a whole new toolbox of reactions for the synthetic organic chemist and (e) major technical advances in the design of photoreactors and, in particular, the widespread availability of high intensity Light Emitting Diodes (LEDs), which provide very compact light sources with much higher electrical efficiency than more traditional light sources. The work in this Thesis is aimed at exploiting some of these technical developments to begin making photochemical reactions more productive and more sustainable. Before explaining these aims in more detail, some existing industrial photochemical processes are described accompanied by the relationship of photochemistry to Green Chemistry.

Green Chemistry and Photochemistry

The drive to produce chemicals with less waste, more easily and more cheaply has been at the heart of much industrial research since its conception. However, the basic principles of Green Chemistry were more readily defined in the early 2000s by Anastas and Warner.[13]

These 12 principles of green chemistry are essentially a convenient "check-list" to help to guide researchers towards more sustainable chemical processes. They allow different processes to be ranked according to the number of principles that they satisfy. The figure below shows a cutdown version of the principles that are frequently used for teaching Green Chemistry - **Figure 3**. In relation to photochemistry, the use of light (photons) as a traceless reagent can greatly improve the *"green credentials"* of a chemical reaction and, in combination with the advancement in lighting technology in the form of cheap light emitting diodes (LEDs), making photochemistry a highly promising area of environmentally conscious chemical research.

<div style="border:1px solid">

12 Principles of Green Chemistry
1. Prevent Waste
2. Atom Economy
3. Less Hazardous Synthesis
4. Design Benign Chemicals
5. Benign Solvents & Auxiliaries
6. Design for Energy Efficiency
7. Use of Renewable Feedstocks
8. Reduce Derivatives
9. Catalysis
10. Design for Degradation
11. Real-Time Analysis for Pollution Prevention
12. Inherently Benign Chemistry for Accident Prevention

</div>

Figure 3: **The twelve principles of green chemistry adapted from Ref** [13]**.**

To be able to measure and compare the "greenness" of a chemical reaction, numerous quantitative methods have been developed.[15] Of these metrics the three most commonly used are atom economy (AE), E factor and process mass intensity (PMI). Atom Economy was developed by Trost through the 1980s.[16]

$$AE\ (\%) = \frac{Molecular\ weight\ of\ product}{Total\ molecular\ weight\ of\ all\ reagents} \times 100$$

Equation 1: **Atom efficiency (AE) equation**

AE (**Equation 1**) considers only the product and the reagents, which means that this method can be easily applied to a number of theoretical synthetic routes to determine which method is the most

efficient.[15] The downside of this is that this metric does not consider solvents, side products or by products. The E-factor which was invented by Sheldon includes all wastes (apart from water).[15,17] Arguably, the E-factor is one of the key concepts that drove the early development of Green Chemistry - **Equation 2**.

$$E = \frac{Total\ mass\ of\ waste}{Mass\ of\ final\ product}$$

Equation 2: E-factor equation

In the best-case scenario, the E-factor of a reaction would be as low as possible as this shows that the least amount of waste is generated. This method is an improvement on the AE method as it considers the greater overall environmental impact of the reaction. However, the E-factor calculation does not account for water as part of the calculations. This is an issue because processes with a low E-factor may require a large amount of downstream aqueous processing, which can be a highly energy intensive.[17] One of the extra applications of the E-factor metric is that it can be applied to whole processes to give an overall view of the environmental impact of a process.

A third, more recent metric is Process Mass Intensity (PMI) which is currently favoured in many parts of the pharmaceutical industry - **Equation 3**.[15]

$$PMI = \frac{Total\ mass\ of\ process\ (including\ water)}{Mass\ of\ final\ product}$$

Equation 3: Process Mass Intensity (PMI) equation

This metric is a further development of the E-factor metric in that it is focused on the whole process to produce the final product and includes water, giving a more holistic view of a reaction when compared to the other metrics. This method is frequently used to compare the environmental impact of processes for the production of Active Pharmaceutical Ingredients (APIs).[15]

Using these metrics, the 12 principles of green chemistry can be applied, measured, and compared to determine which reaction method has the lowest environmental impact. These metrics will be used, together with the 12 principles, in appropriate places throughout this Thesis to assess the possibility of applying different approaches to the development of sustainable processes.

Industrially relevant photochemical reactions

As explained above, photochemical reactions can be categorised in to two major classes. Those activated by UV light and those activated by visible light (mostly blue and green). However, in more recent years there has been a few interesting publications written, which utilise red light to promote reactions. The work in this Thesis however, has focussed on the applications of UV and broadband visible light. In this Section, several larger scale photochemical processes will be examined.

Ascaridole

One of the earliest industrial photochemical reactions was the synthesis of ascaridole, an anthelminthic drug, which was produced in Germany following the Second World War - **Figure 4**.[6, 12]
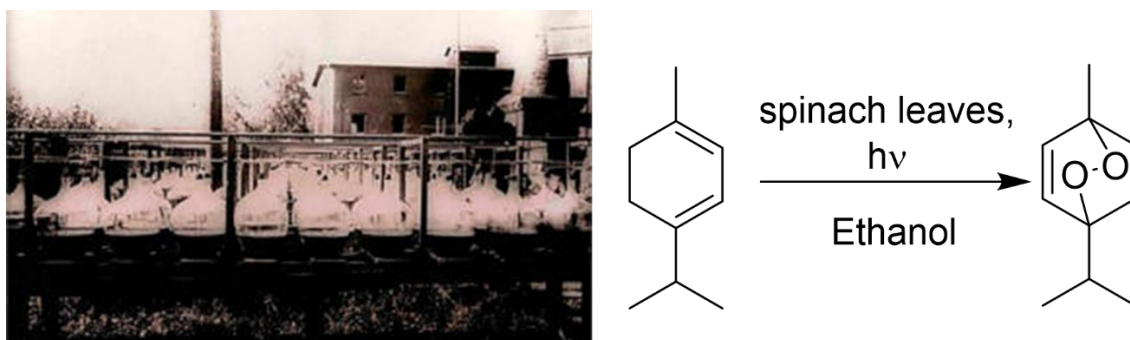

Figure 4: Image of Schenck's ascaridole photochemical plant in operation in Germany in 1948. It used sunlight and the chlorophyll in spinach leaves to generate singlet oxygen to react with α-terpinene (see scheme on the right) Photo Reproduced from Ref 6.

In this simple chemical plant, 200 x 10 L round bottom flasks were exposed to solar light whilst being sprayed with water to keep them cool. This reaction consisted of a photo oxidation of α-terpinene which was shaken frequently and used chlorophyll (from spinach/nettle leaves) as a photosensitiser.[12]

A possible motivation behind the use of photochemistry in this reaction, was that the energy source (the Sun) was free to use and therefore did not add any cost to the process, allowing the much-needed medication to be produced cheaply. Whilst Schenck was able to produce 2 kg of ascaridole in 2 sunny days, this particular compound and method is no longer used as alternative anthelminthic drugs, with fewer side effects, have taken ascaridole's place. Consideration of this classic reaction shows that this process satisfies several of the 12 principles including reduced waste, relatively

benign chemicals, reaction at room temperature, renewable chemicals (α-terpinene and chlorophyll), etc. As the Sun is the ultimate light source to be used for photochemical experiments it is worth examining its emission spectrum - **Figure 5**.[18] There are several important points regarding solar based photochemistry. 1) At sea level there is very little Ultraviolet (UV), making UV photochemistry practically impossible using solar light; 2) Unsurprisingly, the light with the greatest intensity can be found in the visible range making reactions which utilise these wavelengths best suited to solar-based photochemistry; 3) A large percentage of the total solar radiation in the infrared region which heats the reaction mixture unless it is cooled; this would complicate any large scale photochemical process as this would require significant amounts of cooling.
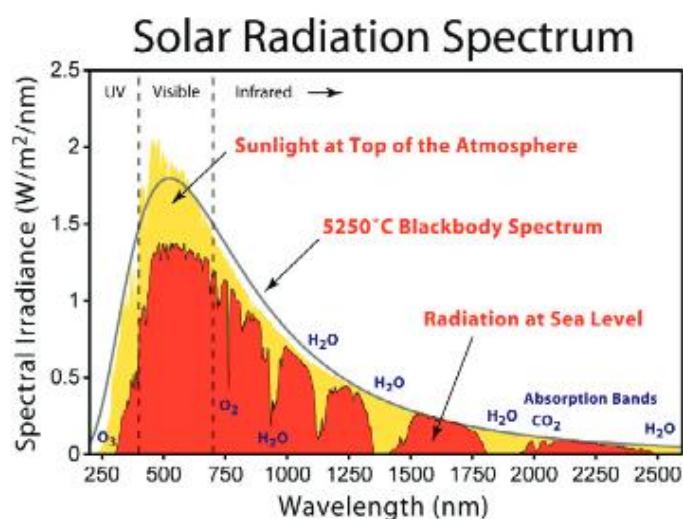

Figure 5: Solar spectrum, showing how the UV component is absorbed in the upper atmosphere and indicating the large portion of the sun's output which lies in the near and mid-IR and can lead to substantial heating when photochemistry is carried out with unfiltered sunlight. Reproduced from Ref [18]

The photochemical reaction of ascaridole is often used to benchmark modern innovations, particularly in reactor development. For example, Noël showed[19] that with the use of micro flow reactors which had been constructed with filters of different colours (red, green or blue) and operation with solar radiation produced ascaridole efficiently and the process easily scaled up - **Figure 6**. Noël and co-workers reported a production rate of 0.274 mol m^{-2} h^{-1}. Using their system, a 1 m^2 reactor could produce a little over 550 g of ascaridole over a day, assuming 12 hours of sunny weather.
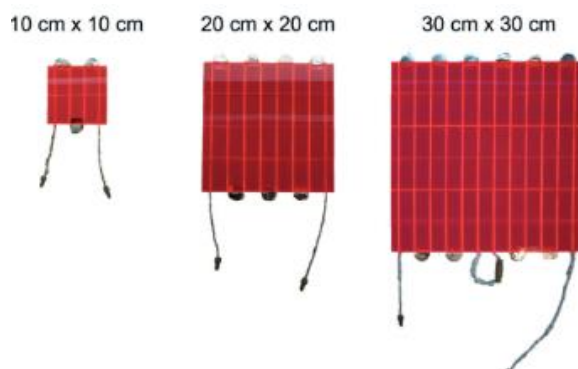
Figure 6: Red coloured solar photoreactor at different scales used by Noël and co-workers to produce ascaridole using ethanol as the solvent. The team were able to use a green version of this reactor to synthesize ascaridole at a rate of 0.274 mol m^{-2} h^{-1} using Rose Bengal (1 mol %) as a photosensitiser; image reproduced from Ref [19]

Rose oxide

The commercial fragrance (Rose Oxide) is typically synthesised by a photooxidation process. Prior to the development of the photooxidation process, Rose Oxide was extracted from the petals of roses (100 kg of roses resulted in 10 g of rose oil) which was expensive and time consuming.[20,21, 22] The photo-oxidation however, reduced both of these factors allowing perfumers to add this desirable fragrance to their products. Furthermore, the photochemical process used citronellol as a starting material which can be readily produced from various natural and synthetic sources.

From the point of view of Green Chemistry this reaction has many similar positive points i.e., relatively benign chemicals, reaction at room temperature, renewable chemicals (citronellol), use of a photosensiter (catalyst)). One aspect which could be improved from a Green Chemistry point of view is the atom efficiency of the reaction (as there are several unwanted side products produced).

In this reaction, the photogenerated singlet oxygen reacts with citronellol to form a peroxide, then is quenched to form an alcohol which is used to produce Rose Oxide – **Scheme 1**.
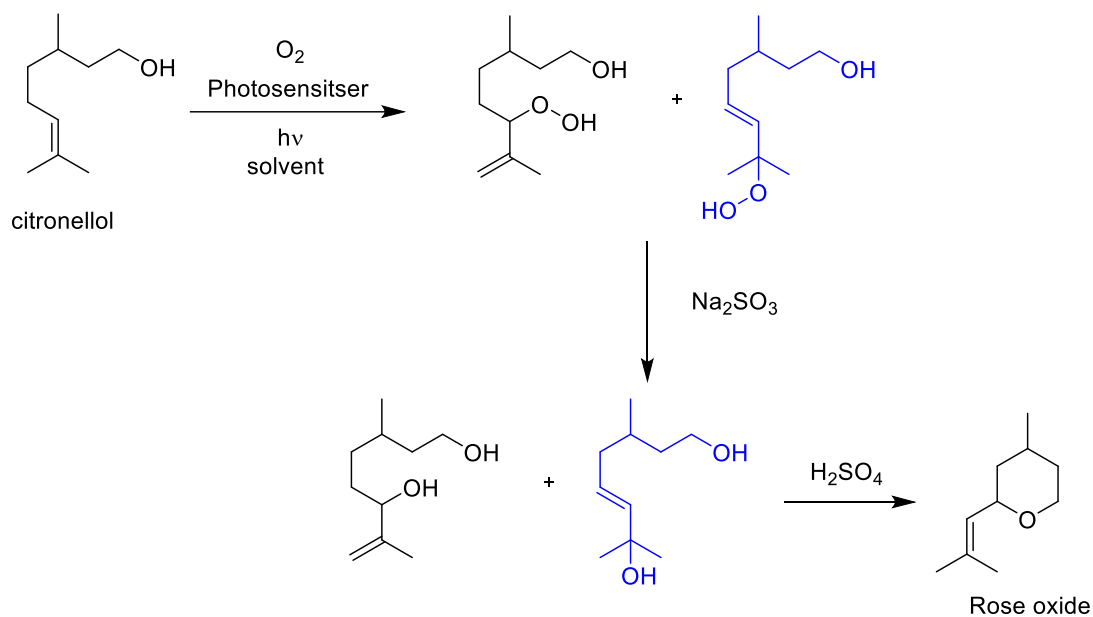
Scheme 1: Photochemical synthesis of rose oxide from citronellol, with desired intermediates highlighted in blue.[23–25]

This reaction usually uses visible light to produce singlet oxygen, in the same fashion to ascaridole, and historically, this visible light photochemical reaction was used to produce 60-100 tonnes/annum of Rose Oxide by Dragoco - **Figure 7**.[3,25] As can be seen in the image below Dragoco used multiple reactors to produce the required amounts of Rose Oxide, which is a good example of scaling-out rather than scaling-up a process.

Figure 7: Photochemical reactor used to produce rose oxide at Dragoco in the 1990s. In this reaction set-up it is possible to observe multiple reactors run in parallel to one another. This allows for a significant increase in product manufacturing capability without the need increasing the size of the reaction vessel. Reproduced from Ref [25]

Recently, Clark *et al.* revisited this reaction using a new type of reactor which they named the 'PhotoVap'.[26] This consisted of a modified rotary evaporator, which enabled the formation of a thin film of solution, allowing excellent (and efficient) LED sourced light penetration into the solution - **Figure 8**.

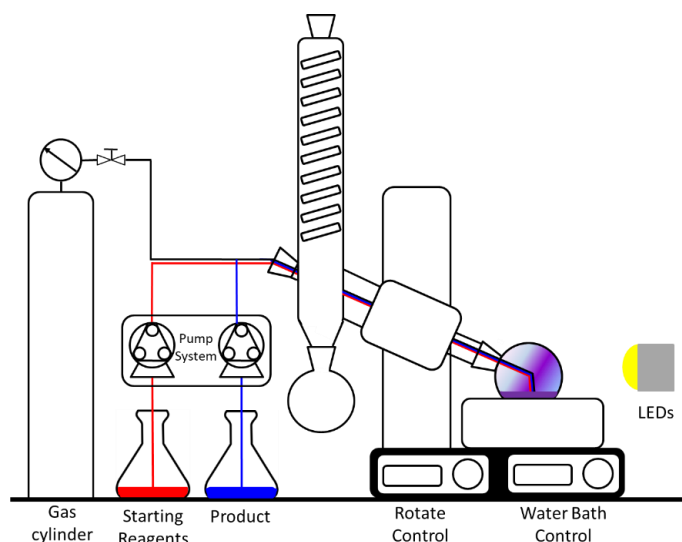Figure 8: Simple diagram of the PhotoVap. In this step-up a rotary evaporator has been adapted to perform photochemistry. The adaptions include the insertion of multiples line into the reaction flask, which allow the addition and recovery of reaction solutions along with a gas line (typically oxygen). The reaction flask is then spun at a known speed to produce a thin film of reaction mixture. This thin film is irradiated with high powered LEDs to enable the desired reaction to take place. Image reproduced from Ref [26]

Oxygen was then added to the system to produce the diol precursor to Rose Oxide in high productivity rates (1.2 mmol/min, ~300 g/day). This shows the potential of modern approaches to produce significant amounts of this product without the need for a large factory. The use of the PhotoVap reactor features in Chapter 3 of this Thesis where it has been used to explore the possibility of conducting photochlorination by exploiting some of the unique features of the PhotoVap's design.

Artemisinin

Another example of larger scale photochemistry was reported by Sanofi in 2014 in the production of the anti-malarial drug, Artemisinin.[27] Malaria effect more than one third of the world's population, mostly in Sub-Saharan Africa, Southern Asia and South America.[28] Historical treatments for malaria

have been based around the use of Quinine, however the malaria parasite has begun to show resistance to these treatments. In the 1970s, using traditional Chinese medicine as a guide, Artemisinin was extracted from *Artemisia annua* and identified as a potential treatment for malaria (work which was awarded the 2015 Nobel prize in Medicine).[29] In 2004, the World Health Organisation recommended the use of Artemisinin as part of the standard treatment of malaria. This resulted in the need for a process to produce Artemisinin which was non-seasonal and low cost, to be competitive with the isolation of the active compound from the plant-based source.

Sanofi reported a semi-synthetic process to produce Artemisinin. Using of synthetic biology and a small number of chemical steps the team were able to produce the artemisinic acid ester, which had a hydroperoxide group installed with a photochemical step - **Scheme 2**.
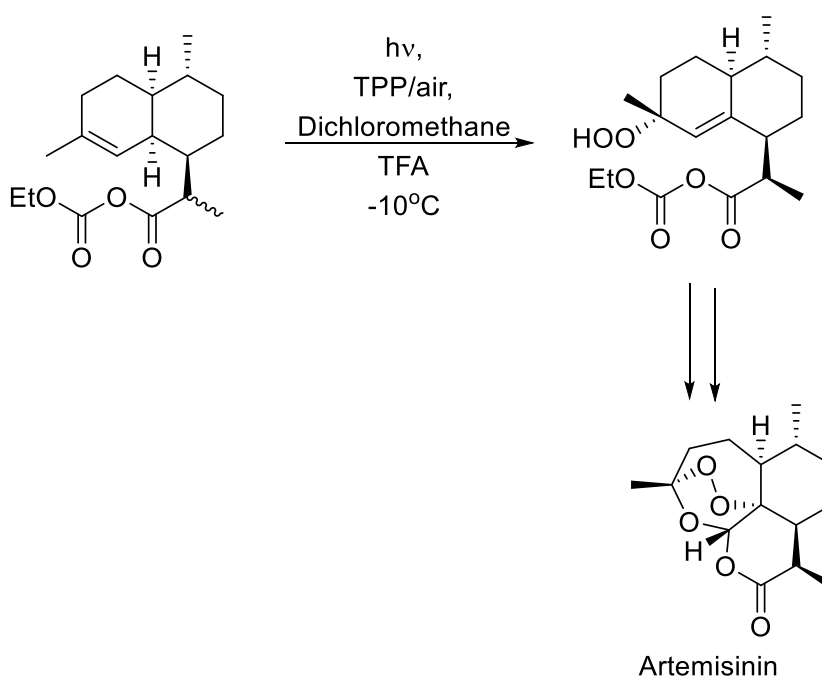
Scheme 2: Sanofi photochemical production of Artemisinin, adapted from Ref [27]

From a Green Chemistry perspective, there are several positive points and drawbacks of this approach. The first major point is the use of synthetic biology to achieve a high level of chemical complexity for the starting material in this process. This is an excellent example of a more benign alternative route, avoiding several complex chemical steps which would be required in a full

chemical synthesis of Artemisinin.[30, 31] Additionally, the photochemical step utilised an organic

photosensitiser (tetraphenylporphyrin, TPP) and sourced the necessary oxygen from the air. This

decreases the hazard associated with the chemical reaction. Interestingly, the use of biology to

reduce the complexity in chemical processes has inspired some of the work in Chapter 2 of this

Thesis where enzymes have been applied to induce chirality into photochemical products.

 Some of the drawbacks of this process were the use of chlorinated (toxic) solvent and low

temperature required - which needs significant amounts of energy to achieve/maintain.

Figure 9: Sanofi's photochemical Artemisinin production plant in Italy.[27] From the image it is possible to observe the photochemical section of the reactor (top left). Using this manufacturing facility Sanofi were able to produce 60 tons of Artemisinin (average batch sizes of 370 kg) in 2014. This crystalline product was of sufficient quality to meet purity requirements of a drug and did not need any further purification.

Using this route, Sanofi reported that their production was at 60 tonnes in 2014 (**Figure 9**), which

could potentially satisfy one third of the world's demand for Artemisinin at the time. However, up to

now the photochemical route to Artemisinin was still not economically competitive as compared

with its extraction from *Artemisia annua,* partially due to the photochemical route having a low

overall yield of ~ 50 %.[28]

Since this time, there have been several reports of alternative methods to produce this compound

with improvements to the synthetic process, showing that this is still an active research area.[19,28,32,33]

One publication of note is the work of Amara *et al.* who reported the use of a binary mixture of

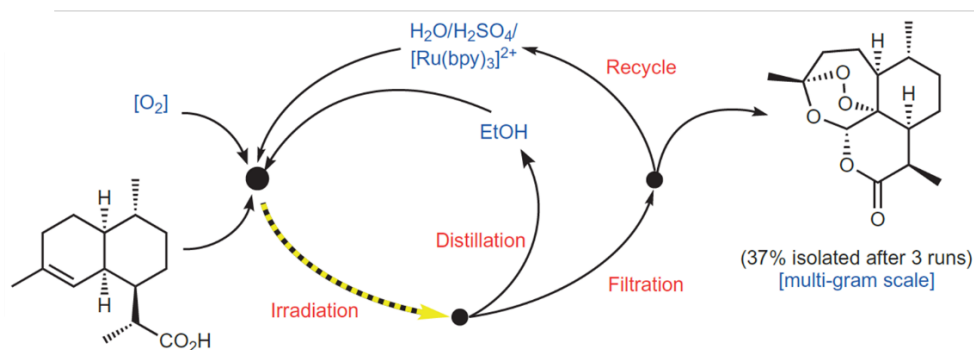aqueous and organic solvents to produce Artemisinin - **Figure 10**.[32]

Figure 10: This method described the chemical step being conducted in an aqueous/ethanol mixture. In this method the team were able to crystalize artemisinin from the solvent following distillation of the ethanol from the blend. This enabled easy recover of the desired component and the potential to recycle the solvent mixture, acid catalyst and photocatalyst giving this process an E-factor of 1.5 which is an improvement on Sanofi's original method (E-factor = 4.8).[32]

Through this work the team showed that Artemisinin could be produced in, and crystallised from, a water/ethanol mixture allowing the solvent, photocatalyst and acid catalyst to be readily recycled and reused. When this method was compared to the commercial process the E-factor was slightly lower, however this was related to the reduced yield of this method, but they then showed that when all the water, oxygen and solvent were excluded from the E-factor calculations (as they could be readily recycled) then this method was ~3 times more efficient than Sanofi's method.

In this paper the team show that the use of a binary mixture of solvents gave highly desirable results for this photochemical reaction. More generally, choice of solvents can have a big effect on both the chemistry and the sustainability of a process. A point which is further explored in Chapter 4 of this Thesis.

Caprolactam

As discussed earlier, whilst there are high levels of visible light resent in the Sun's emission spectrum higher energy light is less abundant. Thus, UV photochemistry had to wait for technology to catch up before being more thoroughly exploited. This need for technology to progress appears to be a pattern which has slowed progress of photochemistry.

An early example of industrial scale UV based photochemistry is the use of a photochemical method to produce polymers. In the 1970s Toray were using a photochemical batch reactor to manufacture precursors for nylon 12 (**Scheme 3**) and nylon 6 (ϵ–caprolactam **Scheme 4**).[34,35] Both were made using the same photochemical methodology which utilises UV light to dissociate nitrosyl chloride to generate NO + Cl; the high reactive NO then reacts with an alkane. The product of this reaction can be used to make a cyclic amide, which is used to make the polyamide structure of nylon.
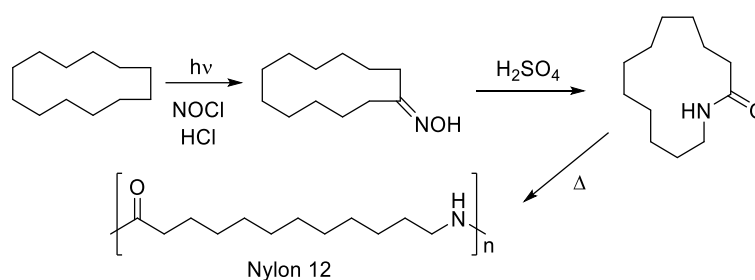
Scheme 3: Photochemical nylon production, adapted from Ref [34]
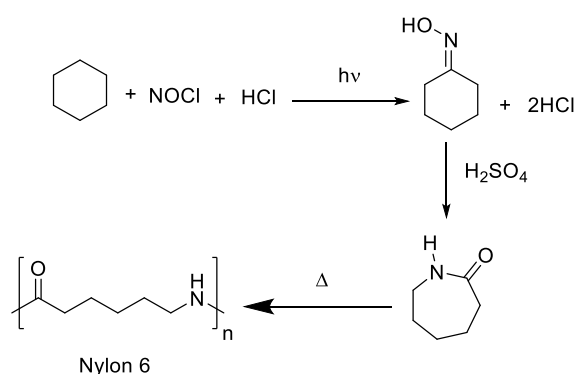
Scheme 4: Photochemical production of ϵ–caprolactam, adapted from Ref [35]

The reactor they were using was a multi-lamp reactor – see **Figure 11**,[34] which has the temperature maintained using a cooling jacket and the system had the capability of adding various gases to facilitate the desired reaction. Following the photochemical reaction, dense oily droplets of product formed sink to the bottom of the reactor to be extracted. This allowed the process to continuous and so became economically viable. However, this photochemical process had many drawbacks such as: expensive reactor lining (titanium), requirement for continuous lamp cooling, poor reaction mixture mixing, regularly replacing burnt out lamps, safety concerns of having a hot lamp (800 °C) next to a flammable liquid and the economic production of reactants.[34]
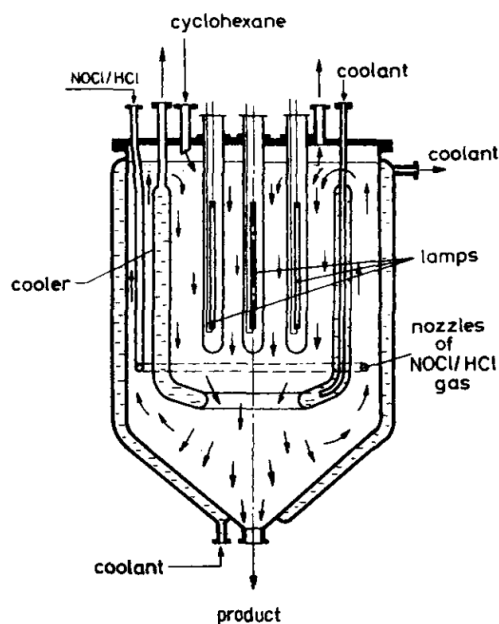
Figure 11:Toray's photochemical batch reactor. From this simple diagram it is possible to see the lamps used in this reaction surrounded by the cooling system. Furthermore, the gas exhaust nozzles are shown to be below the lamps, allowing the gases to mix prior to being exposed the UV light. In addition, the cone design of the reactor vessel allows the product to be collected from the base. Image reproduced from Ref [34]

In Chapter 3, similar problems arise in the photodissociation of gaseous Cl_2 for photochlorination. The Chapter explores potential resolutions of these issues, where a Rotary evaporator is adapted to chlorinate aromatic compounds.

Vitamin D

Another photochemical process which is of industrial interest is the synthesis of vitamin D. The need for vitamin D as a supplement in food stuffs should be thought of as a global issue because historically there has been many instances of rickets (a disease caused by vitamin D deficient) observed in Northern Europe and USA.[36] Historically, this related to the industrial revolution reducing the working population's exposure to sunlight, as vitamin D is produced by the skin as a result of exposure to solar light (290 – 315 nm).[36] Since the earlier 1930s, various food stuffs have been fortified with vitamin D to reduce the instances of rickets and improve bone health in the population. The need to supplement vitamin D into the food chain has remained highly important since this time. Recently, vitamin D has come back into the limelight as it has been reported that it could aid in the treatment of Coronavirus.[37]

Historically, vitamin D was produced from 7-dehydrocholesterol (also known as provitamin D, which is found in wool fat), irradiated with UV light then purified.[38] Whilst this may align with some of the principles of green chemistry (benign materials, less hazardous synthesis) however the atom economy of this reaction is quite low due to the production of numerous side products. This is related to the reaction mechanism. When irradiated with UV light the starting material (provitamin D) undergoes an electrocyclic ring opening to form previtamin D. Once previtamin D is formed a number of reaction pathways can take place. The desired method is a [1,7] sigmatropic rearrangement to form the desired *trans*-vitamin D$_3$, however, this route is endothermic and high temperatures are required to achieve high yields of the desired product - **Scheme 5**. Unfortunately, as the reaction progresses, other unwanted products can also be produced, reducing the efficiency of the reaction.
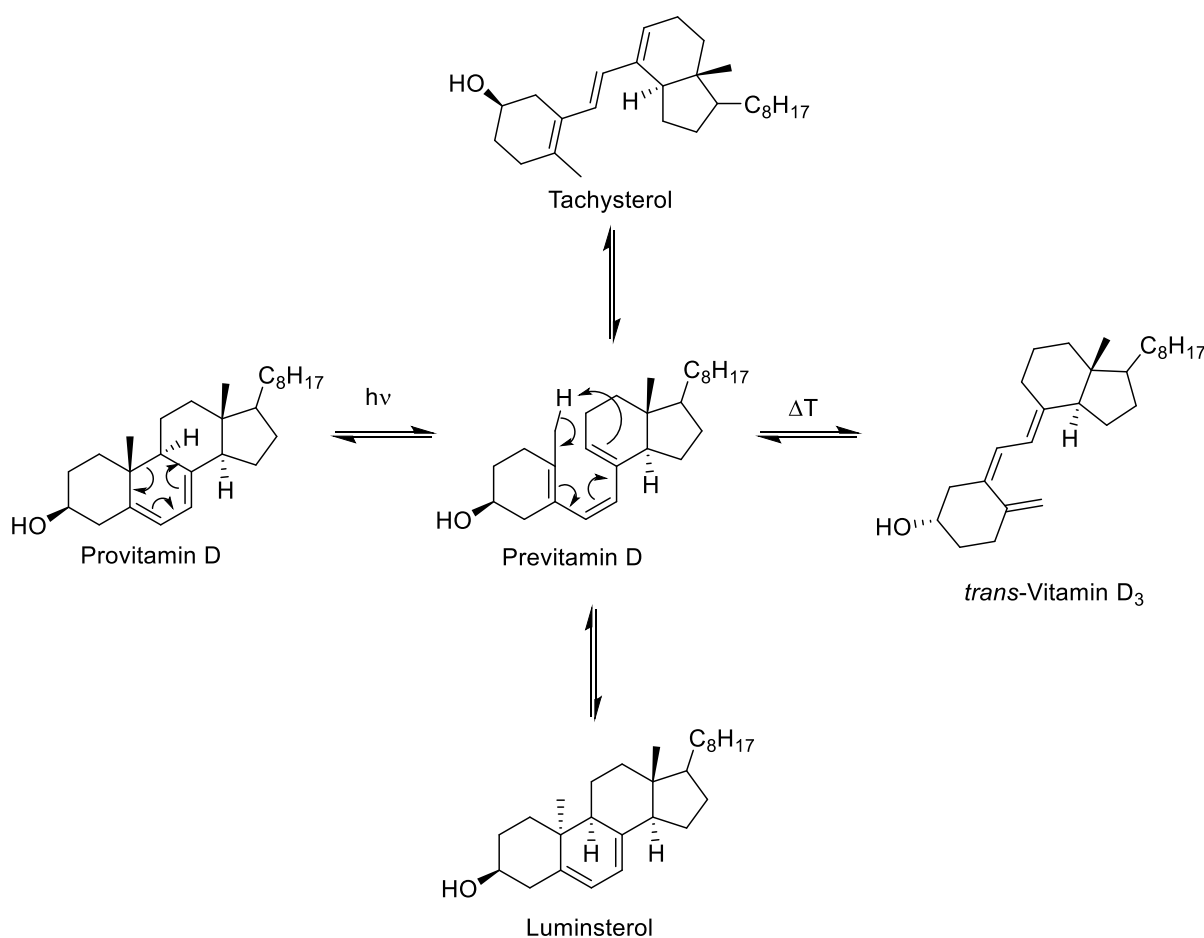
Scheme 5: Vitamin D photochemical synthesis, adapted from Ref [39]

Recently, Hessel, Noël and Escribà-Gelonch published an interesting method to improve selectivity for the continuous-flow production of vitamin D at high temperature - **Figure 12**. [39]
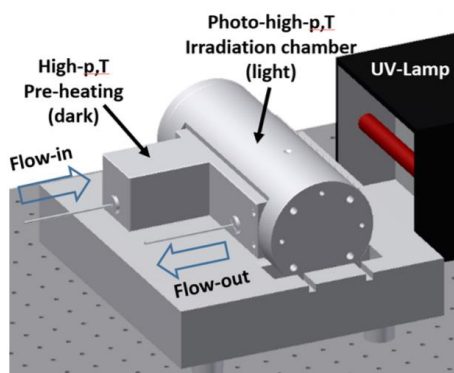

Figure 12: Diagram of high pressure, high temperature photoreactor developed by Hessel and co-workers. This μ-flow reactor makes use of coil of quartz glass to allow excellent penetration of light (280 nm) into the solution. The quartz coil is within the heating aluminium irradiation chamber. The use of aluminium allows for good temperature control (solution was pre-heated before entering the irradiation chamber) and the highly reflective inner surface produced uniform irradiation of the quartz coil. Reproduced from Ref [39]

In this work the team start from the provitamin D, now an industrial synthesised compound obtained from cholesterol and developed a novel reactor design to enable rapid photochemical reactions to be undertaken at high temperatures. This publication reported screening three conditions with this reactor. These were the temperature of the reaction (elevated above the boiling point of the solvent), length of irradiation and concentration of reagents. By studying these points, the group concluded that a short irradiation time at a temperature around 200 °C gave the best results and that varying the concentration did not impede the reaction yield. It is important to note that they were using *tert*-butyl methyl ester (*t*-BME) as the solvent, which was chosen to reduce the potential production of dangerous peroxides which could be produced when working at elevated temperature. The maximum amount of provitamin D which could be solubilised into this mixture was shown to be 0.22 M and the team noted that if an alternate suitable solvent were employed this could reduce the impact this limiting factor of on the process. The reported the production of vitamin D_3 (7.3 g/day) in *t*-BME following 43 seconds of irradiation at temperatures close to 200 °C in a continuous flow system at 34 bar, with 40 % selectivity for vitamin D_3. This method shows that with careful optimisation of reaction conditions, even complex chemical synthesis can be honed to produce desirable outcomes. This is a good illustration of the application of a photochemical

process coupling with additional thermal requirements and novel engineering solutions to overcome industrial issues.

Heraeus Noblelight – anti-cancer treatment

A more recent notable example of industrial scale UV photochemistry and the application of modern engineering techniques is exemplified by the work of Heraeus Noblelight. The company report the photochemical synthesis of 10-hydroxycamptothecin and 7-ethyl-10-hydroxycamptothecin from their corresponding N-oxides, on a multi kilogram scale using a multiple micro-flow reactor (**Figure 13**).[1, 40]
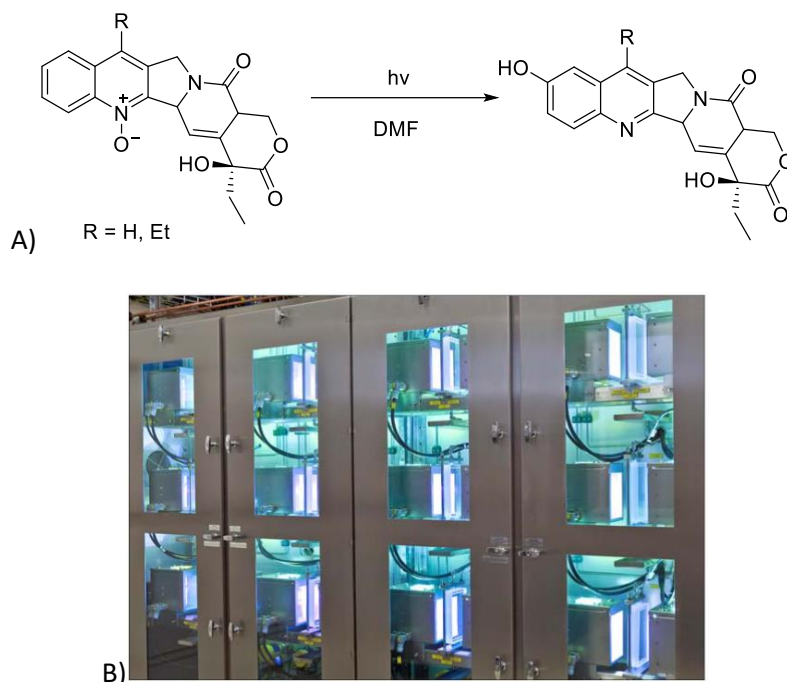
Figure 13: A) Scheme of 10-hydroxycamptothecin and 7-ethyl-10-hydroxycamptothecin photochemical synthesis B) Heraeus Noblelight's photochemical reactor. From this image it is possible to see the employment of multiple μ-flow reactors used to scale-out their process to enable manufacturing of the desired compounds at the required quantities. Image reproduced from Ref [1]

These products are precursors to anti-cancer drugs irinotecan and topotecan which have a current demand of less than 1 tonne/annum.[1] Interestingly, this equates to less than 3 kg of product per day, which is a surprisingly small quantity but indicative of the quantities required for "personalised" medicines. The term "personalised medicine" is a relatively new concept based on the understanding that a patient's response to a medicine can depend on their genetic makeup.[41] This

leads to the potential possibility that a medicine would need to be adapted (or personalised) to be more effective to patients with key genetic markers. To the drug producer this could result in a change in production tactics. This change could be to replace the current multi-tonne production facilities making vast quantities of a single product to a more flexible approach where smaller, volumes of more specialised therapeutic agents are synthesized.

The utilisation of micro-flow reactors has become an area of intense research in recent years and Leblebici and co-workers[42] have recently published an excellent review on the topic which follows on from the a similar article published by Oelgemöller & Shvydkiv[1] showing how the area has developed over time. This is because the use of these reactors allows for highly concentrated solutions to be processed and easily irradiated, due to the very short light pathlengths used. However, this type of reactor also has a few drawbacks when used at large scale such as highly complex piping requirements, need for multiple pumps and easily blocked flow channels which are difficult to clean. In the instance of Heraeus Noblelight when compared to the batch process, the micro-reactor process was 6-times more concentrated – reducing the solvent costs which are a major constraint for large scale synthesis.

Similar to the Artemisinin example discussed earlier, the solvent chosen for this reaction was not ideal from a green chemistry perspective as dimethylformamide (DMF) which is a polar aprotic solvent which can be difficult to recycle. The issues which arise between photochemistry and solvent choice are explored to a greater degree later in this thesis.

AbbVie - Photoredox

In the last decade there has been a significant development in the field of visible light photochemistry with a lot of work focused on photoredox catalysed reactions.[5,43,44] The use of various photoredox catalysts allows for numerous chemical reactions to be conducted which can be complex to achieve via alternative routes. Further to this the application of these catalysts to photochemical reactions agrees with the ninth principle of Green Chemistry, use of catalysts.

The majority of the publications relating to this research area have mostly kept to small laboratory-sized quantities, however in 2018 a team based at AbbVie (a commercial pharmaceutical manufacturer) reported a reactor design which used high powered visible light lasers to carry out photochemical reactions at an industrially relevant scale - **Figure 14.**[45]
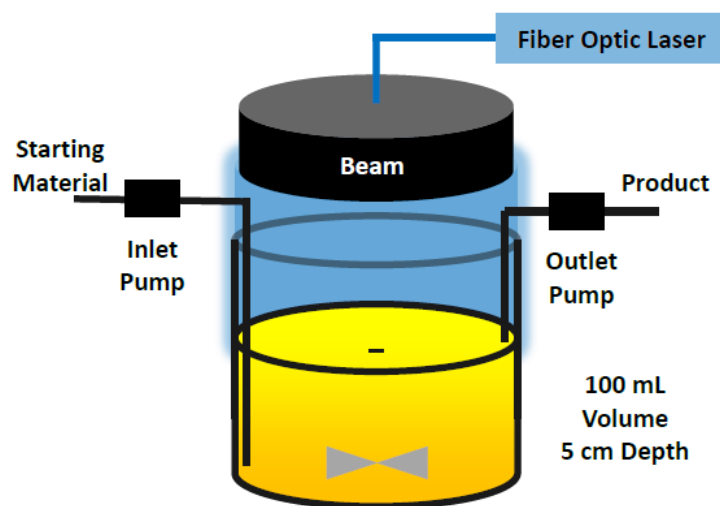
Figure 14: Laser (26 W, 460 nm) driven photoredox continuous flow reaction conducted by AbbVie. This system consists a continuous stir tank reactor, where the quantity of materials is maintained throughout the reaction by balancing the volume of the reagents added with the product remove form the tank. It is important to note that the starting material is added at the base of the tank and the product collected from the top of the reactor. The result of these design choices means that the starting materials are fully irradiated before being removed from the tank. This image was reproduced from Ref [45]

The reaction chosen was a C-N bond formation as this could be used as a model reaction for a collection of pharmaceutical synthetic reactions, which could be of interest in the future - **Scheme 6**. In the absence of a photocatalyst only ~ 3 % conversion was observed after 3 hours however, using their optimised system, the team were able to synthesise 1.5 kg of the desired product in 32 hours which gave a reactor productivity of 1.2 kg/day. As discussed previously, this quantity is in alignment with the production levels required for personalised medicines.
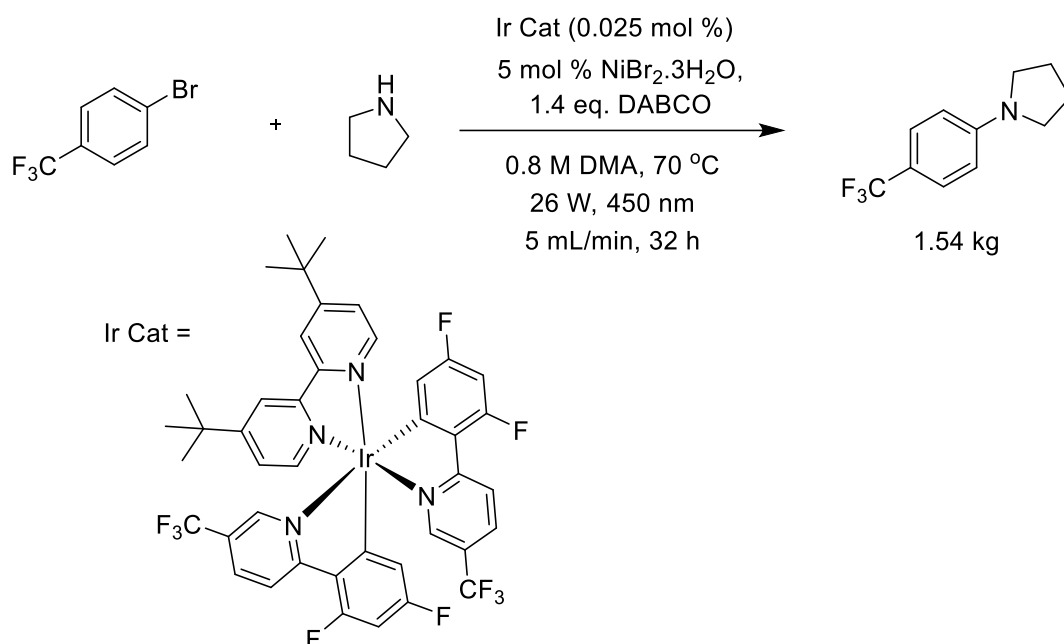
Scheme 6: Visible photoredox reaction conducted at an industrially relevant scale by AbbVie.[45]

This shows the importance of engineers and chemists working together to overcome a few long-standing photochemical issues and to be able to answer the industrial need of an increase in scale for photoredox reactions. However, there are still areas of research worth investigating within this reaction, particularly from a green chemistry angle. Whilst this reaction is catalysed, the catalyst itself is based on iridium (an expensive and rare element), the replacement of this catalyst with an organic alternative could reduce the overall cost of the reaction. Alongside this, the solvent used in the reaction dimethylacetamide (DMA) is both toxic and high boiling (making it difficult to remove from the product mixture). In an attempt to address some of these issues, a similar catalytic photoredox amide bond forming reaction is the focus of the research in the second chapter of this thesis so further discussion on this topic will be conducted in that Chapter.

Conclusion

This Chapter has given a brief, critical overview of several industrial photochemical syntheses with some comments from the perspective of Green Chemistry. From these cases a number of points are clear.

1. Solar based photochemistry does not appear to be well suited to industrial scale synthesis of chemicals.

2. Several examples showed that photochemistry is often conducted in solvents which are not particularly environmentally benign.

3. Reactor design is very important when conducting photochemistry, particularly when conducting reactions with corrosive gases.

4. The recent development of photoredox catalysed reactions to produce industrially relevant products is worth further exploration as unusual reactions can be readily performed, however there are still a number of challenges from a green chemistry perspective.

5. The application of biologically controlled chemical synthesis should be considered in the planning of complex reactions as this can reduce the complexity of the steps required to achieve the desired aims.

Thesis Aims

From the points in the conclusions these Thesis aims have been derived. In all of the aims the common theme will be to use various light sources other than solar.

- The first aim of the Thesis is to explore an industrially relevant photoredox reaction, an amide bond synthesis. This type of reaction was chosen as to the best of my knowledge, it has been the least explored from a green chemistry perspective. Alongside the photochemistry work, the application of biology (in the form of enzymes) will be explored to control the chirality within the product, potentially reducing the level of synthetic complexity. These points will be explored in Chapter 2.

- The second aim will be to develop a reactor which is capable of safely conducting photochlorination reactions using chlorine gas. Once built and tested, the reactor will be used to synthesize several compounds which could be of interest for large scale production. This system was chosen for further exploration as there are only a limited number of publicised methods for conducting this type of reaction and the unique properties of the

PhotoVap could solve a number of long-standing issues. This will be investigated in Chapter

3.

- The final aim of the Thesis will be to study the application of bio-derived solvents for use in

  photochemical reactions, beginning with binary and then ternary mixtures to achieve the

  desired solvent properties.

At the end of this Thesis, the progress made will be evaluated against these aims and suggestions

will be made for further work to carry this research forward.

Bibliography

1. Oelgemöller, M. & Shvydkiv, O. Recent advances in microflow photochemistry. *Molecules* **16**, 7522–7550 (2011).
2. Marzo, L., Pagire, S. K., Reiser, O. & König, B. Visible-Light Photocatalysis: Does It Make a Difference in Organic Synthesis? *Angew. Chemie Int. Ed.* **57**, 10034–10072 (2018).
3. Esser, P., Pohlmann, B. & Scharf, H. -D. The Photochemical Synthesis of Fine Chemicals with Sunlight. *Angew. Chemie Int. Ed. English* **33**, 2009–2023 (1994).
4. Rau, H. Asymmetric Photochemistry in Solution. *Chem. Rev.* **83**, 535–547 (1983).
5. Romero, N. A. & Nicewicz, D. A. Organic Photoredox Catalysis. *Chem. Rev.* **116**, 10075–10166 (2016).
6. Oelgemöller, M. Solar Photochemical Synthesis: From the Beginnings of Organic Photochemistry to the Solar Manufacturing of Commodity Chemicals. *Chem. Rev.* **116**, 9664–9682 (2016).
7. Rehm, T. H. Flow Photochemistry as a Tool in Organic Synthesis. *Chem. Eur. J.* **26**, 16952–16974 (2020).
8. Šima, J. Photochemistry — development and achievements. *Acta Chim. Slovaca* **10**, 84–90 (2018).
9. Protti, S., Dondi, D., Fagnoni, M. & Albini, A. Photochemistry in synthesis: Where, when, and why. *Pure Appl. Chem.* **79**, 1929–1938 (2007).
10. Albini, A. & Fagnoni, M. 1908: Giacomo ciamician and the concept of green chemistry. *ChemSusChem* **1**, 63–66 (2008).
11. Ciamician, G. MODERN civilization is the daughter of coal, for this offers to mankind the solar. *Science (80)* **XXXVI**, 926 (1912).
12. Günther, Schenck, O. & Ziegler, K. Die Synthese des Ascaridols. *Naturwissenschaften* **32**, 157 (1944).
13. Anastas, P. & Warner, J. *Green Chemistry: Theory and Practice*. (Oxford University Press, 2000).
14. Fang, Y. & Li, C. Preference of 4-exo ring closure in copper-catalyzed intramolecular coupling of vinyl bromides with alcohols. *J. Am. Chem. Soc.* **129**, 8092–8093 (2007).
15. Sheldon, R. A. Metrics of Green Chemistry and Sustainability: Past, Present, and Future. *ACS Sustain. Chem. Eng.* **6**, 32–48 (2018).
16. Trost, B. M. The atom economy - A search for synthetic efficiency. *Science (80).* **254**, 1471–

1477 (1991).

17. Sheldon, R. A. The: E factor 25 years on: The rise of green chemistry and sustainability. *Green Chem.* **19**, 18–43 (2017).

18. Wu, H. W., Emadi, A., De Graaf, G., Leijtens, J. & Wolffenbuttel, R. F. Design and fabrication of an albedo insensitive analog sun sensor. *Procedia Eng.* **25**, 527–530 (2011).

19. Cambié, D. *et al.* Energy-Efficient Solar Photochemistry with Luminescent Solar Concentrator Based Photomicroreactors. *Angew. Chemie* **131**, 14512–14516 (2019).

20. Gunes, E. Turkey Rose Oil Production and Marketing: A review on problem and opportunites. *J. Appl. Sci.* **5**, 1871–1875 (2005).

21. Boskabady, M. H., Shafei, M. N., Saberi, Z. & Amini, S. Pharmacological effects of Rosa damascena. *Iran. J. Basic Med. Sci.* **14**, 295–307 (2011).

22. Butler, H. *Poucher's Perfumes, Cosmetics and Soaps.* (2000).

23. Alsters, P. L., Jary, W., Nardello-Rataj, V. & Aubry, J. M. Dark singlet oxygenation of β-citronellol: A key step in the manufacture of rose oxide. *Org. Process Res. Dev.* **14**, 259–262 (2010).

24. Ravelli, D., Protti, S., Neri, P., Fagnoni, M. & Albini, A. Photochemical technologies assessed: The case of rose oxide. *Green Chem.* **13**, 1876–1884 (2011).

25. Monnerie, N. & Ortner, J. Economic evaluation of the industrial photosynthesis of rose oxide via lamp or solar operated photooxidation of citronellol. *J. Sol. Energy Eng. Trans. ASME* **123**, 171–174 (2001).

26. Clark, C. A., Lee, D. S., Pickering, S. J., Poliakoff, M. & George, M. W. A Simple and Versatile Reactor for Photochemistry. *Org. Process Res. Dev.* **20**, 1792–1798 (2016).

27. Turconi, J. *et al.* Semisynthetic artemisinin, the chemical path to industrial production. *Org. Process Res. Dev.* **18**, 417–422 (2014).

28. Kung, S. H., Lund, S., Murarka, A., McPhee, D. & Paddon, C. J. Approaches and recent developments for the commercial production of semi-synthetic artemisinin. *Front. Plant Sci.* **9**, 1–7 (2018).

29. Cook, S. P. The quest for affordable artemisinin. *Future Med. Chem.* **5**, 233–236 (2013).

30. Zhu, C. & Cook, S. P. A concise synthesis of (+)-artemisinin. *J. Am. Chem. Soc.* **134**, 13577–13579 (2012).

31. Wang, Z., Yang, L., Yang, X. & Zhang, X. Advances in the chemical synthesis of artemisinin. *Synth. Commun.* **44**, 1987–2003 (2014).

32. Amara, Z. *et al.* Applying green chemistry to the photochemical route to artemisinin. *Nat. Chem.* **7**, 489–495 (2015).

33. Kopetzki, D., Lévesque, F. & Seeberger, P. H. A continuous-flow process for the synthesis of artemisinin. *Chem. Eur. J.* **19**, 5450–5456 (2013).

34. Fischer, M. Industrial Applications of Photochemical Syntheses. *Angew. Chemie Int. Ed. English* **17**, 16–26 (1978).

35. Funken, K. H., Müller, F. J., Ortner, J., Riffelmann, K. J. & Sattler, C. Solar collectors versus lamps - A comparison of the energy demand of industrial photochemical processes as exemplified by the production of ε-caprolactam. *Energy* **24**, 681–687 (1999).

36. Holick, M. F. The influence of vitamin D on bone health across the life cycle. *J. Nutr.* **135**, (2005).

37. The Lancet Diabetes & Endocrinology. Vitamin D and COVID-19: why the controversy? *Lancet Diabetes Endocrinol.* **9**, 53 (2021).

38. Morales-Gonzalez, O. M., Escribà-Gelonch, M. & Hessel, V. Life cycle assessment of vitamin D3 synthesis: from batch to photo-high p,T. *Int. J. Life Cycle Assess.* **24**, 2111–2127 (2019).

39. Escribà-Gelonch, M., Noël, T. & Hessel, V. Microflow High-p,T Intensification of Vitamin D3 Synthesis Using an Ultraviolet Lamp. *Org. Process Res. Dev.* **22**, 147–155 (2018).

40. Rauter, H., Seliger, R. & Wissmann, F. EP 2 065 387 A2. (2009).

41. Vogenberg, F. R., Barash, C. I. & Pursel, M. Personalized medicine - Part 1: Evolution and

development into theranostics. *P T* **35**, (2010).

42. Kayahan, E. *et al.* Dawn of a new era in industrial photochemistry: The scale-up of micro: The mesostructured photoreactors. *Beilstein J. Org. Chem.* **16**, 2484–2504 (2020).

43. Liu, J. *et al.* Visible-light-mediated decarboxylation/oxidative amidation of α-keto acids with amines under mild reaction conditions using O2. *Angew. Chemie Int. Ed.* **53**, 502–506 (2014).

44. Zhang, L. & Hu, X. Room temperature C(sp2)-H oxidative chlorination: Via photoredox catalysis. *Chem. Sci.* **8**, 7009–7013 (2017).

45. Harper, K. C., Moschetta, E. G., Bordawekar, S. V. & Wittenberger, S. J. A Laser Driven Flow Chemistry Platform for Scaling Photochemical Reactions with Visible Light. *ACS Cent. Sci.* **5**, 109–115 (2019).

Chapter 2- Exploration of photocatalytic amide bond forming reactions

Introduction

The amide functional group is found in a diverse range of chemical products in the chemical industry. For example, of the 38 new small molecule drugs which were approved by the US FDA in 2018, 75 % of these contained at least one amide bond.[1] In view of amide bonds being found in several bioactive/pharmaceutical compounds the focus of the work in this Chapter has been into photocatalytic amide bond formation. Additionally developing more environmentally friendly approaches for the formation of this key bond makes this work significant, particularly as this continues to be a high priority for the chemical industry.[2,3] Despite this apparent ubiquity of the amide bond across the chemical industry, its synthesis can be somewhat challenging.[4–6] An amide bond can be formed via a condensation reaction between a carboxylic acid and an amine and in this unassisted reaction, the elimination of water usually requires high temperatures (> 200 °C) to occur which can be problematic due to the decomposition of the starting materials and/or the formation of unwanted side products.[4] The conversion of OH group of the carboxylic acid to a better leaving group has been used to address this problem.[4] One such method of derivatisation of the carboxylic acid is through the use of Hexafluorophosphate Azabenzotriazole Tetramethyl Uronium or HATU and this allows the more facile formation of amide bonds, see **Scheme 7**.
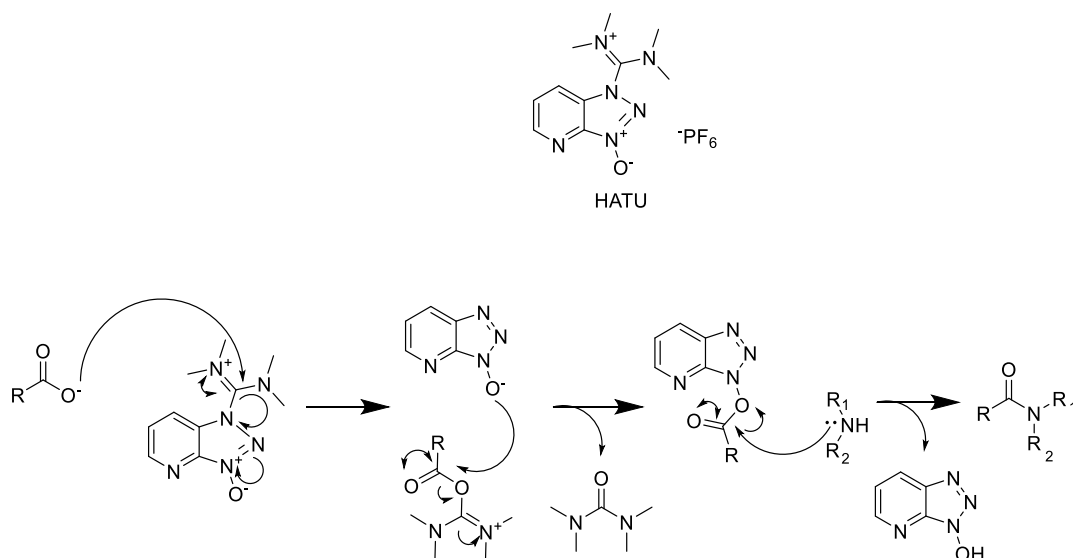
Scheme 7: Amide coupling reagent HATU and the mechanism by which it forms an amide.

Photochemical amide bond formation

The environmental benefits related to the use of photochemistry were discussed in detail in **Chapter 1** and the benefit for amide bond forming reactions are given here. Firstly, light (photons) can be used to drive the catalytic process which synthesise amide bonds. This can be a highly effective method of producing amide bonds as light can be generated cheaply and efficiently using modern light sources (e.g., LEDs). The use of photochemical methods also gives access to a number of alternative chemical functional groups which can be used as starting reagents for amide bond formations. This expands the library of compounds which can be utilised and allows access to amides through a diverse range of routes, some of which are shown below.

Recently, there have been a collection of light catalysed amide bond formations reported in the literature[7–16] however a number of common challenges to many examples of these photochemical amide bond formation reactions can be observed, namely the: (i) small reaction scale currently used; (ii) need for transition metal photocatalysts and (iii) limited substrate scope currently reported. A few recent examples are highlighted here.

Scheme 8:Visible light catalysed amide bond formation proposed by Liu *et al* involving the loss of CO₂ in the amide formation and ruthenium based photocatalyst.[11]

Scheme 8 shows a photocatalytic synthetic method, reported in 2014 by Liu *et al*., for producing

amides from α-keto acids.[11] In this example, the team applied this procedure to produce 18 example

amides from a wide range of both acid and amine starting materials. The mechanism progresses

from the formation of an acyl radical, by the decarboxylation of the α-keto acid with the formation

of carbon dioxide as the only by-product thus producing a highly atom efficient synthesis with a

strong entropic driving force. Furthermore, the work-up of this reaction requires fewer purification

steps compared to the HATU alternative synthesis. However, the reported reaction had long

reaction times (1.5 days) and the scale and concentration used were low (2 mL and 0.5 mmol

respectively) which may present problems for scale-up particularly for industrial manufacturing. The

use of more powerful light sources and different reactor designs than those reported in the

literature may help, in part, to circumvent these limitations.

Scheme 9: Photochemical amide synthesis of amides reported by König and co-workers. Similarly to the previous example this system loses a gas (N₂) to form the amide.[9]

Another example of photochemical amide bond formation is from König and co-workers in 2015,

who studied the photocatalytic amidation of electron-rich heteroarenes with benzoyl azides [9] -

Scheme 9. Through this method they reported the synthesis of 24 different amides including the production of sulfonamide which could have applications for the synthesis of antibiotics. This method has similar positive aspects to the work of Liu *et al.* in that the only waste product of this reaction is gaseous. This reported reaction also had limitations in terms of timescale of reaction (2-24 h), catalyst (transition metal) and solvent (DMSO has a boiling point of 189 °C, making it hard to remove from the reaction mixture) which may be problematic for scale-up.
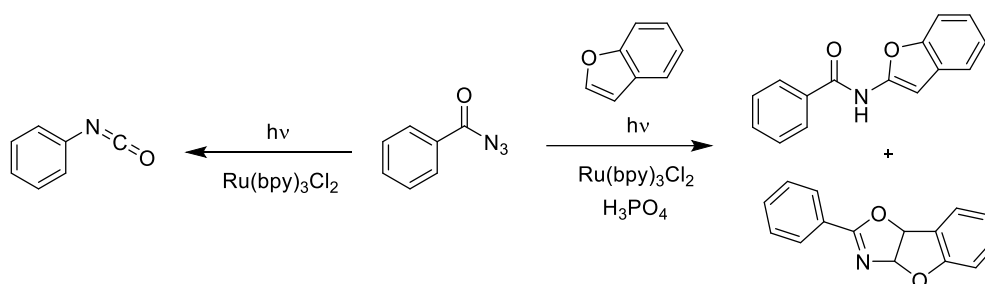

Scheme 10: Variation in product depending on the presence or absence of acid, reported by König and co-workers. **Through the addition of an acid it is possible to form either an amide or an oxazoline, but in the absence of an acid only isocyanates are formed.** [9]

An interesting note with the amide bond formation reported by König and co-workers was the need for phosphoric acid which allows the formation of the desired amide product. In the absence of the acid, only the isocyanate product was observed (see left-hand arrow/side of **Scheme 10**); the authors suggested that the acid is acting as a stabilising agent for the nitrene to be able to react with the desired heteroarene - **Scheme 10**. An oxazolines side product is also produced and these compounds are valuable products in their own right (e.g. Aminorex - **Figure 15**). König and co-workers, also subsequently reported a further detailed optimisation of the photochemical production of these oxazolines.[13]

Figure 15: Aminorex, a weight loss stimulant which contains the Oxazoline moiety, coloured blue.[16]

Photocatalytic amide bond formation has also been achieved using a *N*-chlorosuccinimide or *N*-hydroxyphthalimide to activate the starting aldehyde. Maity and co-workers reported the use of *N*-hydroxy phthalimide combined with a visible photocatalyst to undertake the amidation of a number of aldehydes in 2015.[8] Similarly in 2016, Cho and Iqbal used *N*-chlorosuccinimide for photocatalytic amide bond formation – see both routes in **Scheme 11**.[15]
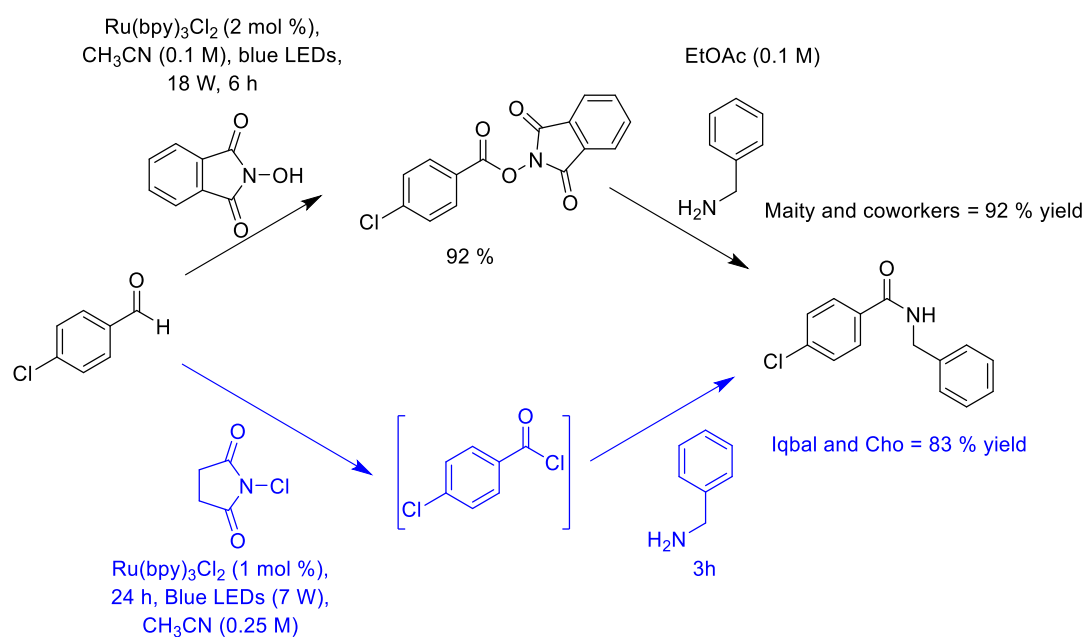

Scheme 11: Two similar photocatalytic methods for the synthesis of the same amide reported by Maity and co-workers [8] and Iqbal and Cho. [15]

It is possible to gain some insight into the pros and cons of each method by comparing these last two examples. Firstly, the photochemical step reported by Maity and co-workers appears to be faster than Cho and Iqbal's method. However, it is important to note that Maity and co-workers report the use of a light source which is 2.5-times more powerful and uses twice the quantity of photocatalysts than Cho and Iqbal. The use of the higher-powered lamp and greater quantity of photocatalyst could be the cause of this decrease reaction time.

Although both methods use a metal photocatalyst, they also use easily recyclable reagents

(phthalimide and succinimide), which potentially could allow reagents to be recycled.

Unlike Maity, Cho and Iqbal did not isolate the intermediate of the reaction. This lack of isolated

intermediate could reduce the complexity associated with the intensification process making this

route more favourable than Maity's.

A thought-provoking example of photochemical amide bond forming approach was reported by

Sahani and co-workers in 2018 which used trichlorobromomethane as a radical carrying reagent to

produce 37 example amides[12] - **Scheme 12**. Through this method the team were able to couple

aldehydes and secondary amines to be able to form amides.
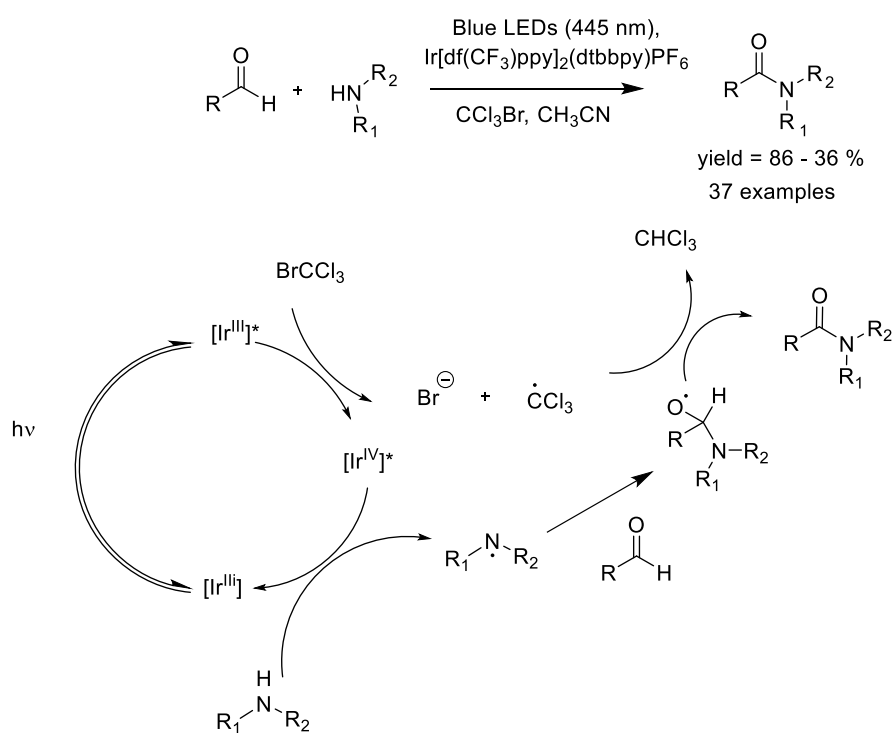
Scheme 12: Photochemical amide bond synthesis reported by Sahani and co-workers. This method uses
trichlorobromomethane to aid in the production of this desired amide.[12]

This method is notable for two reasons. Firstly, the use of trichlorobromomethane is unusual as this

molecule belongs to a family of compounds which are known ozone depleting agents making them

disfavoured when attempting to carry out more sustainable chemical reactions. Secondly, the

formation of secondary amides is unusual as the majority of the reported amides formed

photochemically typically tend to be primary – thus allowing for a greater range of products to be

synthesised.

Like the previous examples, the route reported by Sahani and co-workers employs a transition

metal-based catalyst, but in this case the metal is iridium. This is not an unusual photocatalyst;

however both transition metals typically used as photocatalysts (ruthenium and iridium) are very

scarce with iridium being the less abundant.[17]

In 2016, Papadopoulos and Kokotos also used aldehydes to form 26 different example amides[14] -

Scheme 13. Interestingly, unlike the majority of the other works discussed previously in this report

the amides are mostly aliphatic instead of aromatic. A highlight of this work was that the team were

able to synthesise the antidepressant Moclobemide with a reasonable yield (49 %).
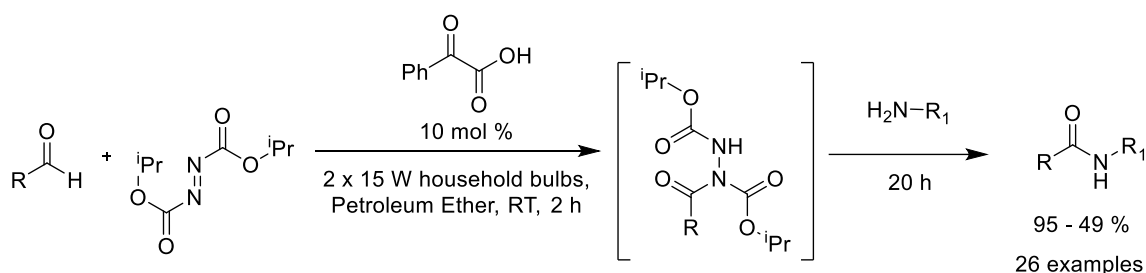
Scheme 13: Use of an organic photocatalyst to produce amides, reported by Papadopoulos and Kokotos. The notable point of this reaction is the use of an organic photocatalyst. [14]

This example exploits an organic α-keto acid as the photocatalyst. As far as I am aware, this is the

only reported photochemical method for amide bond formation which does not use a transition

metal photocatalyst. One can draw parallels between this method and the HATU approach to

forming amides (**Scheme 7**) in that both reactions use stoichiometric amounts of starting reagents

which generate significant quantities of waste products.[14]

The final example of photochemical amide bond formation to be discussed here is the 2018 work of

Ng *et al.* [18] which is the starting point for the work described in this Chapter - **Scheme 14**.
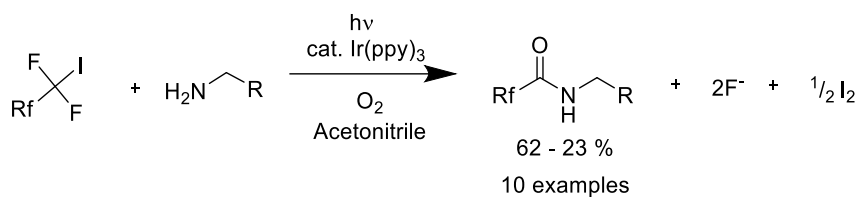
Scheme 14: Summary of the photochemical amide formation work by Ng *et al.* [18] This work is noteworthy for a number of reasons. Primarily, the limited number of by-products produced by this reaction is very low (two fluoride and one iodide atoms). This makes this reaction a highly atom efficient method of forming amides, but also the use of perfluoroalkyl chains means that some unusual amides could be produced by this technique.

This reaction maybe considered a potential improvement over the original HATU amide bond forming approach in that it is photocatalytic and more atom efficient (AE) i.e., 62 % compared to 43% for the HATU reaction - see **Appendix** for details of the calculation. Along with a significant reduction in waste, this method allows for the addition of perfluoroalkane groups into the amide product. This is important because fluorinated groups can be added to biological compounds to improve their bioavailability, modulate lipophilicity, induce conformational changes and improve metabolic stability.[19] Thus it is possible that this approach could be used to synthesise and subsequently allow a study on the effects of fluorinated alkyl chains on the C-terminal of an amide bond in biologically active compounds such as Valsartan (a blood pressure reducing agent) - **Figure 16**.
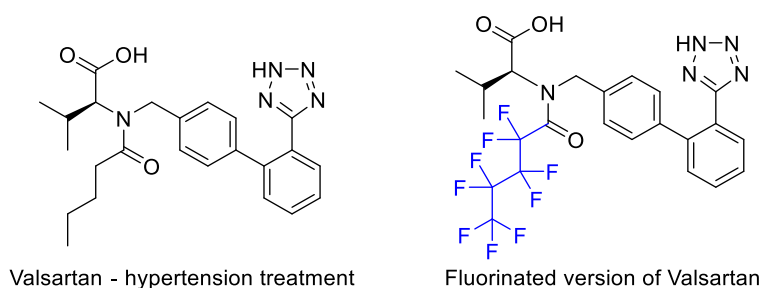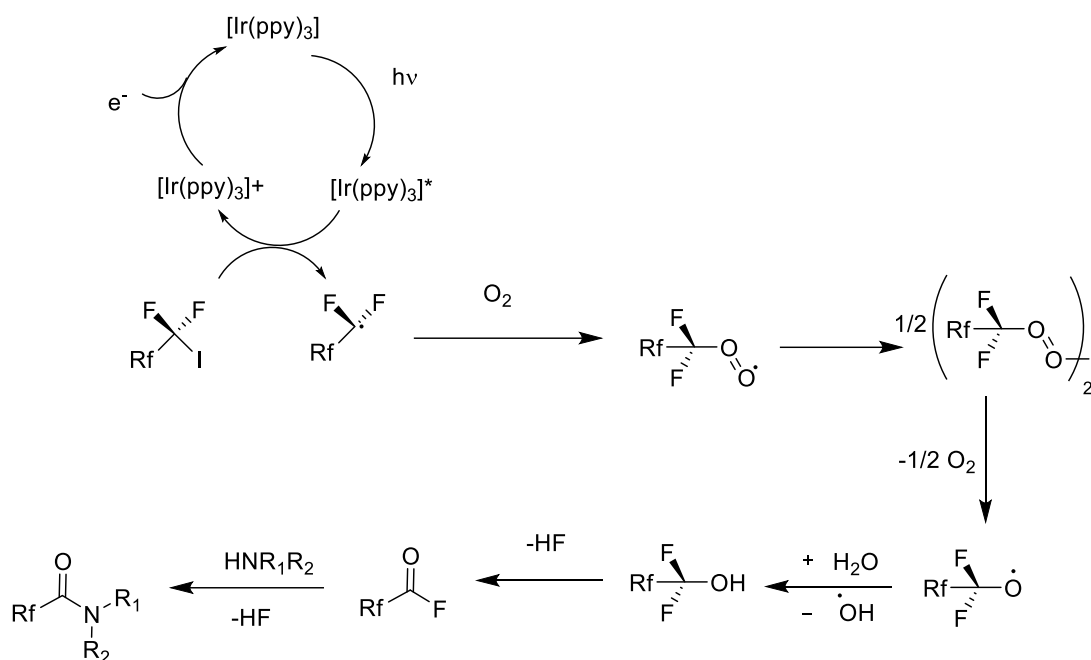

Valsartan - hypertension treatment   Fluorinated version of Valsartan

Figure 16: Potential use of the work of Ng *et al* to introduce fluoride atoms to active pharmaceutical ingredients.

The mechanism proposed for the reaction reported by Ng *et al.* is quite complex and is shown in **Scheme 15**.

Scheme 15: Proposed mechanism by which the photoamidation precedes.

The first step in the reported mechanism is the photoexcited iridium catalyst undergoing single electron transfer, passing an electron to the perfluoroiodoalkyl chain. This electron promotes loss of iodide and formation of a stable perfluoro-radical. Next, this perfluoro-radical species reacts with atmospheric O_2 to quench the radical and form an acyl fluoride (*via* the loss of HF). The acyl fluoride subsequently reacts with an amine via a nucleophilic substitution reaction, eliminating a second molecule of HF and forming the desired amide. This is an atypical reaction mechanism as the oxygen atom in the amide group originates from gaseous O_2 and also this reaction produces two equivalents of HF. The production of HF is somewhat concerning as it is a highly corrosive and harmful acid. However, it can be readily quenched through the addition of calcium carbonate to form insoluble calcium fluoride. Despite the promise of this method, there are a number of remaining issues that need to be addressed (i) the current small scale of the reactions; (ii) the use of the metal photocatalyst and (iii) the limited substrate scope that has been reported.

A key area of interest to the chemical industry is the development of asymmetric synthetic routes to biologically active compounds and the development of this approach to produce chiral amides

would be of considerable interest. It has often been difficult to achieve asymmetric photochemistry

and existing methods require the use of polarised light, bulky cage-like structures or intricately

designed photocatalysts.[20–23] However, the developments in enzymatic catalysis could allow a

combination of photochemical and enzymatic reactions[24] to be developed into a process for the

production of enantiomerically pure amides.

Enzymes have become valuable catalysts for the synthesis of chiral compounds, but their use can

sometimes be more challenging compared with more traditional synthetic chemistry routes.

However, there is a growing biocatalyst toolbox now available for retrosynthesis.[25–29] One such

application is the use of transaminase (TA) enzymes for synthesis, particularly, because of the

prevalence of chiral amines in bioactive natural products and pharmaceutical drugs.[30–36] Of

particular relevance to this Chapter is the recent report by O'Reilly and co-workers of a biocatalytic

disconnection for the regio- and stereo-selective synthesis of a range of 2,6-disubstituted

piperidines, relying on a key ω-TA triggered intramolecular aza-Michael reaction and subsequent

epimerization[37] - **Scheme 16**.
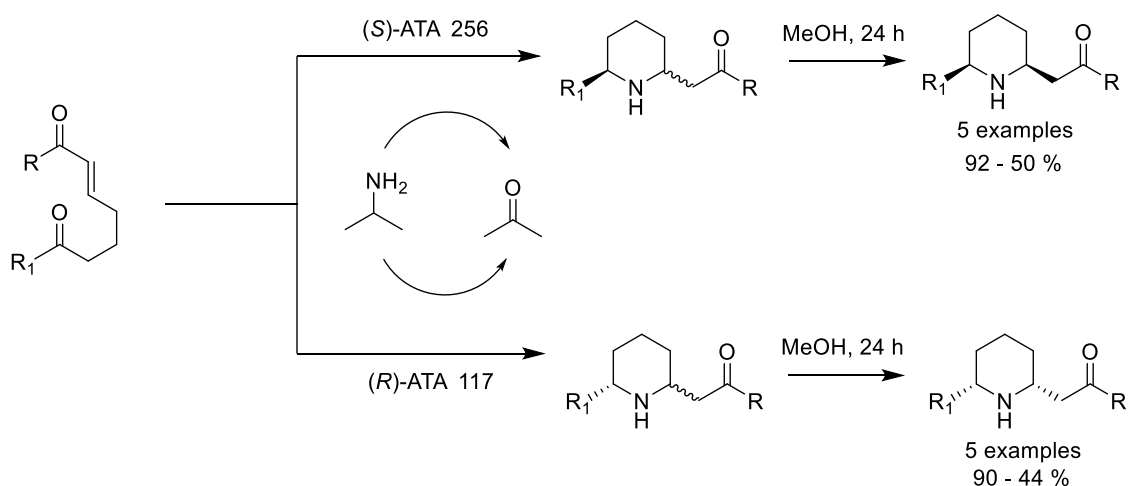
Scheme 16: Enantioselective synthesis of disubstituted piperidines, through the use of transaminases.[37]

Aims for this Chapter

Thus, this Chapter focuses on the use of light to drive the synthesis of amide bonds with the specific aims:

- To explore whether novel reactors can be used to readily intensify the scale of an unusual amide bond forming reaction.
- To investigate whether organic photosensitisers can be used as a more sustainable photocatalyst for amide bond formation.
- To establish whether biocatalytic amine formation can be daisy chained with photocatalysis to produce a new route and process for producing chiral amides.
- To probe whether this amide bond forming reaction can be conducted electrochemically rather than photochemically.
- To compare and contrast the effectiveness of the different approaches for amide formation.

Results & Discussion

<u>General Strategy</u>

Following on from the Aims of this Chapter, the next section describes the general strategy that was undertaken for the work presented in this Chapter:

1. The goal in this part was to investigate intensification by increasing the concentration of the reactants and observing the effect on yield and productivity. Initially, a number of small-scale batch reactions were conducted to monitor if there were any changes in the reaction outcomes when the concentration was increased compared to the results reported in the literature.[18] Following these batch reactions, the most effective concentration was used to run the reaction in a number of different reactors. Thus, allowing exploration of the length of reaction time when using various synthetic set-ups.

2. The goal in this part was to establish whether alternative photocatalysts could be used to produce a more effective process based on photocatalytic amide bond formation. The reduction potential required to break the C-I bond was used to identify[38,39] an excited state oxidation potential high enough to allow the reduction (and breaking) of the C-I bond. The

amide bond forming reaction with/without the organic photosensitiser was conducted to allow comparison between selected sensitisers.

3. To examine whether enzymatic reactions could be coupled with photochemical amide bond formation thus opening up the possibility of producing chiral precursors and ultimately chiral amides. Initially a commercially sourced enantiomerically pure amine was used to conduct the photochemical reaction and determine whether the chiral purity is retained. Following this an enzymatic reaction to produce an enantiomerically pure amine was carried out and subsequently used to make an enantiomerically pure amide via a photochemical reaction. Next the process was repeated using a single solvent media for both the enzymatic and photochemical reactions and this process can be daisy chained together into a flow process to produce a number of chiral amides.

4. To investigate whether the transition metal photocatalysts could be eliminated by an alternative electrochemical approach. The electrochemical amide bond forming reaction was probed using cyclic voltammetry of perfluorobutyl iodide (PBI) with/without a chiral amine. The process was repeated in the presence and absence of oxygen. Following this the process would be compared with the photochemical method to attempt to determine the more sustainable route.

Aim 1: Process intensification

The first step in the intensification process was to repeat the literature reported conditions (**Table 1 – entry 1**) for the photocatalytic production of amides from amines and perfluoroiodoalkanes reported by Ng *et al.* (see **Scheme 14** above) initially using conventional equipment such as a round bottomed flask. It can be seen from entry 1 that it was possible to obtain similar results to those reported in the literature and this was an important first step in the method development activities. Following this initial experiment, the concentration of the reagents was increased 10-fold and the reaction repeated, (**Table 1 – entry 2**) good yields were achieved and the productivity increased by

ca. x30. The amount of benzyl amine was increased slightly to account for the potential reaction between HF acid and benzylamine.

 Following this, the oxygen source was varied between pure oxygen, compressed air, and atmospheric air (**Table 1 – entry 2, 3 & 4**). These experiments were conducted in order to determine the influence of varying the source of oxygen on the yield of the reaction. When pure O_2 was replaced by air the reaction yield decreased. As these experiments were being carried out, it was noticed that the reaction mixture became cloudy as a result of a precipitate forming, which appeared to slow the reaction down. This precipitate was suggested to be benzyl ammonium fluoride salt by comparison of the ^1H, ^{19}F and ^{13}C NMR with the reported literature values.[40] Such salts are readily water soluble and therefore additional experiments were undertaken where a small amount of water was added. **Table 1 – entry 5** shows that this addition of water increased the yield of the reaction significantly with the solution remaining clear and these conditions were carried forward to further experiments.

Table 1: Results from small scale batch reactions, [a] GC Yield, [b] isolated yield, [c] 3 % water added.
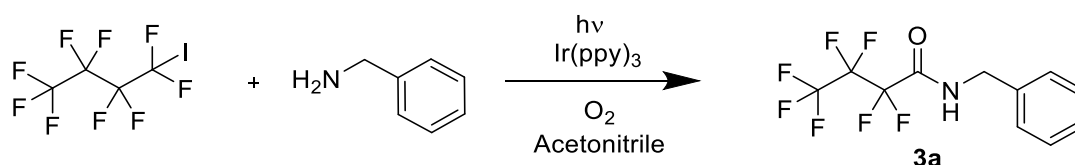
Entry	Reaction atmosphere	Perfluorobutyl iodide (mM)	Benzyl amine (mM)	Cat loading (mol %)	Reaction time (min)	Yield of 3a (%)	Productivity (g/day)
Lit value[18]	O_2	6.7	10	1	600	67[a], 62[b]	0.024
1	O_2	6.7	10	1	420	70[a], 47[b]	0.026
2	O_2	67	133	1	720	70[a]	0.85
3	Compressed air	67	133	1	720	57[a], 45[b]	0.55
4	Atmospheric air	67	133	1	720	55[a]	0.53
5[c]	O_2	67	133	1	720	93[a]	0.90

A number of different trials in various reactors produced rather unsuccessful initial results

(**Appendix - Appendix**

Table 7**, Table 8, Table 9, Table 10**) but the photocatalytic amide bond formation reaction in the

PhotoVap - **Table 2** showed positive results. The yield was increased slightly (**Table 2 – entry 2**) when

compared with the previous set of results (**Table 1 – entry 5**) however there was a significant

reduction in reaction time (2 h vs. 12 h) through the use of this reactor. **Table 2 – entry 3** shows the

further increase in reactant concentration by an extra factor of 10. This entry showed an overall

productivity increase of 470 when compared with the original reported result.

Table 2: Reaction yields when conducted in the PhotoVap in a 1 L round bottom flask. [a] GC Yield, [b] Isolated Yield
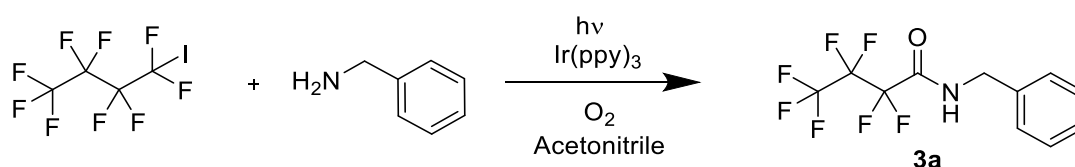

Entry	Reaction atmosphere	Perfluorobutyl iodide (mM)	Benzyl amine (mM)	Catalyst loading (mol %)	Reaction time (mins)	Yield of 3a (%)	Productivity of 3a (g/day)
Lit value[18]	O_2	6.7	10	1	600	67[a], 62[b]	0.024
1	Atmosphere air	67	133	1	60	38[a]	5.55
2	O_2	67	133	1	120	100[a], 84[b]	6.14
3	O_2	670	1333	0.1	180	23[a]	11.2

The PhotoVap has features that allow the reaction to proceed well and one possibility was that there

was good surface contact between oxygen and the reaction solution facilitating the oxygen to readily

dissolve into the solution. To further explore this, the reaction was investigated using different sized

flasks and thus investigating the effect of the available surface area and oxygen diffusion - **Table 3**.

Interestingly, by varying the flask size (0.5L, 2L, to 3 L) the yield of the reaction could be varied by ~

10 % suggesting that this change in oxygen diffusion surface area could be having a significant effect on the yield of the reaction.

Table 3: Photochemical amide bond forming reaction conducted in different size flasks on the PhotoVap.
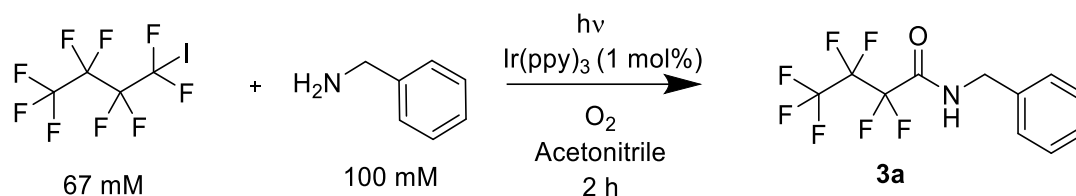
Irradiation Time (mins)	0.5 L Flask - GC Yield (%)	2 L flask - GC Yield (%)	3 L Flask- GC Yield (%)
30	18	20	21
60	29	29	32
90	32	37	42
120	40	45	48

This section of work explored the process intensification of the photocatalytic production of an amide. This was conducted through a series of small-scale batch reactions followed by testing in a number of different reactors. The reported amide bond forming reaction could be carried out on a ca. 500-fold scale through a combination of increasing the reagent concentration and use of a more efficient photochemical reactor, the PhotoVap.

Aim 2: Alternative photocatalyst

All of the work in the previous section was carried out using the iridium (Ir(ppy)$_3$) catalyst. However, it is expensive, and supplies are scarce. This raises the question of whether there might be a more sustainable, inexpensive, and possibly more efficient alternative. Therefore, to be able to examine potential alternative photocatalysts the reduction potential of perfluorobutyl iodide was determined (**Figure 17**) to be -1.23 V vs. SCE.
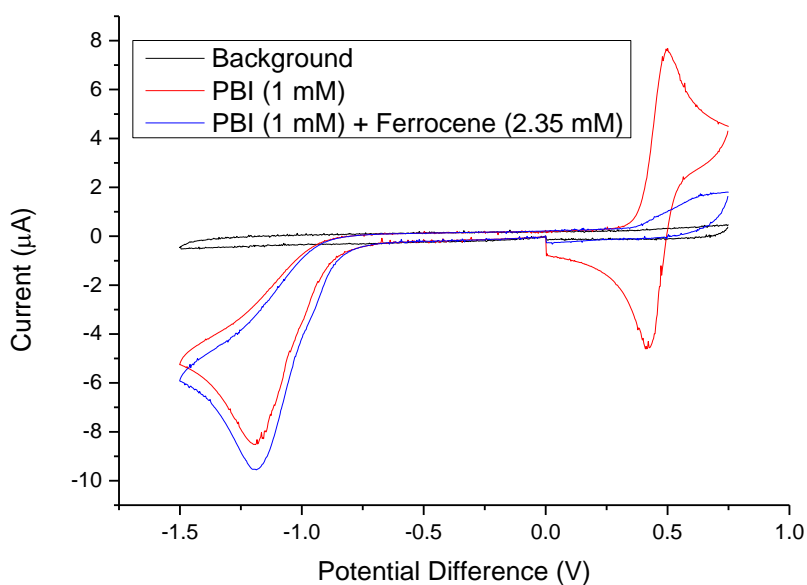
Figure 17: Cyclic voltammogram of (a) degassed background solvent, (b) perfluorobutyl iodide (PBI) and (c) perfluorobutyl iodide and ferrocene measured vs. Ag/AgCl reference electrode.

This could be compared with the oxidation potentials of a number of different photocatalysts (**Figure 18**) and Michler's Ketone (MK) was identified as a potential alternative photocatalyst. MK was acquired, the UV/vis spectrum of MK (**Appendix - Figure 23**) showed a strong, broad absorption band (λ_{max} = 352 nm). Initial reactions using MK and a medium pressure mercury arc lamp source (**Appendix - Table 11**) did not show any difference in results with and without MK. Experiments using the XeCl excimer lamp (308 nm) as an excitation source did show more promise (see **Table 4**).
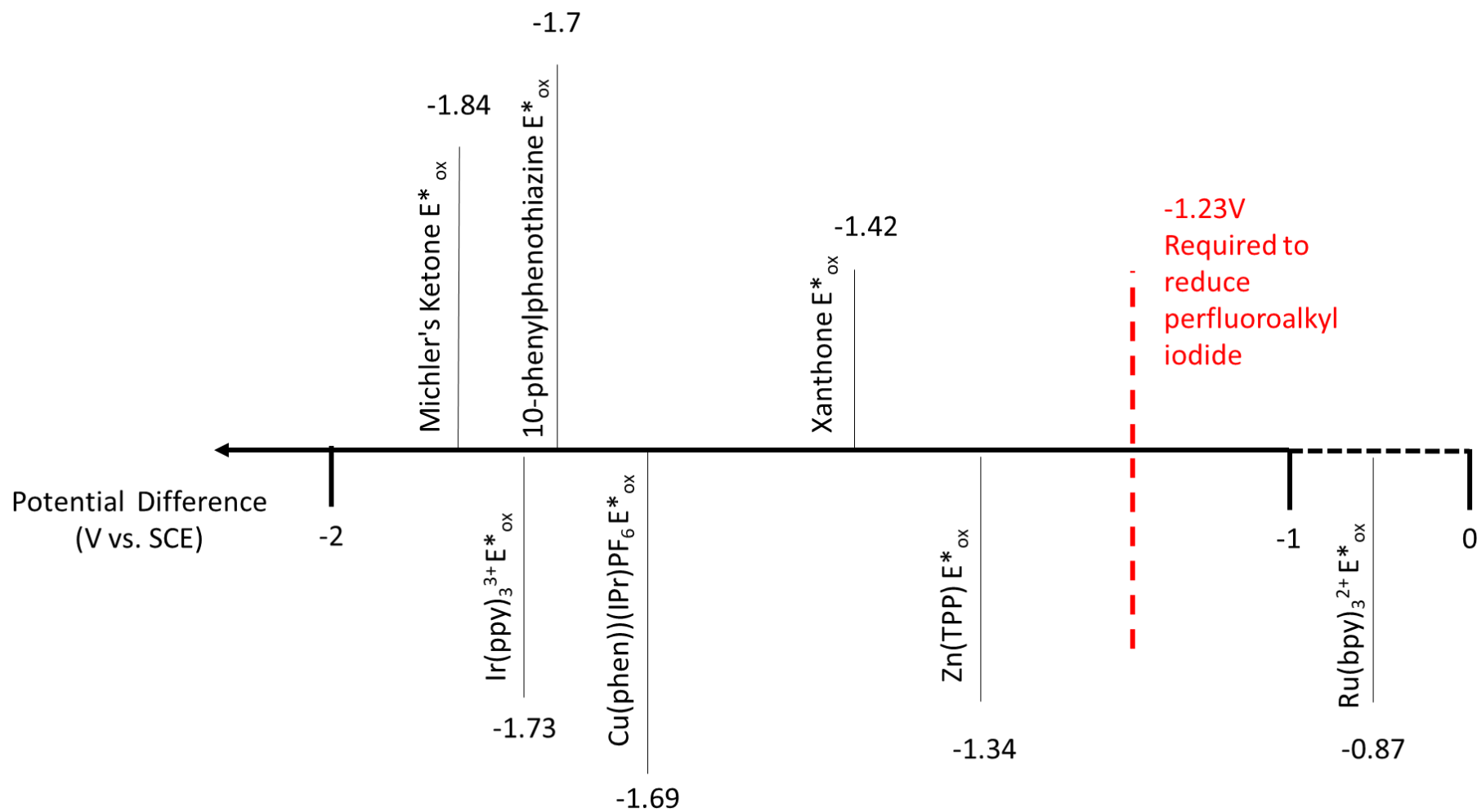
Figure 18: Excited state oxidation potentials of a number of common photocatalysts compared to the reduction potential required to initiate the photoamidation reported by Ng *et al*. Values from Ref [38-39]

Through the use of the XeCl excimer lamp various different conditions were investigated in an attempt to improve the yield of the desired amide. The highest yield (**Table 4 – entry 4**) only showed a modest yield of **3a** through the addition of MK and a small amount of water. The greatest amount of water (10 %) tested, resulted in the yield of **3a** decreasing and the production of the desired amide could not be increased simply by the addition of more water.

Table 4: Excimer lamp exeperiments using MK as a photocatalyst to carry out photochemcial amide bond forming reactions

Reaction number	MK loading (mol %)	Water loading (%)	GC Yield of 3a (%)
1	0	0	10
2	1	0	11
3	10	0	13
4	10	1	14
5	10	10	7
6	50	1	10

Overall, the conculsion from these experiements was that there was no obivously better alternative to the original Iridium-based catalyst. However, these experiments have not been wasted because the electrochemical measurements prompted the idea that the reaction could perhaps proceed electrochemically rather than photochemically without the need for any catalyst. As described in a later section of this chapter, that electrochemical approach has turned out to be really quite promising.

Aim 3: Combination of enzymatic and photochemical reaction

As stated above, there is significant interest in producing chirally pure amides, in this case via photochemistry. The aim here is not to induce the chirality using photochemistry but rather to produce a chiral amine using enzyme catalysis and then to convert that amine to the corresponding amide photochemically. Therefore, the initial step was to undertake a control reaction by conducting the photochemical reaction using a commercially sourced enantiomerically pure amine ((R)-(+)-α-Methylbenzylamine) to determine whether the chiral centre was retained throughout the reaction. The results of this experiment are shown in **Scheme 17.** The chirality of the product was confirmed by chiral HPLC (**See Appendix - Figure 24**) showing that the enantiomeric purity of the amine starting material had been fully retained in the amide product.
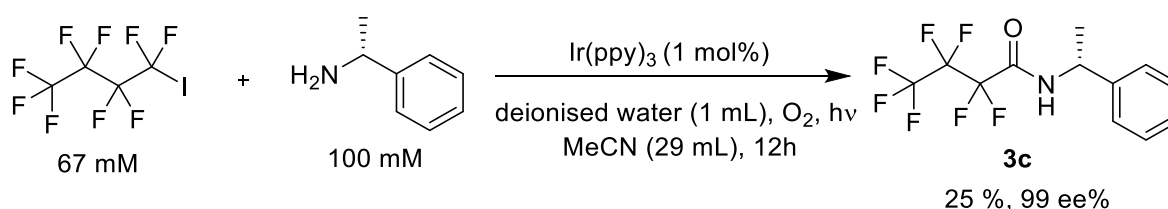
Scheme 17: Use of a commercially sourced enantiomerically pure amine to make a chiral amide.

Once this had been established, the enzymatic production of the enantiomerically pure amine was investigated - **Table 5**. Typically, this type of enzymatic reaction is carried out in purely aqueous media.[37] In this case, however, the ultimate aim was to combine the enzymatic and photochemical reactions into a single integrated process and the photochemistry could not be carried out in pure water. Therefore, a series of aqueous solvent mixtures were investigated for their compatibility with both the enzymatic and photochemical reactions. The aim was to establish whether there was a mixture of enzymatic reaction medium (aqueous buffer) and the photochemical reaction solvent (acetonitrile) which would work for both reactions. If this strategy was not successful, the fallback position would be to use a solvent change between the two reactions. This could still work in a

telescoped reaction sequence, provided that the two solvents were immiscible, because immiscible

solvents can be continuously separated, for example by a Zaiput membrane separator.[41]

Table 5: Conversion of acetophenone to (S)-1-phenylethan-1-amine using transaminase enzyme (ATA 256) across a range of aqueous/organic phase mixtures (1 mL), when left for 24 hours.
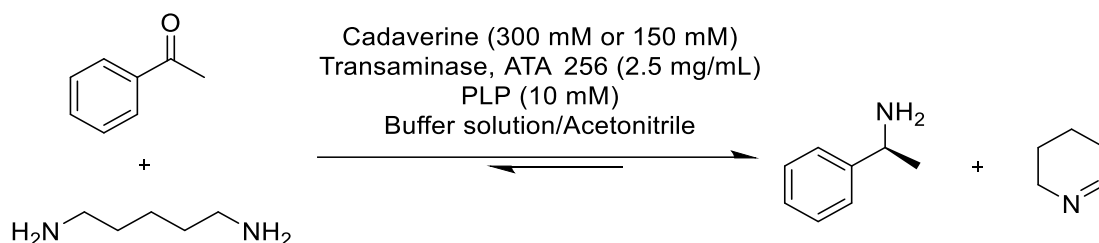
Acetonitrile (%)	Phosphate buffer (%)	Acetophenone concentration (mM)	GC Conversion (%) (99 %ee)
50	50	100	18
20	80	100	17
10	90	100	12
5	95	100	0
50	50	50	34
20	80	50	29
10	90	50	28
5	95	50	1

The starting point was to investigate the effect on the yield of chiral amine by adding various

quantities of acetonitrile to the phosphate buffer used for the enzymatic reaction. As can be seen

from **Table 5**, the highest amine yield (34 %) was obtained with the 50:50 aqueous/organic mixture.

These reactions were carried out on a 1 mL scale. When, however, these conditions were scaled up

to 5 mL volume, no conversion of the starting material was observed. This was believed to be a

response to the large amount of acetonitrile in the reaction mixture denaturing the enzyme thereby

preventing the reaction progressing. Therefore, the percentage of acetonitrile was reduced to 10 %

with the result that the reaction proceeded with a conversion of the ketone to amine of 13 % after

24 hours. Since this conversion was still rather low, the pH of the solution was measured once all

the reagents had been added and was found to be 8.5, probably because of the high levels of

cadaverine used as the amine donor in this reaction. By contrast, the optimum pH for the

transaminase enzyme to work is known to be much higher, between 10-11. Therefore, when the pH

was adjusted to 11 following the addition of all the constituents, there was a significant increase in

the conversion to 97 %. This product solution mixture was then used without any purification to

carry out the photochemical step of the reaction. Disappointingly, this first attempt at telescoping

the enzymatic and photochemical reaction did not yield any of the desired amide product, **3d**.

In an attempt to improve the photochemical step of the process, the buffer used in the enzymatic

reaction was exchanged (Phosphate replaced with Tris) and the reaction repeated. When this

aqueous/organic solution was combined with the photochemical step the amide **3d** was produced in

low yield (15 %). The production of **3d** via this telescoped method was quite a positive step.

However, the low yield meant that it was not a very productive method for producing amides -

Scheme 18. The reason for the low yields may have been that the additional water in the telescoped

mixture was hindering the photochemical process, similar to the results previously shown in the

alternative photocatalyst study (**Table 4**).

i) Tris buffer/MeCN (9:1)
ATA 256 (2.5 mg/mL),
300 mM cadaverine,
10 mM PLP, 24 h

ii) PBI, Ir(ppy)$_3$ (1 mol%)
O$_2$, hν, MeCN, 12 hr

100 mM

3d   15 %
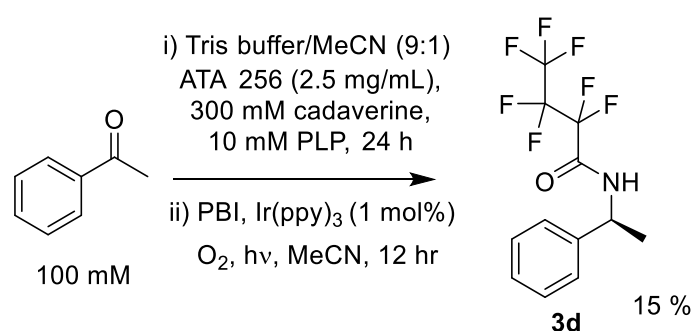
Scheme 18: Use of transaminase enzymes to synthesis chiral amines and used directly to produce the desired amide with structures.

To increase the overall yield of the reaction, it was decided to revert to the strategy of solvent exchange. Therefore, the chiral amine was extracted from the organic/aqueous mixture using ethyl acetate before the amine was used in the photochemical step. This was successful - **Scheme 19**. Even without optimisation, a reasonable yield (39 %) of the desired amide **3d** was obtained.

3d, X = H 39 %,
3e, X = F 43 %,
 X = OMe 0 %
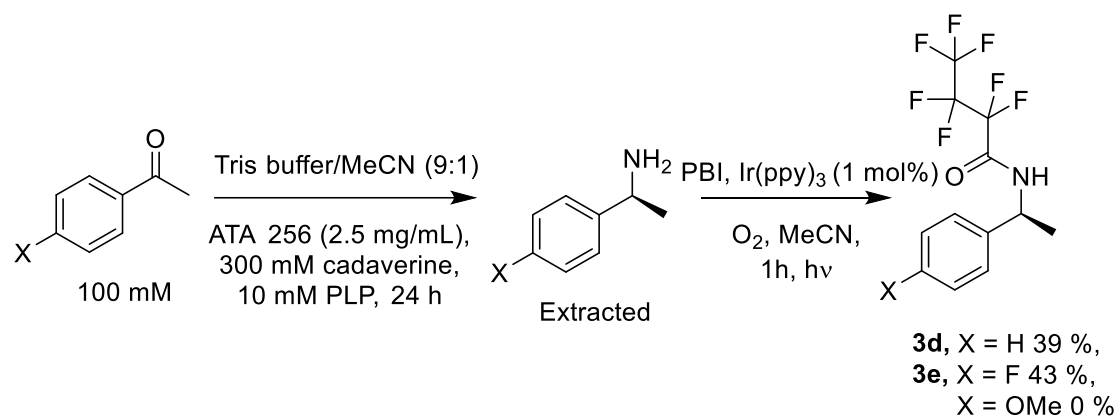
Scheme 19: Use of transaminase enzymes to synthesis chiral amines, the product amine was then extracted and used directly to photochemically produce the desired amide.

Since the solvent exchange appeared to be an effective approach, it was repeated for a number of different amides to establish the scope of this method with chirality established using X-ray crystallography (**Figure 19**). Under the same reaction conditions the *para*-fluoro amide, **3e**, was produced in a yield (43 %) similar to **3d** whilst the *para*-methoxy amide, was not produced at all. The lack of yield could be attributed to the low conversion of the starting ketone (10 %) by the enzyme rather than any failure of the photochemistry.
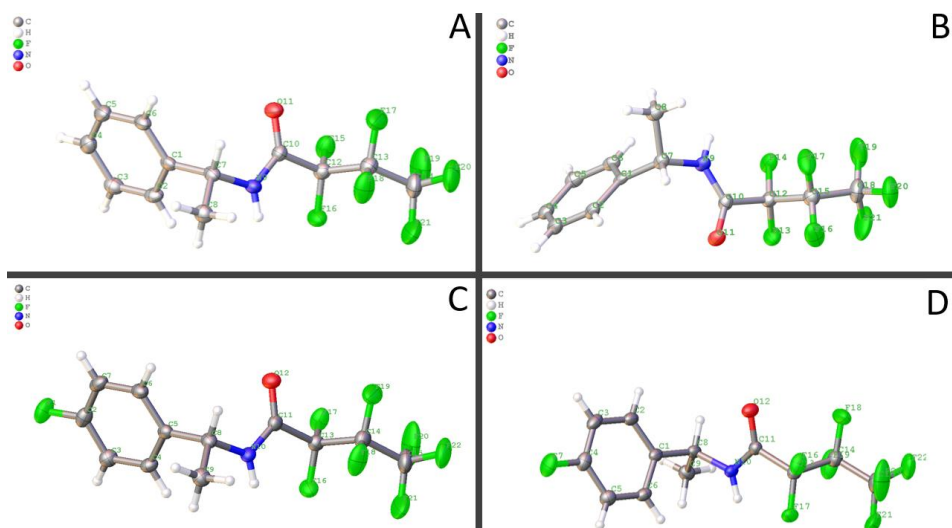
Figure 19: Crystal structures obtained of various amides produced through this project. A = 3a produced photochemically from a commercially sourced enantiomerically pure amine, B = 3c produced photochemically from an enzymatically produced enantiomerically pure amine (extraction), C = 3f produced thermally from a commercially sourced enantiomerically pure amine, D = 3d produced photochemically from an enzymatically produced enantiomerically pure amine (extraction).

Through this reported work it has been shown that chiral amides can be produced photochemically when enantiomerically pure amines are used. This concept was further explored by producing chiral amines via an enzymatic reaction which was then coupled with the photochemical reaction to make a number of chiral amides. Initially, this was conducted in a single solvent media however greater yields were achieved through the extraction of the enantiomerically pure amine and its subsequent use in a photochemical reaction.

Future experiments could be conducted to expand the substrate scope of this work and to improve the unification between enzymatic and photochemical processes into a single process.

Aim 4: Exploration of electrochemical route

The next section describes investigation in to whether the amide formation reaction can be achieved in the absence of a transtion metal catalyst by driving the reaction using electrochemcistry. The initial experiment was to obtain the Cyclic Voltammogram (CV) of perfluorobutyl iodide in the presence and absence of an amine in degassed CH_3CN - **Figure 20**. Similar to the photochemical reactions described above, a chiral amine was used as this also allowed the investigation of whether this approach could be used to generate the chiral amides.
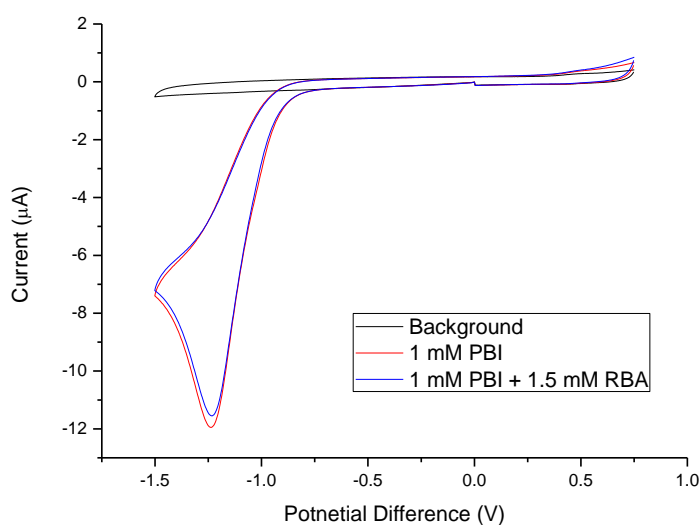
Figure 20: Cyclic voltammogram of a) degassed background solvent b) perfluorobutyl iodide c) perfluorobutyl iodide and (R) + 1-phenylethylamine measured vs. Ag/AgCl reference electrode.

It was observed that there was very little change in the current for the reduction of the perfluorobutyl iodide in the presence and absence of the amine and a further element was needed to allow the reaction to proceed. As the photochemical reaction had been shown to required oxygen to form the desired amide, the electrochemical experiment was repeated in the presence of oxygen (**Figure 21**). In this CV there was a new peak which can be assigned to oxygen reduction and this occurs at a lower potential difference than the perfluorobutyl iodide reduction and thus showing that oxygen will be preferentially reduced under these conditions. Closer examination of **Figure 21** shows that the oxygen oxidation peak was much smaller than the reduction peak (0.5 µA vs. -5 µA respectively) and this ca. 10-fold difference in current suggested that some of the reduced oxygen

had reacted. To explore this further, the solution was purged of oxygen and the CV repeated, the

current of the reduction peak of perfluorobutyl iodide decreased from -11 μA to -2 μA.
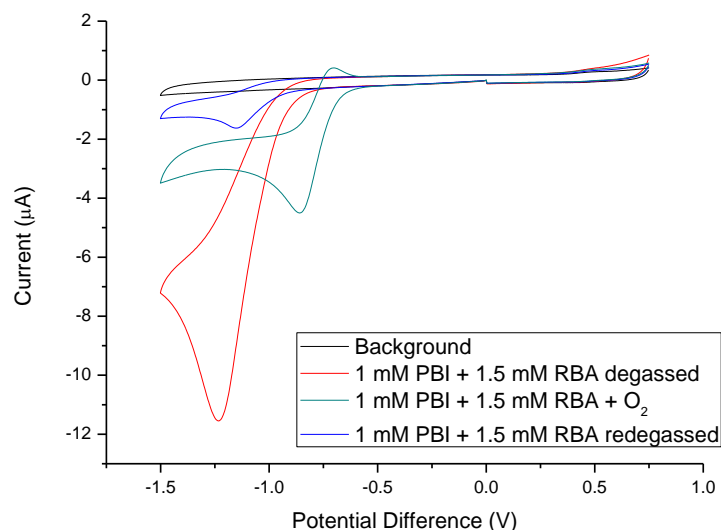

Figure 21: Cyclic voltammogram of a) degassed background solvent b) perfluorobutyl iodide and (*R*) + phenylethylamine degassed c) perfluorobutyl iodide and (*R*) + phenylethylamine gassed with oxygen d) perfluorobutyl iodide and (*R*) + phenylethylamine (purged of oxygen) vs. Ag/AgCl reference electrode.

These results suggested that the perfluorobutyl iodide may have reacted with the reduced oxygen to

form a new compound and this could potentially be the desired amide. Bulk electrolysis reaction was

conducted, and the major product was isolated - **Scheme 20**. This was identified by chiral HPLC

(**Appendix - Figure 25**) to be the desired amide and showed that the enantiomeric purity of the

amine had been retained during the formation of the amide bond.
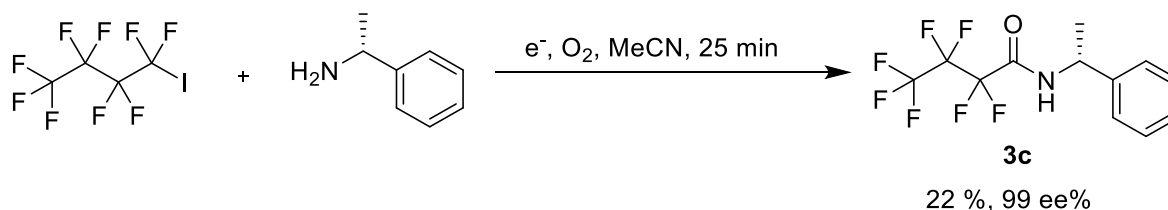
Scheme 20: Bulk electrolysis reaction using a commercially sourced chiral amine.

As the electrochemical method was able to produce the desired amide, the electrochemical and

photochemical methods could be compared. The literature, highest yield batch (from **Table 1**) and

PhotoVap (from **Table 2**) are compared to the electrochemical method in **Table 6**.

Table 6: Comparison table between different methods. [a]GC Yield, [b]Isolated Yield

Method	PBI concentration (mM)	Reaction time (mins)	Yield (%)	Productivity (g/day)
Literature value[18]	6.7	600	67[a], 62[b]	0.024
Photochemical – batch reactions	67	720	93[a]	0.9
Photochemical - PhotoVap	670	180	23[a]	11.2
Electrochemical	20	25	22[b]	1.58

From this comparison it is possible to see that the electrochemical method has a high productivity, greater than the photochemical batch method. This is due to the very short reaction time required. Further experiments are required to fully optimise and expand the applicability of the two methods.

Summary of results

This work has explored the aims discussed earlier. Some of these aims have resulted in the desired outcome, while others have produced unexpected results which require further exploration to fully answer the aim.

1. The initial objective was to investigate intensification of the amide bond forming reaction because the published work had very low productivity. This objective has been successfully achieved with a substantial increase in productivity. **Table 1** shows the results of the increase in the concentration of the chosen amide bond reaction where the productivity was increased by *ca.* 40 times. This was completed in a number of small-scale batch reactions and compared to the results reported in the literature.[18] Following this, the same concentration was applied in a number of different reactors to see whether through the change in reactor the reaction time could be decreased. The system with the most applicability for the amide bond forming reaction was shown to be the PhotoVap (**Table 2**). In the PhotoVap the reaction scale intensity of **3a** was increased by a factor of ca. 500. An interesting side note was that through the use of a larger flask (0.5 L vs 3 L, **Table 3**) the reaction yield could be varied by ~10 %.

2. The target of this part was to establish whether an alternative photocatalyst could be used to produce a more effective process based on photocatalytic amide bond formation. The answer was somewhat disappointing as within the range of photocatalysts studied, the process probably cannot be significantly improved. The reduction potential of perfluorobutyl iodide was measured (-1.23 V vs. SCE - **Figure 17Error! Reference source not found.**) and this value was used to identify[38,39] a possible alternative photosensitiser -Michler's Ketone (MK). The amide bond forming reaction was conducted with/without MK to determine whether MK catalysed the reaction. A subtle increase in yield was observed when using the excimer lamp with 10 mol % MK and 1% water (**Table 4**). This showed that the MK may have some ability to catalyse the amide bond forming reaction, but more work is required to find the optimal conditions for this catalyst.

3. The third objective was to combine enzymatic catalysis with photocatalytic amide formation in a two-stage process. This objective was fully achieved laying the foundations to carrying out both steps as flow processes. Initially, a commercially sourced enantiomerically pure amine was used to conduct the photochemical reaction to demonstrate that the chiral purity was retained in **3c** - **Scheme 17**. Following this, an enzymatic reaction to produce an enantiomerically pure amine was conducted and this optically active product was then used to make an enantiomerically pure amide via a photochemical reaction using the same solvent (aqueous buffer/acetonitrile) for both steps, resulting in a modest yield (15 %) of **3d** - **Scheme 18**. In an attempt to improve the yield of the amide, I used my fall-back plan to extract the amine and then to change the solvent prior to the photochemical step. This strategy resulted in higher yields of two different enantiomerically pure amides **3d** and **3e** - **Scheme 19**.

4. The final aim was to investigate if the transition metal photocatalysts could be eliminated by using an alternative electrochemical approach. This proved to be very promising. The first step was to conduct cyclic voltammetry (CV) of perfluoro butyl iodide (PBI) with/without a

chiral amine (**Figure 20**). The process was repeated in the presence of O_2 (**Figure 21**). These experiments suggested that a reaction of the chiral amine with perfluorobutyl iodide might be taking place in the presence of O_2. To investigate this further, a bulk electrolysis reaction was conducted under the same conditions and **3c** was isolated from the reaction mixture. The chiral purity of the amine was retained in the amide and the reaction time was reduced compared with the photochemical process.

Conclusions

This work has addressed some of the issues facing the larger scale use of amide bond forming reactions. In particular, the work has demonstrated increasing the scale of a photocatalytic method, improving the substrate scope, and reducing the reliance on transitions metal as catalysis. This has been achieved through the use of the novel PhotoVap reactor, application of biocatalysis and the use of electrosynthesis. Whilst the level of success has varied, the most promising results come from the combination of enzymatic and photochemical methodologies to produce chiral amides, because such products have many potential applications in the chemical industry.

Future work

The enzyme/photochemistry methodology needs to be developed further. Both enzymatic and photochemical reactions are frequently carried out as flow processes. Therefore, it should be possible to develop a single integrated flow enzymatic reaction feeding directly into a photochemical flow reactor to give a process for the continuous production of chiral amides.

The other topic which should be explored further is the electrochemical method. It would be interesting to explore the development of a flow electrochemical divided cell, which could be used to produce chiral amides. It would also be interesting to test whether the electrochemical method could be coupled with the enzymatic system as this could potentially be a rapid method of producing chiral amides from achiral starting materials.

Bibliography

1. Jarvis, L. M. The new drugs of 2019. *C&EN Glob. Enterp.* **98**, 30–36 (2019).

2. Constable, D. J. C. *et al.* Key green chemistry research areas—a perspective from pharmaceutical manufacturers. *Green Chem.* **9**, 411–42 (2007).

3. Bryan, M. C. *et al.* Key Green Chemistry research areas from a pharmaceutical manufacturers' perspective revisited. *Green Chem.* **20**, 5082–5103 (2018).

4. Valeur, E. & Bradley, M. Amide bond formation: Beyond the myth of coupling reagents. *Chem. Soc. Rev.* **38**, 606–631 (2009).

5. De Figueiredo, R. M., Suppo, J. S. & Campagne, J. M. Nonclassical Routes for Amide Bond Formation. *Chem. Rev.* **116**, 12029–12122 (2016).

6. Pattabiraman, V. R. & Bode, J. W. Rethinking amide bond synthesis. *Nature* **480**, 471–479 (2011).

7. Rueping, M. *et al.* Dual catalysis: Combination of photocatalytic aerobic oxidation and metal catalyzed alkynylation reactions-C-C bond formation using visible light. *Chem. Eur. J.* **18**, 5170–5174 (2012).

8. Dinda, M., Bose, C., Ghosh, T. & Maity, S. Cross dehydrogenative coupling (CDC) of aldehydes with N-hydroxyimides by visible light photoredox catalysis. *RSC Adv.* **5**, 44928–44932 (2015).

9. Brachet, E., Ghosh, T., Ghosh, I. & König, B. Visible light C-H amidation of heteroarenes with benzoyl azides. *Chem. Sci.* **6**, 987–992 (2015).

10. Marzo, L., Pagire, S. K., Reiser, O. & König, B. Visible-Light Photocatalysis: Does It Make a Difference in Organic Synthesis? *Angew. Chemie Int. Ed.* **57**, 10034–10072 (2018).

11. Liu, J. *et al.* Visible-light-mediated decarboxylation/oxidative amidation of α-keto acids with amines under mild reaction conditions using O2. *Angew. Chemie Int. Ed.* **53**, 502–506 (2014).

12. Pandey, G., Koley, S., Talukdar, R. & Sahani, P. K. Cross-Dehydrogenating Coupling of Aldehydes with Amines/R-OTBS Ethers by Visible-Light Photoredox Catalysis: Synthesis of Amides, Esters, and Ureas. *Org. Lett.* **20**, 5861–5865 (2018).

13. Bellotti, P. *et al.* Visible Light-Induced Regioselective Cycloaddition of Benzoyl Azides and Alkenes to Yield Oxazolines. *J. Org. Chem.* **84**, 6278–6285 (2019).

14. Papadopoulos, G. N. & Kokotos, C. G. One-Pot Amide Bond Formation from Aldehydes and Amines via a Photoorganocatalytic Activation of Aldehydes. *J. Org. Chem.* **81**, 7023–7028 (2016).

15. Iqbal, N. & Cho, E. J. Visible-Light-Mediated Synthesis of Amides from Aldehydes and Amines via in Situ Acid Chloride Formation. *J. Org. Chem.* **81**, 1905–1911 (2016).

16. Frump, J. A. Oxazolines. Their preparation, reactions, and applications. *Chem. Rev.* **71**, 483–505 (1971).

17. David R. Lide. Abundance of Element's in the Earth crust and in the sea. in *CRC Handbook of Physics and Chemistry* (ed. 84th) 14–17 (2003).

18. Ng, C. O. *et al.* Photoredox Catalysis of Cyclometalated IrIII Complex for the Conversion of Amines to Fluorinated Alkyl Amides. *Asian J. Org. Chem.* **7**, 1587–1590 (2018).

19. Purser, S., Moore, P. R., Swallow, S. & Gouverneur, V. Fluorine in medicinal chemistry. *Chem. Soc. Rev.* **37**, 320–330 (2008).

20. Rau, H. Asymmetric Photochemistry in Solution. *Chem. Rev.* **83**, 535–547 (1983).

21. Griesbeck, A. G. & Meierhenrich, U. J. Asymmetric photochemistry and photochirogenesis. *Angew. Chemie Int. Ed.* **41**, 3147–3154 (2002).

22. Brimioulle, R., Lenhart, D., Maturi, M. M. & Bach, T. Enantioselective catalysis of photochemical reactions. *Angew. Chemie Int. Ed.* **54**, 3872–3890 (2015).

23. Richardson, R. D. *et al.* Dual wavelength asymmetric photochemical synthesis with circularly polarized light. *Chem. Sci.* **6**, 3853–3862 (2015).

24. Schmermund, L. *et al.* Photo-Biocatalysis: Biotransformations in the Presence of Light. *ACS Catal.* **9**, 4115–4144 (2019).

25. Turner, N. J. & O'reilly, E. Biocatalytic retrosynthesis. *Nat. Chem. Biol.* **9**, 285–288 (2013).

26. de Souza, R. O. M. A., Miranda, L. S. M. & Bornscheuer, U. T. A Retrosynthesis Approach for Biocatalysis in Organic Synthesis. *Chem. Eur. J.* **23**, 12040–12063 (2017).

27. Wells, A. & Meyer, H. P. Biocatalysis as a strategic green technology for the chemical industry. *ChemCatChem* **6**, 918–920 (2014).

28. Hönig, M., Sondermann, P., Turner, N. J. & Carreira, E. M. Enantioselective Chemo- and Biocatalysis: Partners in Retrosynthesis. *Angew. Chemie Int. Ed.* **56**, 8942–8973 (2017).

29. Green, A. P. & Turner, N. J. Biocatalytic retrosynthesis: Redesigning synthetic routes to high-value chemicals. *Perspect. Sci.* **9**, 42–48 (2016).

30. Patil, M. D., Grogan, G., Bommarius, A. & Yun, H. Recent advances in ω-transaminase-mediated biocatalysis for the enantioselective synthesis of chiral amines. *Catalysts* **8**, (2018).

31. Guo, F. & Berglund, P. Transaminase biocatalysis: Optimization and application. *Green Chem.* **19**, 333–360 (2017).

32. Slabu, I., Galman, J. L., Lloyd, R. C. & Turner, N. J. Discovery, Engineering, and Synthetic Application of Transaminase Biocatalysts. *ACS Catal.* **7**, 8263–8284 (2017).

33. Kelly, S. A. *et al.* Application of ω-Transaminases in the Pharmaceutical Industry. *Chem. Rev.* **118**, 349–367 (2018).

34. Savile, C. K. *et al.* Biocatalytic Asymmetric Synthesis of Sitagliptin Manufacture. *Science (80).* **329**, 305–310 (2010).

35. Gomm, A. & O'Reilly, E. Transaminases for chiral amine synthesis. *Curr. Opin. Chem. Biol.* **43**, 106–112 (2018).

36. Fuchs, M., Farnberger, J. E. & Kroutil, W. The Industrial Age of Biocatalytic Transamination. *European J. Org. Chem.* **2015**, 6965–6982 (2015).

37. Ryan, J. *et al.* Transaminase Triggered Aza-Michael Approach for the Enantioselective Synthesis of Piperidine Scaffolds. *J. Am. Chem. Soc.* **138**, 15798–15800 (2016).

38. Teegardin, K., Day, J. I., Chan, J. & Weaver, J. Advances in Photocatalysis: A Microreview of Visible Light Mediated Ruthenium and Iridium Catalyzed Organic Transformations. *Org. Process Res. Dev.* **20**, 1156–1163 (2016).

39. Romero, N. A. & Nicewicz, D. A. Organic Photoredox Catalysis. *Chem. Rev.* **116**, 10075–10166

(2016).

40. Klopotek, D. L., Hobrock, B. G., Kovacic, P. & Jones, M. B. Reactions of Primary and Secondary Amines with Fluoronitrene Generated from Isopropyl N,N-Difluorocarbamate. *J. Org. Chem.* **45**, 1665–1667 (1980).

41. Mata, A. *et al.* Acyl azide generation and amide bond formation in continuous-flow for the synthesis of peptides. *React. Chem. Eng.* **5**, 645–650 (2020).

42. Clark, C. A., Lee, D. S., Pickering, S. J., Poliakoff, M. & George, M. W. A Simple and Versatile Reactor for Photochemistry. *Org. Process Res. Dev.* **20**, 1792–1798 (2016).

43. Wzorek, A., Kamizela, A., Sato, A. & Soloshonok, V. A. Self-Disproportionation of Enantiomers (SDE) via achiral gravity-driven column chromatography of N-fluoroacyl-1-phenylethylamines. *J. Fluor. Chem.* **196**, 37–43 (2017).

44. Stanko, O. V. *et al.* Diastereoselective synthesis of polyfluoroalkylated α-aminophosphonic acid derivatives. *J. Fluor. Chem.* **216**, 47–56 (2018).

Experimental

Experiment section content

Chemicals and equipment

All chemicals were purchased from commercial sources and used without further purification unless otherwise stated. Crystallography data was collected by Dr S. Argent at the University of Nottingham, School of Chemistry Crystallography Service. The GC-FID used for reaction monitoring

used was a Shimadzu GC-2010 fitted with a Supleco SPB70, 30 m length, 0.25 mm diameter, 0.25 μm particle size max temperature = 350 °C, GC column. The GC program used was started at 50 °C which was increased to 300 °C over 10 mins and kept this temperature for a 5 mins. The reaction media samples (1 mL) were filtered under gravity through a cotton wool plug which was placed in to the top of glass pipette. The samples were injected into the GC instrument using an autosampler. The carrier gas: Helium at a flow rate of 40 ml/min H$_2$ flow = 40ml/min, Air flow = 400 ml/min. The chiral GC-FID analysis was performed on Agilent 6850 equipped with a CP CHIRASIL-DEX CB (25 m × 0.25 mm). Helium carrier gas at a flow rate of 1 mL/min. NMR data was collected on a 400 MHz Bruker spectrometer and NMR data was processed using MestraNova software and the values are reported in ppm.

Small scale batch reactions

Literature repeat

To a round bottom flask (25 mL) a solution of acetonitrile (8 mL), perfluorobutyl iodide (9 μL, 18 mg, d = 2.01 g/mL, 0.05 mmol), benzyl amine (9 μL, 9 mg, d = 0.981 g/mL, 0.08 mmol) and Ir(ppy)$_3$ (0.5 mg, , 0.0007 mmol, 1 mol %) was added. This solution was purged with oxygen 5 mins and then left under an oxygen atmosphere through the use of a balloon. This was irradiated for 7 hours with white LEDs (fan cooled, 5 x 1000 lumen, 5 cm between LEDs and vessel). The solution was continually stirred over the course of the reaction. In the first 5 mins of the reaction a yellow precipitate (benzyl ammonium fluoride) was observed in the reaction solution.

Samples were collected every hour, filtered through cotton wool, and submitted for GC analysis (maximum GC yield was 70 % after 7 hours). Additionally, the crude reaction mixture was washed with perfluorinated solvent (HFE-7500, 20 mL x 3), as the produce was found to be soluble in this solvent. The fluorinated washings were collected and dried under *vacuo*. This resulted in an off-white solid of *N*-benzyl-2,2,3,3,4,4,4-heptafluorobutanamide (**3a**) (7.1 mg, 47 %).
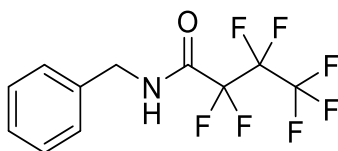
¹H NMR (400 MHz, Chloroform-*d*) δ 7.40 – 7.24 (m, 5H, 1-5), 7.08 – 7.00 (br, 1H, 8), 4.52 (d, *J* = 5.9

Hz, 2H, 7). **¹³C** (101 MHz, Chloroform-*d*) δ 157.7 (t, *J* = 26.0 Hz, 9), 136.0 (6), 129.1 (2/4), 128.3 (3),

127.9 (1/5), 117.5 (qt, *J* = 287.8, 33.6 Hz, 12), 108.5 (m, 10/11), 44.1 (7). **¹⁹F NMR** (376 MHz,

Chloroform-*d*) δ -80.58 (t, *J* = 8.8 Hz, 3F, 12), -120.62 (q, *J* = 8.8 Hz, 2F, 10), -126.86 (2F, 11). **HRMS**:

Mass calculated $[C_{11}H_7F_7NO]^-$ = 302.0415, mass found 302.0410.

The data matched with the data reported by Ng *et al.*[18] However, the interpretation of the data is

different to that in the literature for the ¹³C NMR. This difference of interpretation is based on the

large coupling constant (288 Hz) observed. This is likely to be caused by the three (quartet) fluorine

atoms bonded directly to the carbon (^1J coupling*). This signal is then split by into triplets via a

smaller coupling constant (34 Hz). Within the **3a** only the carbon in the terminal position of the

fluorinated chain could have this signal. Therefore, the other signals in the multiplet are likely to be

the other two carbons.

Figure 22: ¹³C NMR spectrum of 3a
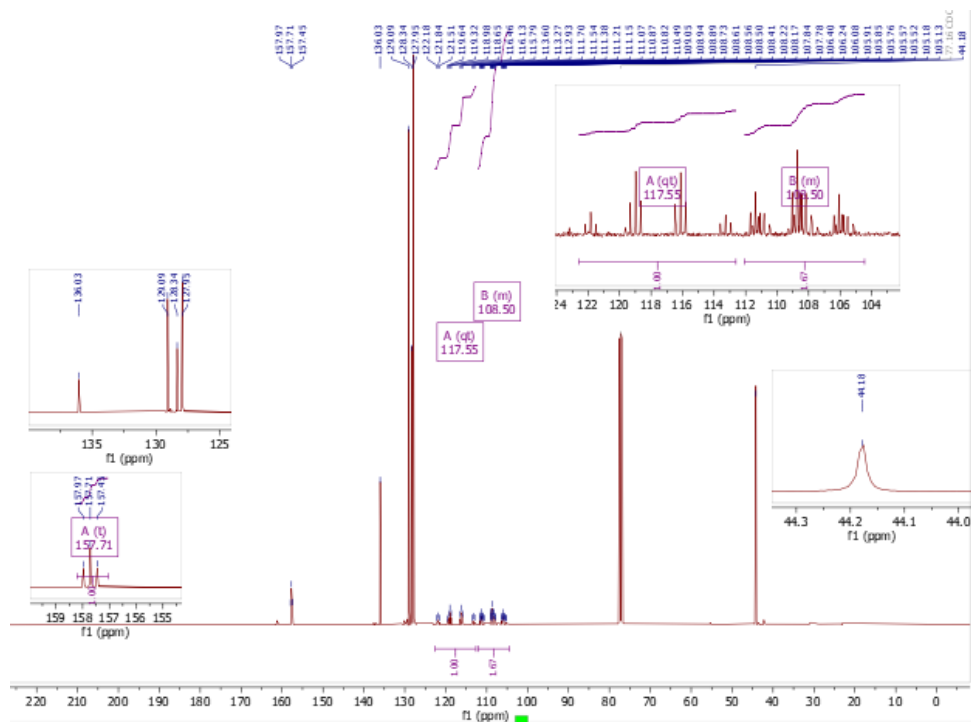
Oxygen atmosphere

To a two-necked round bottom flask (100 mL) a solution of acetonitrile (30 mL), perfluorobutyl iodide (350 µL, 0.704 g, d = 2.01 g/mL, 2 mmol), benzyl amine (450 µL, 0.441 g, d = 0.981 g/mL, 4 mmol) and Ir(ppy)$_3$ (13.5 mg, 0.02 mmol, 1 mol %) was added. This solution was purged with oxygen for 5 mins and then left under an oxygen atmosphere. This was irradiated for 12 hours with white LEDs (fan cooled, 5 x 1000 lumen). The solution was continually stirred over the course of the reaction. In the first 5 mins of the reaction, a yellow precipitate (benzyl ammonium fluoride – **3b**) was observed in the reaction solution.
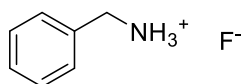
^{1}**H NMR** (400 MHz, D$_2$O) δ 7.49 (m, 5H), 4.20 (s, 2H). ^{19}**F NMR** (376 MHz, D$_2$O) δ -122.21.

This data matched with the literature data reported by Klopotek et al.[40]

Following this, a sample was filtered through cotton wool and submitted for GC analysis to produce *N*-benzyl-2,2,3,3,4,4,4-heptafluorobutanamide.

Compressed air atmosphere

The previous procedure (in 4.2.2) was repeated however, this solution was purged with compressed air for 5 mins and then left under a compressed air atmosphere. Following this, a sample was filtered through cotton wool and submitted for GC analysis (yield = 57 % after 12 h). As before, the crude reaction mixture was washed with perfluorinated solvent and the fluorinated washings were dried under *vacuo* resulting in an off-white solid of *N*-benzyl-2,2,3,3,4,4,4-heptafluorobutanamide (273.4 mg, 45 %).

Atmospheric air atmosphere

The protocol in the previous section was repeated, but the solution was purged with atmospheric air 5 mins and then left under an atmospheric air atmosphere. Following this, a sample was filtered through cotton wool and submitted for GC analysis.

Oxygen atmosphere with additional water

Previous protocol was repeated with the addition of deionised water (1 mL) and the solution was purged with oxygen for 5 mins and then left under an oxygen atmosphere. No precipitate was observed in this reaction. Following this, a sample was then filtered through cotton wool and submitted for GC analysis.

Photochemical reaction conducted using the PhotoVap

Use of the PhotoVap is fully reported by Clark *et al.*[42] Briefly, a 1 L round bottom flask was charged with the reagents & then attached to an adapted rotary evaporator, which had a thermocouple and gas piping inserted through the system into the reaction solution. The round bottom flask was then spun at a set speed (150 rpm) to create a thin film. The solution was then irradiated with high powered white LEDs (Asynt, 360 W) with a distance of *ca.* 5 cm between the flask and the light source. The light source was cooled using ethylene glycol/water solution (50:50, Julabo).

3-hour irradiation – no additional oxygen

A solution of acetonitrile (29 mL), perfluorobutyl iodide (0.35 mL, 0.704 g, d = 2.01 g/mL, 2 mmol), benzyl amine (0.45 mL, 0.441 g, d = 0.981 g/mL, 4 mmol), Ir(ppy)$_3$ (13.9 mg, 0.02 mmol, 1 mol %) and deionised water (1 mL) were attached to the PhotoVap. The solution was irradiated for 3 hours under an air atmosphere. Every hour, samples were collected & then filtered through cotton wool, then submitted for GC analysis.

2-hour irradiation – additional oxygen

The previous method was repeated (4.3.1) however, oxygen was bubbled through the solution for 2 hours at a rate of 32 cm^3/min over the course of the reaction. Every 30 minutes samples were collected, filtered through cotton wool, and then submitted for GC analysis (GC yield = 100 % after 2 h). Following this, the crude solution was dried under *vacuo* and then purified by flash chromatography (pentane/dichloromethane, 1:1). This resulted in yellow solid (0.506 g, 84 %) of the desired product.

3-hour irradiation – additional oxygen – 10-fold increase in concentration

The protocol from section 4.3.1. was repeated however, the reagents concentrations were altered to be: perfluorobutyl iodide (3.43 mL, 6.89 g, d = 2.01 g/mL, 20 mmol, 667 mM), benzyl amine (4.3 mL, 4.21 g, d = 0.981 g/mL, 40 mmol) Ir(ppy)$_3$ (13.4 mg, 0.02 mmol, 0.1 mol %). As before oxygen was bubbled through the solution at the same rate as the previous method, over the course of the reaction (3 h).

Batch reactions conducted in various sized flasks.

A solution of perfluorobutyl iodide (0.35 mL, 2.01 mmol), benzylamine (0.32 mL, 3 mmol) and Ir(ppy)$_3$ (13.2 mg, 0.02 mmol, 1 mol %) in acetonitrile (30 mL) was placed into either a 0.5, 2 or 3 L round bottom flask. Oxygen was bubbled through the solution through the course of the reaction. Samples were taken every 30 mins for two hours, whilst the reaction solution was being irradiated. These samples were filtered through cotton wool and then analysed by GC.

This set of experiments was performed by C. Wilding, a Master's student in the Nottingham Group, under the supervision of the author.

Excimer lamp experiments

A solution of acetonitrile (90 mL), perfluorobutyl iodide (1 mL, 2.01 g, d = 2.01 g/mL, 6 mmol), benzyl amine (1 mL, 0.981g, d = 0.981 g/mL, 9 mmol). This solution was purged with oxygen for 5 mins then left under an oxygen atmosphere. This was irradiated for 3 hours with a XeCl excimer lamp (229 W, 308 nm). The solution was continually stirred over the course of the reaction. Following this samples were collected, filtered through cotton wool, and then submitted for GC analysis.

This was repeated with various levels of Michler's ketone (14.5 mg, 0.06 mmol, 1 mol %), (180 mg, 0.7 mmol, 10 mol %) or (0.8 g, 3 mmol, 50 mol %) and water (0.9 ml, 1 %) or (9 mL, 10 %).

Photochemical synthesis of chiral amide from a commercial sourced amine

To a round bottom flask (100 mL) a solution of acetonitrile (29 mL), perfluorobutyl iodide (350 µL, 0.704 g, d = 2.01 g/mL, 2 mmol), (*R*)-1-phenylethan-1-amine (400 µL, 0.376 g, d = 0.940 g/mL, 3 mmol) deionised water (1 mL) and Ir(ppy)$_3$ (13.9 mg, 0.02 mmol, 1 mol %) was added. This solution

was purged with oxygen for 5 mins and then left under an oxygen atmosphere. This was irradiated for 12 hours with white LEDs (fan cooled, 5 x 1000 lumen). The solution was continually stirred over the course of the reaction. No precipitate was observed in this reaction. Following the reaction, the crude mixture was concentrated under *vacuo* then purified by flash chromatography (dichloromethane/cyclohexane (1:1)). This gave an off-white solid (155.7 mg, 25 %, 99 % ee) of (*R*)-2,2,3,3,4,4,4-heptafluoro-*N*-(1-phenylethyl)butanamide (**3c**).
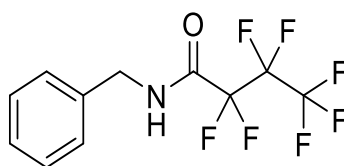
1H NMR (400 MHz, Chloroform-*d*) δ 7.51 – 7.16 (m, 5H, **1-5**), 6.81 (s, 1H, br, **8**) 5.17 (p, *J* = 7.1 Hz, 1H, **7**), 1.58 (d, *J* = 6.9 Hz, 3H, **13**). **13C NMR** (101 MHz, Chloroform-*d*) δ 156.8 (t, *J* = 26.0 Hz, **9**), 141.0 (**6**), 129.0 (**2/4**), 128.2 (**3**), 126.2 (**1/5**), 117.5 (qt, *J* =287.2, 33.4 Hz, **12**), 108.5 (m **10/11**), 50.1 (**7**), 20.9 (**13**). **19F NMR** (376 MHz, Chloroform-*d*) δ -80.74 (t, *J* = 8.7 Hz, 3F, **12**), -120.86 (q, *J* = 8.7 Hz, 2F, **10**), -127.05 (2F, **11**). **HMRS** $[C_{12}H_{10}F_7NONa]^+$ calculated = 340.0548, found = 340.0537.

This data matched with the data reported by Wzorek *et al.*[43] However, the interpretation varies for the same reasoning as with **3a**.

Crystal structure collected from this sample.
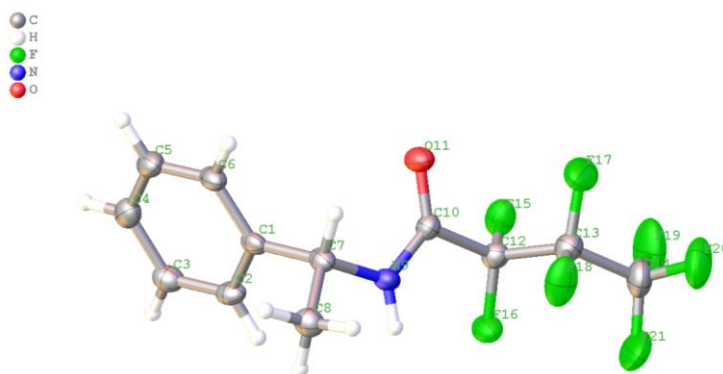
Enzymatic reaction

Scoping ratios of organic/aqueous solvent mixture for the enzymatic reaction

10 different conditions were initially tested. In each case the aqueous phase was potassium phosphate buffer (0.1 M, pH = 10.8) and the organic phase was acetonitrile. Initially, a stock acetophenone solution (232 µL, 2M) in acetonitrile (1 mL) was made. This solution (50 µl) was diluted in various quantities of acetonitrile (0, 50, 150 or 450 µl) to reach the desired concentration (100 mM). This was then mixed with phosphate buffer (750, 700, 600, or 300 µl) to reach the desired co-solvent percentage (5, 10, 20, 50 %). A second stock solution of cadaverine (0.5270 g, 3M) in potassium phosphate buffer (0.1 M, pH = 10.8, 1mL) was produced. This stock solution (100 µL) was added to each of the samples. A third stock solution of enzyme (50 mg, ATA 256) was dissolved into potassium phosphate buffer (0.1 M, pH = 10.8, 2 mL). To this stock Pyridoxal phosphate (PLP, 5.3 mg, 10 mM) was added. 100 µL of this solution was added to the reaction mixture. This process was repeated to reach a desired acetophenone concentration of 50 mM. In this system the same acetophenone stock solution was used however the stock solution (25 µL) was diluted with acetonitrile (25, 75, 175 or 475 µL) and the same quantities of buffer solution were added. The same enzyme solution was used in the same quantities however an alternative cadaverine solution was used in this case. A cadaverine stock (0.2691 g, 1.5 M) in phosphate buffer (0.1 M, pH = 10.8, 1 mL) was used instead. 100 µL was added in each case still. These solutions were left at 30 °C overnight stirring at 200 RPM. The next day the product was extracted from each mixture by adding ethyl acetate (400 µL) and sodium hydroxide (saturated, 10 µl) to each sample. These samples were mixed well, then centrifuged for 2.5 min at 15000 RPM. The organic layer was collected, then acetic anhydride (10 µL) and triethylamine (10 µL) was added. The resulting mixture was submitted to chiral GC analysis, which had been previous calibrated to determine conversion of acetophenone to (S)-1-phenylethan-1-amine.

Enzymatic reaction conducted in Phosphate buffer/acetonitrile (50:50, 5ml)

Acetophenone (232 µL, d =1.03 g/ml, 0.239 g, 2 mmol) dissolved in acetonitrile (768 µL) to make a stock solution. This stock solution (125 µL, 2.6 M) diluted to 100 mM by added to acetonitrile (2375 µL). This diluted acetophenone solution (2.5 mL, 100 mM, 0.25 mmol) was added to the phosphate buffer solution (1500 µL, 0.1 M, pH = 10.8). To this mixture cadaverine solution (133.2 mg in 500 µL phosphate buffer, 1.5 M) was added. Pyridoxal phosphate (6 mg) was then dissolved in phosphate buffer (2 mL, 0.1 M, pH = 10.9). This PLP solution (500 µL) was added to the enzyme (12.5 mg, ATA 256) and this solution was added to the phosphate/acetonitrile mixture. These solutions were left at 30 °C for 48 hours stirring at 200 RPM. Following this a sample (250 µL) of the product was extracted from each mixture and both ethyl acetate (400 µL) and sodium hydroxide (saturated, 10 µl) were added. These samples were mixed well, then centrifuged for 2.5 min at 15000 RPM. The organic layer was collected, then acetic anhydride (10 µL) and triethylamine (10 µL) were added. The resulting mixture was submitted to chiral GC analysis, which had been previous calibrated to determine conversion of acetophenone to (S)-1-phenylethan-1-amine.

Enzymatic reaction conducted in Phosphate buffer/acetonitrile (90:10, 5ml)

A stock solution of acetophenone (232 µL, 2M) dissolved in acetonitrile (768 µL) was produced. The stock solution (125 µL) was diluted to 100 mM by adding it to acetonitrile (375 µL) this was then added to phosphate buffer solution (3500 µL, 0.1 M, pH = 10.8).
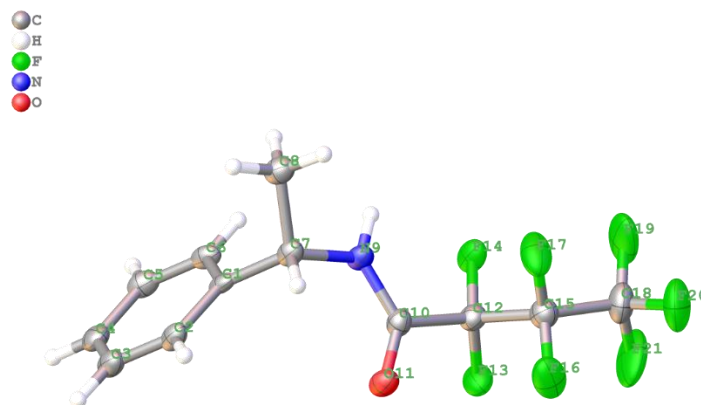
Following this point procedure was the same as the previous method.

Enzymatic reaction conducted in Phosphate buffer/acetonitrile (90:10, 5ml) with pH adjustment

In this example following the addition of cadaverine solution to the mixture, the reaction solution pH was adjusted to 10.9 from 8.6. This resulted in (S)-1-phenylethan-1-amine conversion being 97 % (99 %ee).

Photochemical amidiation reaction using an amine produced enzymatically

The product mixture ((S)-1-phenylethan-1-amine, 97 mM, in 4.5 ml phosphate buffer/0.5 ml acetonitrile) (described above) was put into a round bottom flask (100 mL) and acetonitrile (20 mL)

was added. This resulted in ((S)-1-phenylethan-1-amine, 20 mM, 0.5 mmol) dissolved in

acetonitrile/phosphate buffer (20.5 ml/ 4.5 mL (82:18)). To this mixture, Ir(ppy)$_3$ (1.4 mg, 0.002

mmol, 1 mol %) and perfluorobutyl iodide (30 µL, 60 mg, d = 2.01 g/mL, 0.2 mmol, 8 mM) was

added. This solution was purged with oxygen for 5 mins and then kept under an oxygen atmosphere.

The solution was irradiated for 12 hours. Following the reaction mixture was analysed by GC.

Repeat of the enzymatic reaction conducted in tris(hydroxymethyl)aminomethane (Tris) buffer/

acetonitrile (90:10)

The enzymatic reaction described above was repeated using Tris buffer instead of phosphate buffer.

The next day the product was extracted from each mixture, by adding ethyl acetate (5 mL) and

sodium hydroxide (saturated, 50 µl) to each sample. These samples were mixed well, then

centrifuged for 2.5 min at 15000 RPM.

The organic layer was collected dried under *vacuo* to give a colourless oil of (S)-1-phenylethan-1-

amine (58.1 mg, 96 % (99 %ee)).

The oil (58.1 mg, 0.5 mmol, 48 mM) was put into a round bottom flask (1 L) and acetonitrile (10 mL)

was added. Additionally, to this, Ir(ppy)$_3$ (1 mg, 0.002 mmol, 1 mol %) and perfluorobutyl iodide (36

µL, 72 mg, d = 2.01 g/mL, 0.2 mmol, 20 mM) were added. This solution was purged with oxygen for 5

mins and then kept under an oxygen atmosphere (60 cm^3/min). The solution was irradiated for 1

hour on the PhotoVap and rotated at 150 RPM. Following the reaction mixture was analysed by GC.

The product of this reaction was washed with HFE-7500 (5 mL) and the perfluoronated phase was

collected. This was dried under *vacuo* to give the desired (S)-2,2,3,3,4,4,4-heptafluoro-N-(1-

phenylethyl)butanamide (**3d**) (26 mg, 41 %).

Matched the NMR & HMRS data of the (R)-2,2,3,3,4,4,4-heptafluoro-N-(1-phenylethyl)butanamide.

Crystal structure collected from this sample.

Production of (*S*)-2,2,3,3,4,4,4-heptafluoro-*N*-(1-(4-fluorophenyl)ethyl)butanamide through the combination of enzymatic and photochemical processes

Process repeated with 4'fluoroacetophenone. The enzymatic reaction gave a colourless oil (*S*)-1-(4-fluorophenyl)ethylamine (67.4 mg, 97 % (99 %ee)) and gave the desired product following the photochemical reaction of (*S*)-2,2,3,3,4,4,4-heptafluoro-*N*-(1-(4-fluorophenyl)ethyl)butanamide (**3e**) (30 mg, 45%).
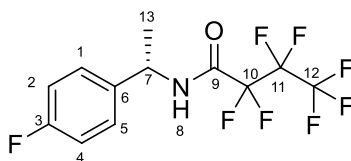
^{1}**H NMR** (400 MHz, Chloroform-*d*) δ 7.29 (m, 2H, **1/5**), 7.06 (m, 2H, **2/4**), 6.48 (s, 1H, br, **8**), 5.16 (p, *J* = 7.1 Hz, 1H, **7**), 1.58 (d, *J* = 6.9 Hz, 3H, **13**). ^{13}**C NMR** (101 MHz, Chloroform-*d*) δ 162.50 (d, *J* = 246.6 Hz, **3**), 156.89 (t, *J* = 26.0 Hz, **9**), 136.95 (d, *J* = 3.29 Hz, **6**), 127.98 (m, **1/5**) 118.96 (qt, *J* = 293.06, 33.5 Hz, **12**), 115.86 (m, **2,4**), 108.57 (m, **10/11**), 49.48 (**7**), 20.94 (**13**). ^{19}**F NMR** (376 MHz, Chloroform-d) δ -80.80 (t, *J* = 8.7 Hz, 3F, **12**), -114.20 (m, 1F, **3**), -120.92 (q, *J* = 8.7 Hz, 2F **10**), -127.10 (s, 2F, **11**).

Crystal structure collected from this sample.
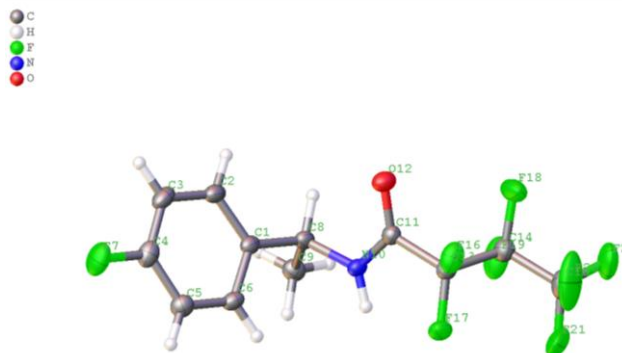
Enzymatic conversion of 4'methoxyacetophenone

Process repeated with 4'methoxyacetophenone however, only 10% conversion of the starting material was observed by GC 48 hours after starting the enzyme step of the chemistry.

Telescoped enzymatic and photochemical reactions

The enzymatic product solution (5 mL, 97 % conversion of acetophenone to (S)-1-phenylethan-1-amine) was added acetonitrile (20 mL) perfluorobutyl iodide (29 μL, d = 2.01 g/mL, 0.2 mmol) and Ir(ppy)$_3$ (1 mg, 0.002 mmol). This was purged with oxygen for 5 mins and then kept under an oxygen atmosphere. Subsequently, the solution was irradiated for 12 hours. Following this, the reaction mixture was analysed by GC and showed the desired product (12 %). Additionally, HFE-7500 (10 mL) was added to the crude mixture. The perfluorinated layer was collected and dried under *vacuo.* This gave the desired product of (S)-2,2,3,3,4,4,4-heptafluoro-*N*-(1-phenylethyl)butanamide (10 mg, 16%).

Cyclic Voltammogram experiments

A solution of acetonitrile (25 mL, dry) and tetrabuytlammonium tetrafluoroborate (3.2532 g, 10 mmol) was made and put into the electrochemical cell. This solution was purged of oxygen for 10 – 15 mins by flowing argon through the stirred solution. Using a glassy carbon working electrode, platinum wire counter electrode and silver/silver chloride reference electrode a background CV was taken. To this mixture perfluorobutyl iodide (2.5 μL (measured with a GC syringe), 5 mg, d = 2.01 g/mL, 0.015 mmol) was added and another CV collected. Next ferrocene (4.7 mg, 0.025 mmol) was added, and a final CV collected.

With a fresh solution of purged (argon ~10 mins) acetonitrile (25 mL, dry), perfluorobutyl iodide (2.5 µl, 5 mg, d = 2.01 g/mL, 0.015 mmol) and tetrabuytlammonium tetrafluoroborate (3.25 g, 10 mmol, 0.4 M), (R)-1-phenylethan-1-amine (3.6 µL, 3 mg, d = 0.940 g/mL, 0.03 mmol) was added. Following the collection of a CV, oxygen was bubble through the solution (~1 min) and another CV was collected. Finally, the oxygen was removed from the solution (argon purge ~ 10 mins) and a final CV collected.

Bulk electrolysis synthesis

A solution of acetonitrile (20 mL, dry) perfluorobutyl iodide (65 µL, 130 mg, d = 2.01 g/mL, 0.4 mmol), tetrabutylammonium tetrafluoroborate (3.25 g, 10 mmol) and (R)-1-phenylethan-1-amine (75 µL, 70 mg, d = 0.940 g/mL, 0.6 mmol) was made and oxygen bubbled (~2 min) through the solution. This solution was placed into a divided electrochemical cell (vitreous carbon working electrode, platinum gauze counter electrode with a glass frit and a saturated calomel electrode as reference electrode) and oxygen bubbled through the stirred solution. The experiment was conducted by passing current through the solution at a voltage of -1.5 V. The experiment was carried out for ~30 mins by which time ~65 Coulomb had passed through the solution.

Following this, the solution was dried under *vacuo* and purified by flash chromatography (dichloromethane/cyclohexane (1:1)). This resulted in the desired product of (R)-2,2,3,3,4,4,4-heptafluoro-N-(1-phenylethyl)butanamide (27.5 mg, 22 %, 99 % ee).

Thermally produced standards

2,2,3,3,4,4,4-heptafluoro-N-(1-phenylethyl)butanamide

The enantiomerically pure amides were synthesised via the method reported by Stanko *et al.*[44] Briefly, methyl heptafluorobutyrate (3.1 mL, d = 1.47 g/mL, 20 mmol) was dissolved in diethyl ether (10 mL). To (R)-1-phenylethan-1-amine (2.6 mL, d = 0.952 g/mL, 20 mmol) and a further diethyl ether (7 mL) was added. This was left stirring overnight at room temperature. The next day the solvent

was removed under *vacuo* to give a white solid. This white solid was recrystallized in chloroform

forming fine white needle like crystals (6.0263 g, 95 %).

This was repeated for (*S*)-1-phenylethan-1-amine, final yield (5.7187 g, 90 %).

These products were used as standards for chiral HPLC studies.

2,2,3,3,4,4,4-heptafluoro-N-(1-(4-fluorophenyl)ethyl)butanamide

The previous method was repeated; however, the quantities were changed slightly. Methyl

heptafluorobutyrate (2.3 g, 10 mmol) was dissolved in diethyl ether (10 mL). To this (*R*)-1-(4-

fluorophenyl)ethan-1-amine (1.2 g, 9 mmol) and a further diethyl ether (7 mL) was added. This white

solid was recrystallized in chloroform forming fine white needle like crystals of (*R*)-2,2,3,3,4,4,4-

heptafluoro-*N*-(1-(4-fluorophenyl)ethyl)butanamide (**3f**) (1.4641 g, 44 %).
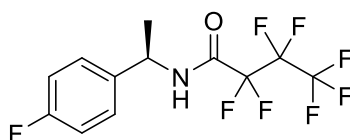
Matched the NMR data of the (*S*)-2,2,3,3,4,4,4-heptafluoro-*N*-(1-(4-fluorophenyl)ethyl)butanamide.

Crystal structure collected from this sample.
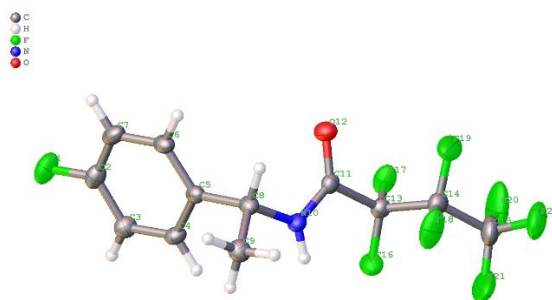
This was repeated for (*S*)-1-(4-fluorophenyl)ethan-1-amine, final yield (1.0575 g, 32 %).

Appendix

Table 7: Vortex reaction results. [a] GC Yield, [b] (R)-1-phenylethan-1-amine used, [c] benzyl amine

Reaction number	Reactor	Perfluorobutyl iodide (mM)	Benzyl amine (mM)	Cat loading (% mol)	Reaction time (min)	Yield of 3a (%)
Lit value	8 mL glass tube	6.7	10[c]	1	600	67[a], 62[b]
1	Vortex – Ambient Air (0.5 ml/min)	67	100[c]	0.01	30	0.7[a]
2	Vortex – Ambient Air (1 ml/min)	67	100[c]	0.01	15	0.6[a]
3	Vortex – Ambient Air (2 ml/min, 4000 RPM)	67	100[c]	0.01	7.5	0.5[a]
4	Vortex – Ambient Air (0.5 ml/min)	67	100[c]	0.1	30	1.7[a]
5	Vortex – Ambient Air (1 ml/min)	67	100[c]	0.1	15	1.4[a]
6	Vortex – Ambient Air (2 ml/min, 4000 RPM)	67	100[c]	0.1	7.5	1.1[a]
7	Vortex – Ambient Air (2 ml/min, 3000 RPM)	67	100[c]	0.1	7.5	1.0[a]
8	Vortex – Ambient Air (2 ml/min, 2000 RPM)	67	100[c]	0.1	7.5	0.8[a]
9	Vortex – Ambient Air (1 ml/min, 4000 RPM)	67	100[b]	0.1	15	3[a]
10	Vortex – Ambient Air (1 ml/min, 4000 RPM)	34	50[b]	0.1	15	4.3[a]
11	Vortex – Ambient Air (1 ml/min, 4000 RPM), no water	34	50[b]	0.1	15	3.2[a]
12	Vortex – Ambient Air (1 ml/min, 4000 RPM)	17	25[b]	0.1	15	6.5[a]
13	Vortex – Ambient air (0.1 ml/min)	67	100[c]	1	750	3.2[a]
14	Vortex – Ambient Air (0.5 ml/min)	67	100[c]	1	150	2.4[a]
15	Vortex – Ambient Air (1 ml/min)	67	100[c]	1	15	2.0[a]
16	Vortex – Ambient Air (2 ml/min)	67	100[c]	1	7.5	1.6[a]
17	Vortex - O_2 (10 sccm) (flow rate 0.1 ml/min)	67	100[c]	1	150	5.0[a]

Table 8: Yield of FEP flow reaction with and without additional glass beads irradiated with the "lightsabre", [a] Isolated Yield [b] GC Yield

Flow rate (mL min⁻¹)	Beaded reactor Yield of 3a (%)	Non-beaded reactor Yield of 3a (%)
2	1.4[a], 4.7[b]	4.03[b]
5	1.3[a], 4.5[b]	2.3[a], 2.4[b]
7	1.1[a], 4.2[b]	2.1[a], 2.6[b]

Table 9: Yield of FEP flow reaction with and without additional glass beads irradiated with a 125W medium pressure mercury arc lamp, [a] Isolated Yield [b] GC Yield. This set of experiments was performed by C. Wilding, a Master's student in the Nottingham Group, under the supervision of the author.

Flow rate (mL/min)	Beaded System Yield of 3a (%)	Non-beaded System Yield of 3a (%)
2	1.8[a], 1.2[b]	1.5[a], 3.25[b]
5	0.6[a], 0.3[b]	1.3[a], 1.9[b]
7	0.4[a], 0.3[b]	0.9[a], 1.6[b]

Table 10: Yield of photochemical amide bond forming reaction carried out in the flow excimer (XeCl, 308 nm) reactor.

Reaction number	Flow rate (ml/min)	GC Yield of 3a (%)
1	0.5	3
2	1	2

Table 11: Initial experiments using MK as a photocatalyst to carry out photochemcial amide bond formation

Reaction number	MK loading (%)	GC Yield (%)
1	0	5
2	1	5

Metric calculation

Atom efficiency
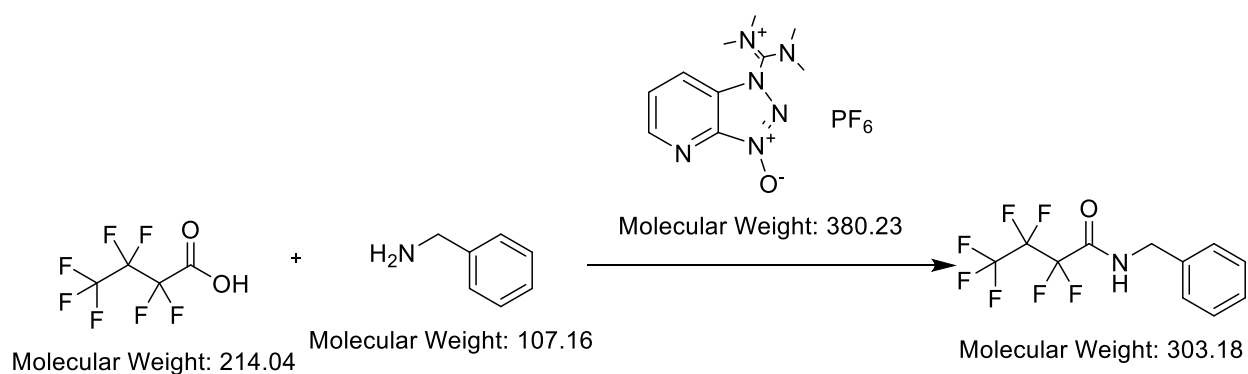
Scheme 21: HATU reaction used to calculated atom efficiency

$$Atom\ Efficeny\ (AE)\ \% = \frac{mol\ weight\ of\ product}{mol\ weight\ of\ reagents}\ x\ 100$$

$$Atom\ Efficeny\ (AE)\ \% = \frac{303}{107 + 214 + 380}\ x\ 100$$

$$Atom\ Efficeny\ (AE)\ \% = \frac{303}{701}\ x\ 100$$

$$Atom\ Efficeny\ (AE)\ \% = \ 43.2\ \%$$

Molecular Weight: 345.93

Molecular Weight: 32.00

Ir cat.

Molecular Weight: 107.16

Molecular Weight: 303.18
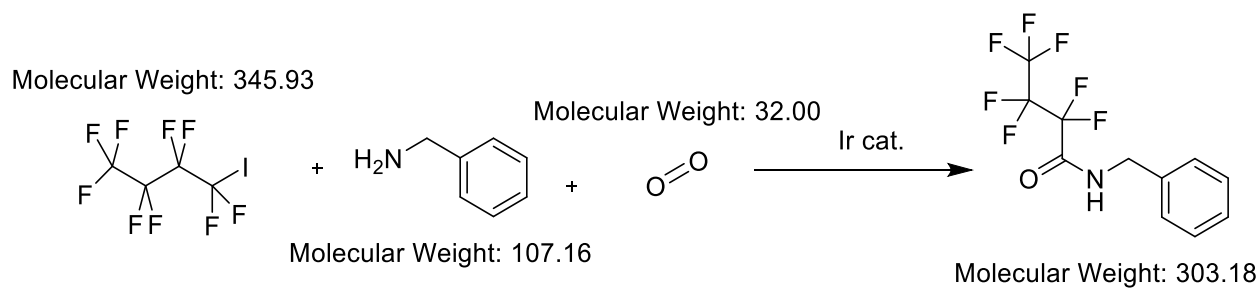
Scheme 22: Photoredox amide bond formation used to calculate atom efficiency, catalysts are not included in atom economy calculations

$$Atom\ Efficeny\ (AE)\ \% = \frac{mol\ weight\ of\ product}{mol\ weight\ of\ reagents}\ x\ 100$$

$$Atom\ Efficeny\ (AE)\ \% = \frac{303}{107 + 346 + 32}\ x\ 100$$

$$Atom\ Efficeny\ (AE)\ \% = \frac{303}{484}\ x\ 100$$

$$Atom\ Efficeny\ (AE)\ \% = \ 62.6\ \%$$

E – Factor

6.8 g, 3.4 mL   4.3 mL, 4.2 g   8.58 g   1.38 g
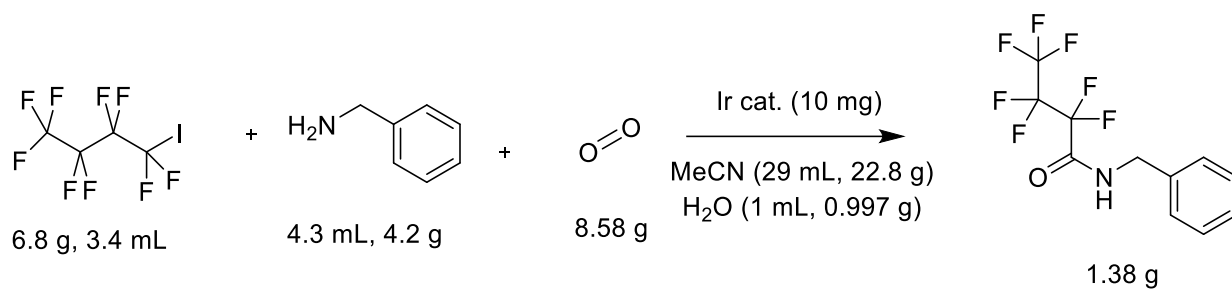
Oxygen mass calculation:

flow rate $= 32 \ cm^3/min$

$= 0.032 \ L \ x \ 180 \ mins$

$= 5.76 \ L$

$= 5.76 \ L \ x \ 1.49 \ kg/L$

$= 8.58 \ g$

$$E - factor = \frac{mass \ of \ waste}{mass \ of \ product}$$

$$E - factor = \frac{((22.8 + 4.2 + 6.8 + 8.58 + 0.997 + 0.01) - 1.38)}{1.38}$$

$$E - factor = \frac{(42.00)}{1.38}$$

$$E - factor = \ 30.4$$
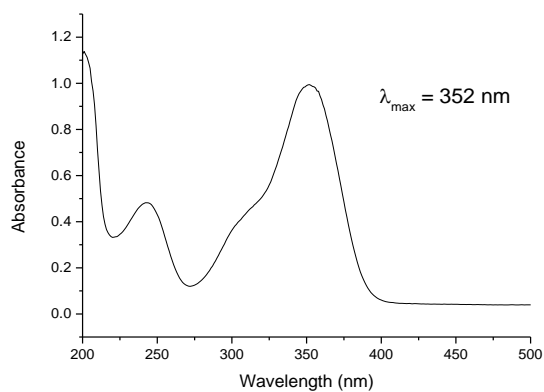
Figure 23: Michler's ketone, 1 mm cuvette in acetonitrile, 75 µM

REACH SEPARATIONS

Sample ID : JH177
Reach ID : NN153
Project ID : Hunter
Job Type : Chiral Analysis
Analyst : A.Brien
Date Received : 12-02-2019
Client declared mwt: 317.21
Client declared amount: 4mg

Results Summary:

NN153;
Chemical purity : 91.58%
Enantiomeric excess : 99.8 - in favour of the second eluting isomer

Method:

JH177 (assigned internally as lot number NN153) was dissolved to 1 mg/mL in EtOH and was then analysed by SFC. The conditions are described in the table below and are the same conditions used to analyse sample JH184_A Pseudo Racemate.

Figure 24: Chiral HPLC report of 3c produced by the photocatalytic method

REACH SEPARATIONS

Sample ID : JH268
Reach ID : NN171
Project ID : Hunter
Job Type : Chiral Analysis
Analyst : A.Brien
Date Received : 00-00-0000
Client declared mwt: 318
Client declared amount: 4mg

Results Summary:

NN171;
Chemical purity : 80.78% , m/z = 318.07
Enantiomeric excess : 99.7 in favour of the second eluting isomer.

Method:

JH268 (assigned internally as lot number NN171) was dissolved to 1 mg/mL in MeCN and was then analysed by HPLC. The conditions are described in the table below and are the same conditions used to analyse sample JH181 (NN154).

Please note there is a small shift in RT compared to NN154.

Figure 25: Chiral HPLC report of 3c produced by the electrochemical method

Chapter 3 – Development of a novel reactor to conduct photochlorination reactions

Introduction

This Chapter focuses on laboratory-scale photochlorination and particularly, on developing a new reactor to carry this reaction out more simply and safely. In recent years, efforts have been made to conduct chlorination reactions in a safer and more efficient manner.[1] This has led to the utilisation of micro and continuous flow methods which can allow for the *in-situ* generation of chlorine, therefore negating some of its inherent hazardous nature.[1,2] The application of a continuous flow system means that there is a reduction in the risk of a build-up of chlorine gas or over chlorination occurring, both of which could be possible batch-based systems.

Laboratory scale chlorination

Laboratory scale photochlorination has been an attractive area of research for many years. This is due to the highly reactive nature of chlorine and its pervasiveness through the chemical industry and also the fact that chlorine is often found in bioactive compounds - **Figure 26**.[3, 4]
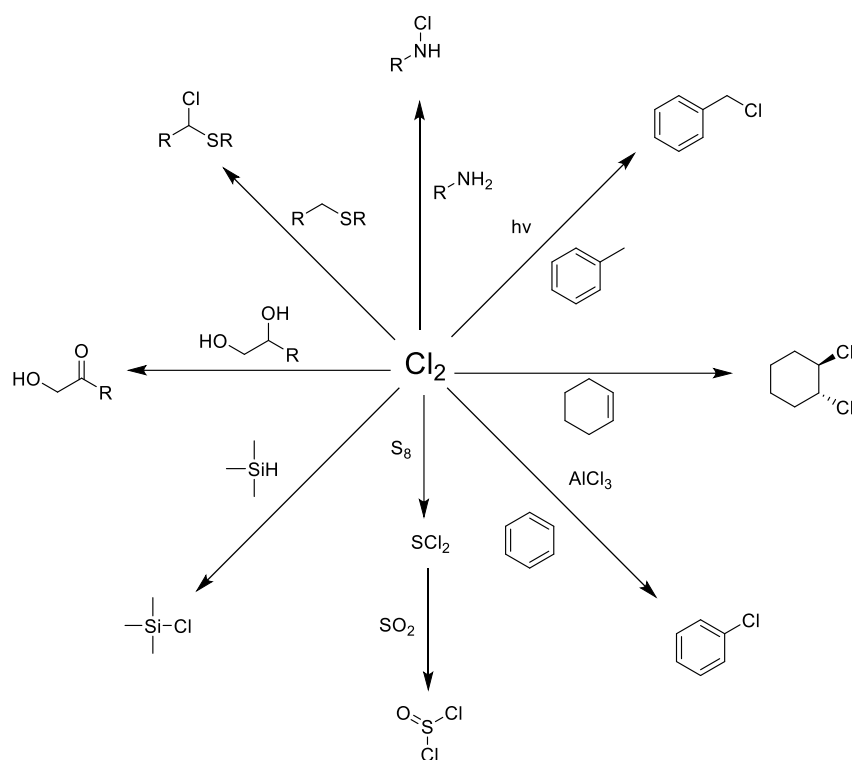
Figure 26: Common uses of chlorine gas in chemical reactions.[1,3,4]

Subsequently, there have been many methods for the generation of chlorine for the use in

chemical synthesis, some of which are shown in **Table 12**. One of the most well documented

molecules to study in these methods is the chlorination of toluene to produce benzyl chloride.[2,

5–9] When these methods are compared a number of features become apparent.

Table 12: Collection of published conditions for the chlorination of toluene

Conditions	Time (h)	Temperature (°C)	Authors
HCl, KCl, AgCl, H$_2$O, visible light	5-8 h	25	Whiting and co-workers [5]
N-hydroxyphthalimide, carbon tetrabromide, dichloromethane, Cu(OAc)$_2$, trichloroisocyanuric acid	22 h	25	Schreiner and co-workers[6]
K$_2$S$_2$O$_8$, NaCl, acetonitrile	15-24h	90	Hu and Zhang[7]
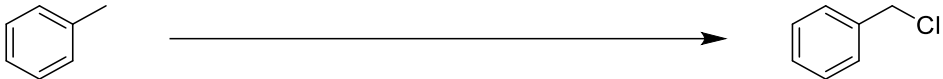
HCl, NaOCl, CHCl$_3$ (thermal or photochemical)	0.25	40	Kappe and co-workers[2]
Cl$_2$ excited with either UV light, heat, γ-rays or fast electrons	1 second (fast electrons)	Not reported	Cox and Swallow[8]
SO$_2$Cl$_2$, peroxide	0.5	110	Brown and Kharasch[9]

Firstly, one of the fastest methods tends to be using UV light and elemental chlorine **Table 12 –** Kappe and co-workers/Cox and Swallow. This makes these methods highly attractive from a green chemistry perspective as this method is highly atom efficient, but also energy efficient due to the high quantum yield of this reaction.

Secondly, the methods proceeding via different pathways typically tend to be slower and require high temperatures and/or metal catalysts e.g., **Table 12** – Hu and Zhang /Schreiner and co-workers.

Alternatively, other more complex reagents can be used (**Table 12** Brown and Kharasch) however; this can significantly affect the atom efficiency of a chlorination method, therefore making it less attractive.

For these reasons, the focus of this work has been into photochemical methods of chlorination.

Flow chlorination methods

A number of noteworthy examples of recent chlorination work are reported by Hessel and co-workers[10], Jähnisch and co-workers[11], and Kappe and co-workers.[2] These examples are worth discussing in more detail as they use either chlorine or anhydrous hydrochloric acid gas as the source of chlorine therefore, significant thought has had to be placed into the safe handling of these materials.

In the work of Hessel and co-workers the reactor system is divided into two sections, a dry and wet zone - **Figure 27**.[10] The anhydrous hydrochloric acid feeds through a mass flow controller before reacting with neat alcohol. This gives excellent control over the amount of gas being fed into the system however, it does require a constant positive flow of dry gas through the system

to prevent moisture entering the reactor and causing corrosion to occur. Hessel *et al.* used this system to carry out a number of thermal chemical reactions, including the synthesis of benzyl chloride in high yield (96 %). The micro-flow reactor was a positive step in terms of safety, as the small volume meant that if a leak occurred then the release of hydrochloric acid gas would be small.
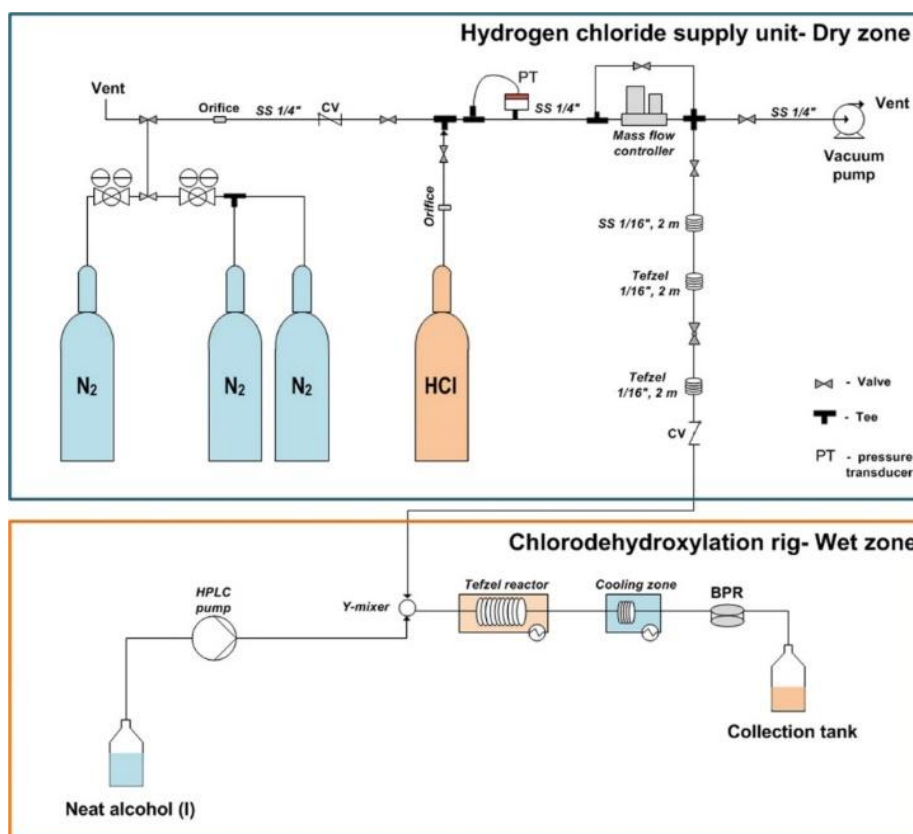
Figure 27: Reactor diagram used by Hessel *et al.* In this system the reactor is split into two sections. A dry and wet zone. The dry is free from moisture to prevent the HCl reacting and corroding the equipment. Figure reproduced from Ref [10]

Kappe and co-workers had an interesting approach to flow chlorination - **Figure 28**.[2] During their work, they combined two common chemical laboratory reagents together in flow, HCl and NaOCl. This allowed for the *in-situ* generation of chlorine gas, thus negating the hazards associated with transporting and storing the dangerous gas. With this method of chlorine generation in hand, the team went on to carry out both thermal chlorination reactions and photochemical chlorination reactions. Interestingly, concurrently a similar method of in-situ chlorine generation and utilisation of the gas for photochlorination was published by Ryu and co-

workers - **Figure 28**.[12] This shows the desire amongst the chemical community for a simple and versatile method of being able to perform photochlorination reactions on a laboratory scale.
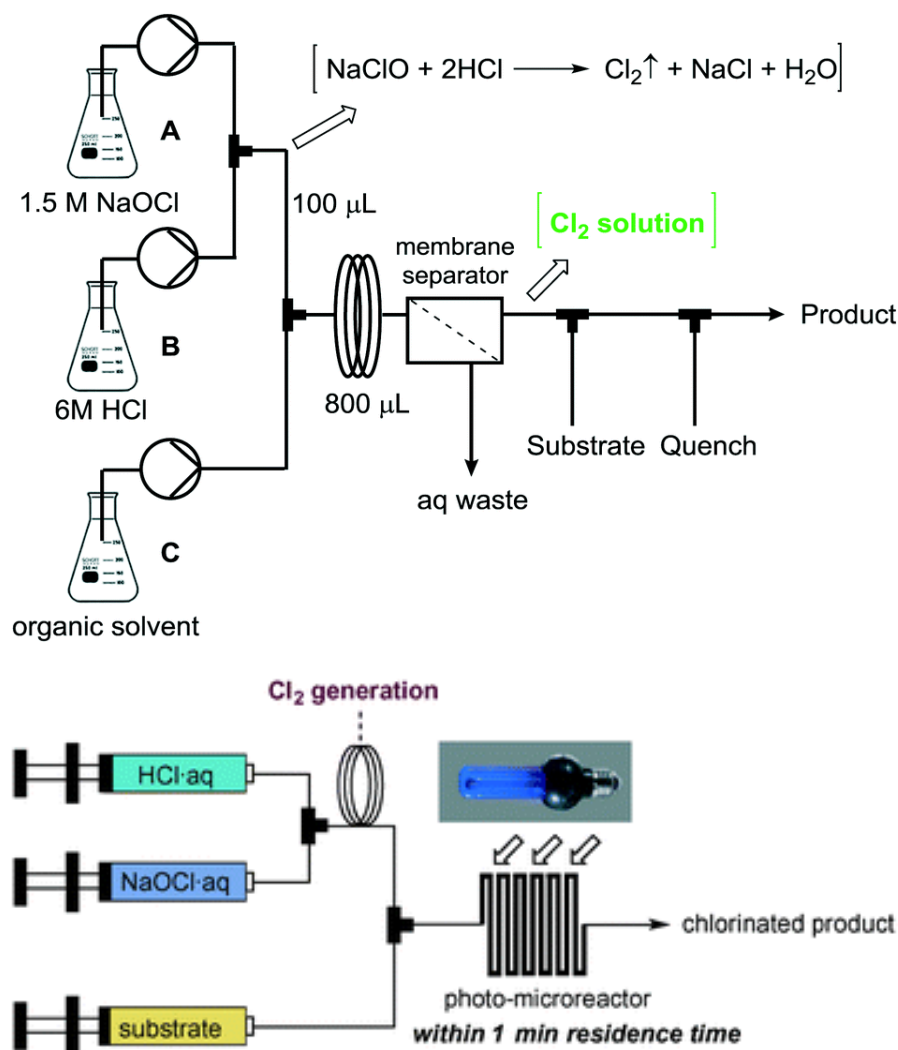
Figure 28: *In-situ* chlorine generation methods reported by (top) Kappe and co-workers[2] (bottom) Ryu and co-workers.[12] Images reproduced from respective reference

Finally, Jähnisch and co-workers developed a falling film reactor for the photochlorination of toluene derivatives.[11] In this system chlorine gas was fed into the reactor and bubbled though the falling film solution. This falling film reactor used a quartz window and a xenon arc lamp (1 kW, 190 – 2500 nm, λ_{max} = 800 nm) to conduct the photochemical reaction. Throughout this work the authors were able to significantly increase the space-time yield of the photochlorination reaction, by comparing the batch and flow processes (1.3 vs. 400 mol L^{-1} h^{-1}).

Whilst these are excellent example of photochlorination at laboratory scale, the application of these types of reactors has been limited. One reason for this could be the somewhat specialised equipment and expertise required to build a chlorinating reactor.

Aim

The aim of the work in this chapter is focused on the use of chlorine gas for the direct photochlorination of organic compounds. The initial aim of this work is to determine whether a new design of reactor could facilitate the use of chlorine gas for direct photochlorination. The intention is to investigate whether the established Nottingham PhotoVap concept could be re-engineered, to readily conduct photochlorination reactions and to test its use with a range of benchmark reactions.

The final aim will be to apply the photochlorination method to the preparation of several compounds that are key intermediates for API synthesis.

Strategy

The strategy for answering the first aim will be to develop a reactor to address some of the problems of lab-scale photochlorination. The objective is to handle chlorine gas safely and then to carry out a few chlorination reactions with toluene,, to understand the effect of the reactor conditions for photochlorination (amount of chlorine, repetitions, length of time irradiation, etc).

Following the realisation of a successful reactor, its performance will be assessed by using it to photochlorinate toluene and a selection of its derivatives to establish how it compares with previous methods of chlorinating these compounds in regard to ease of use, reaction time, etc. After this, the preparation of chlorinated compounds will be attempted, which are or could be key intermediates for synthesis of known APIs.

Finally, given the hazards of storing large quantities of chlorine gas in the laboratory, alternative sources of chlorine gas will be investigated particularly the electrolysis of aqueous NaCl to

produce *in situ* chlorine gas. This approach is analogous to the electrolytic generation of H_2 from H_2O in the commercial Thales Nano H-cube and could greatly reduce the waste from photochlorination, as well as increasing its safety.

Results and Discussion

Requirements

To allow for a gas-liquid photochemical reaction to take place, numerous requirements need to be satisfied for the reaction to progress well. These include containment of gas and liquid in near proximity with good mass transfer between gas and liquid phases. Furthermore, the required wavelength of light should be able to penetrate the reactor and reach the photoactive component (chlorine) of the reaction. Finally, there should be good control of the reaction temperature over the course of the reaction.

In addition to these points, the use of chlorine requires further safety and material compatibility considerations. This means that any chlorine gas used should be fully contained and the quantity of gas minimized for each reaction, reducing the exposure risk should there be a leak. Once the gas is in the reactor, any excess gas should be easily purged from this system and quenched prior to removal of reaction products from the reactor. Finally, the chlorine gas should not encounter any corrodible or reactive materials (e.g., steel, grease).

At the beginning of this work, it was proposed that an adapted version of a photoreactor, developed previously at Nottingham, might be able to overcome the majority of these issues. The initial design was adapted from the one used and reported for the "UV PhotoVap"**- Figure 29**.[13] This choice was made, as the design was well suited for the containment of gases - such as oxygen and this design had already been shown to be highly applicable to conducting photochemical reactions. Starting from a reactor which has been previously shown to be applicable to gas-liquid photochemical reactions, addresses several of the reactor requirements stated above. Additionally, this system had already been shown to permit good temperature

control when using high powered mercury lamps. These lamps would be required for a photochlorination reaction because the UV light needs to be ~ 310 nm and UV-LEDs at such wavelengths are not particularly powerful. One downside of using these lamps, is that they are not very efficient and generate significant amounts of heat. To try to limit the impact of the heat generated, the lamps were switched on for a short duration and the water bath was kept cool by adding ice to the water between experiments. Prior to the start of the photochemistry, the UV Photovap had to be adapted to overcome some of the other points which would allow it to be used for photochlorination reactions.
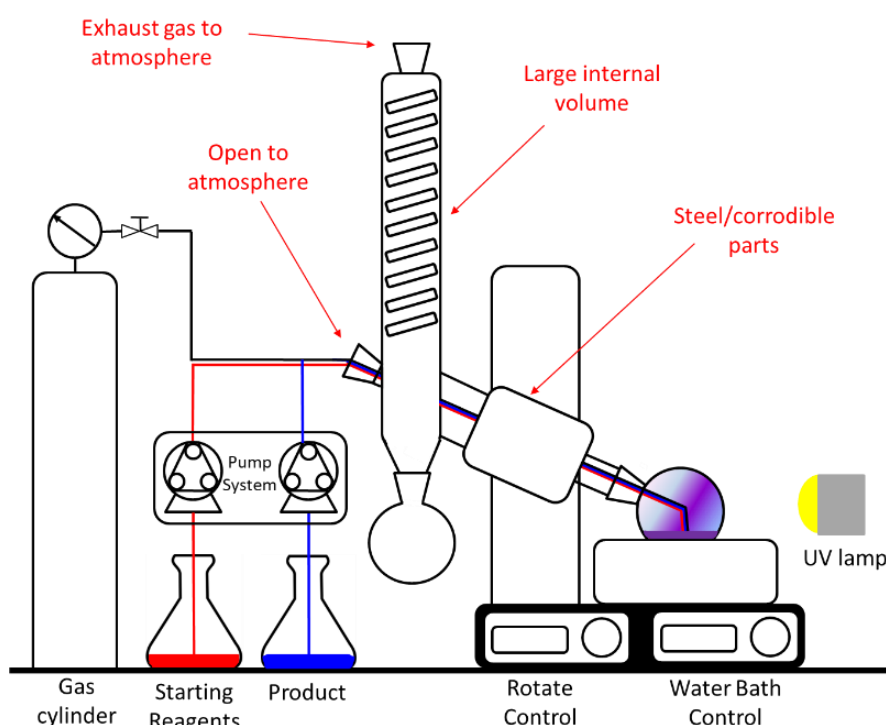
Figure 29: Diagram of the UV Photovap with notation identifying section which are not compatible with photochlorination. Adapted from ref [13]

Reactor development - ChloroVap

The first of these changes was to investigate a number of material choices which had to be considered when designing and building the reactor. Chlorine gas forms hydrogen chloride when it encounters water, and this acid is highly corrosive to steel and the many plastic components. To overcome this issue all connectors and piping were made of PTFE (manufactured by Bola) as PTFE is resistant to concentrated hydrochloric acid. The thermocouple (3 mm k-type Inconel 600,

RS) was chosen for several reasons. Firstly, the extra thickness would increase the lifetime of the thermocouple as corrosion would take longer before the thermocouple stopped working but also, Inconel is an alloy of nickel and chromium, which is corrosion resistant. The thermocouple was coated in a heat shrink PTFE (Bola) cover to further protect it from chlorine gas exposure. The downside of this thickness and PTFE wrap, is that the temperature measured by the thermocouple had a slower response time but appeared to give an acceptable indication of the temperature of each reaction. These alterations answer the inherent material compatibility issues associated with chlorine gas.

The next point was to use an adapted piece of glassware to replace the condenser of the rotary evaporator. This was made in house by School of Chemistry glass blowers to eliminate several problems: (i) extra ports had been added; (ii) the removal of the water condenser and receiving flask which add unnecessary volume to the apparatus. The extra glass ports were required for the thermocouple and water aspirator connectors. The removal of the condenser/receiving flask significantly reduced the volume of this section of the reactor (from ~ 3 L to ~ 0.5 L) meaning that only a relatively small amount chlorine would be held in the dead volume of the reactor, with majority of the total reactor volume being the reaction flask itself. An additional benefit of this reduced reactor volume meant that any chlorine which needed to be removed by the water aspirator would be very rapid.

The final adaption was the grease used for the glass tap (T4) and glass-plastic seals. These points were greased with Fomblin (perfluorinated grease) to allow easier movement of this tap and sealing of the joints without any reaction occurring between the grease and chlorine gas. Normally, Fomblin is unnecessarily expensive to use in a standard rotary evaporator set up, however it was essential for this system.

These adaptions allowed the system to safely contain the chlorine gas for the photochemical reaction and the adapted reactor was given the colloquial title of the "ChloroVap" - **Figure 30**.

The basic concept consists of placing the reaction solution into the reactor flask, then chlorine being fed into the reactor flask - **Figure 30**. The flask is then spun which allows for excellent surface contact between the reactive gas and the reaction solution – aiding mass transfer. Next, the flask is irradiated with UV light causing the chlorine to undergo homolytic bond cleavage to form chlorine radicals. Following the completion of the reaction, a water aspirator was used to remove the excess chlorine and quench the reaction. This was achieved by using an alkaline scrubbing solution which was placed between the reaction flask and the water aspirator, meaning that the extracted gas is bubbled through alkaline solution and neutralising it. Additionally by blowing nitrogen gas into the flask, this aids in the removal of the reaction gases. To complete the safety requirements, the ChloroVap was placed inside a fume hood to give a further layer of protection, should any chlorine gas leak from the reactor.

Once the reactor had been built and a standard operating procedure was drawn up – see **Appendix**. A number of initial tests were run, to give clearer understanding of how well this reactor had worked compared to other photochlorination reactors.
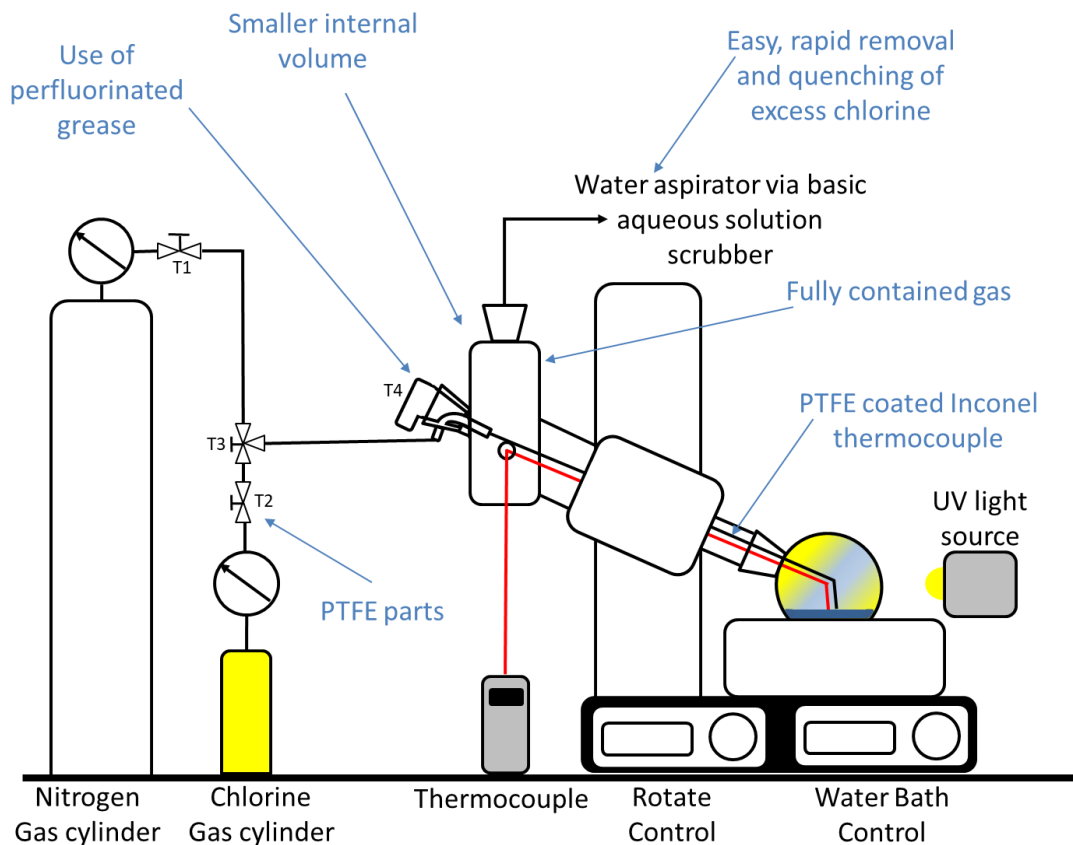
Figure 30: Top: Schematic diagram of ChloroVap reactor with specific alterations noted, Bottom: Image of the actual prototype "ChloroVap".

Initial experimentations

Toluene
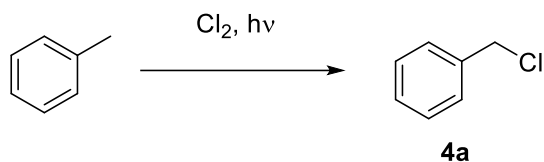
Scheme 23: Test experiment, the photochlorination of toluene

The first photochemical reaction conducted in the ChloroVap was the chlorination of toluene. A full table of results is shown in **Table 13**. This reaction was used to gain a preliminary understanding of the performance of the reactor. Additionally, this reaction has been reported many times in literature, allowing the ChloroVap to be benchmarked against other photochlorination methods. Moreover, **4a** is not the only product of the photochlorination of toluene; therefore, the use of this reaction means that the ChloroVap's selectivity for mono chlorinated photochemical products can be assessed. Whilst the optimisation was conducted using a calibrated GC method, the reaction mixture was also analysed using GCMS showing that the minor products were benzoyl chloride and benzal chloride. However, as the singly chlorinated species was more desirable, this was the focus of the optimisation experiments. The experimental factors for initial investigation were:

- Length of Irradiation

- Quantity of chlorine required

- Initial starting temperature

- Flask size

- Concentration of toluene

Since the aim is to promote photochemical chlorination, it was essential to run a control experiment right at the beginning, where exposing toluene to chlorine in the dark, established whether any reaction occurred in the absence of light. In this case, only a very small quantity

(0.7 %) of benzyl chloride (**4a**) was produced (**Table 13 – experiment 1**). This is in keeping with the precedent as previous studies have determined that the chlorination of toluene can be performed under thermal conditions. Alternatively, it could be due to the residual amount of ambient light present in the fume hood when the reaction is conducted. In hindsight, a further control experiment where chlorine was exposed to toluene at a high temperature in the dark should have been conducted however, this only became apparent once the project was completed.

For safety reasons, it was decided not to flow the chlorine gas while the ChloroVap was running. The total volume of the reactor (with a 1 L flask attached) excluding the narrow bore tubing was ca. 1.5 litres. Therefore, a decision was made to fill the reactor with 3g, which is slightly less than a total fill of the reactor, but given the high density of the gas, it would probably displace any air in the system and pool in the flask. This represents 42 mmol of chorine and the corresponding volume of toluene (47 mmol) was 5 mL was used for two reasons. Firstly, this was a convenient amount for creating a film of solvent in the flask and the slight excess of toluene, should reduce the various polychlorinated products produced.

Table 13: Various conditions tested with the ChloroVap to better understand the proper conditions for its use.

4a
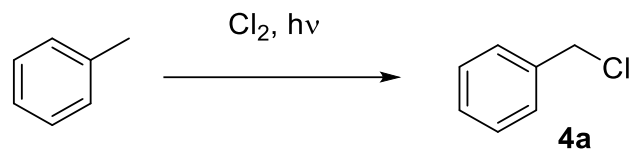
Reaction No.	Flask size (L)	Irradiation time (mins)	Chlorine added (g)/mole equivalent to toluene	Selectivity for 4a (%)	Conversion of toluene (%)	Yield of 4a (%) (GC)
1	1	0	3/ 0.9	65	1	0.7
2	1	1	3/0.9	83	36	30
3	1	2.5	3/0.9	84	55	46
4	1	5	3/0.9	78	51	40
5	1	10	3/0.9	77	54	42
6	1	2.5	1/0.3	75	54	41
7	1	2.5	10/3	74	62	46
8	1	2.5	2 x 3 (total = 6g)/ 1.8	69	60	41
9	1	2.5	3 x 3 (total = 9 g)/2.7	52	98	51
10[b]	1	2.5	3/0.9	34	62	21
11[c]	1	2.5	3/0.9	76	58	44
12	3	2.5	3/0.9	69	66	45
13	0.5	2.5	3/0.9	66	52	34
14[d]	1	2.5	3/90	55	96	53, 52[a]
15[e]	1	2.5	3/900	52	95	49

Reaction run with 5 mL of neat toluene, with starting temperature of 25 °C. [a] Isolated Yield, [b] starting temperature *minus* 50 °C, [c] starting temperature 50 °C, [d] 1 M toluene in chloroform, [e] 0.1 M toluene in chloroform.

The first set of photochemical experiments conducted focused on the effect of variation of irradiation time - **Table 13 experiment 2 - 5**. Initially, it was hypothesised that only a minimal amount of time may be required, due to the high quantum yield of photochlorination reactions. It was found that 2.5 mins appeared to give a good balance between conversion and selectivity - **Table 13 experiment 3**. Irradiation times shorter than 2.5 min (**Table 13 experiment 2**) gave higher **4a** product selectivity, but the conversion of the starting material was low. When the solution was irradiated for longer than 2.5 min, the selectivity for **4a** decreased (**Table 13 experiment 4 and 5**) and the conversion of the starting material did not significantly increase. There are two possible explanations, either the chlorine gas was depleting and there was secondary photolysis of the **4a**, or **4a** could be more reactive towards chlorine than toluene.

The next series of experiments focused on how much chlorine should be added to the reaction. When the quantity of chlorine varied, only a small difference in the yield of **4a** was observed (**Table 13 experiment 6 and 7**). This is an interesting finding as in the experiment where 1 g of chlorine was added to the flask there was a high yield of **4a** suggesting that there was good mass transfer between the gaseous and liquid phases. Somewhat surprisingly, when a threefold molar excess of chlorine gas was used, the yield did not change significantly from the use of 3 g. This is likely to be due to the small reactor volume, meaning that the extra chlorine was not retained in the reaction flask but was entering the rest of the reactor. In an attempt overcome this issue, multiple rounds of photochlorination on the same sample were conducted. In these experiments the chlorine gas (3 g) was replenished following each 2.5 min of irradiation. **Table 13 experiment 8 – 9** shows that near full conversion of toluene was achieved following 3 successive rounds of photochlorination reactions. This suggests that in the first round of photochlorination, the gas is absorbing enough UV light to be fully utilised as the concentration of **4a** only increased when subsequent rounds of photochlorination were performed. However, the yield of **4a** did not increase above 51 % due to the reducing selectivity for this product with each successive round of photochlorination. This is not

surprising as with each subsequent round of photochlorination, there is more **4a** available to react and form unwanted side products.

The effect of lowering the temperature of the reaction to -50 ^{O}C or rising it to +50 ^{O}C was investigated next. The temperature of the reaction could have several effects from influencing changing the reaction kinetics, to varying the amount of chlorine dissolved in the toluene. Increasing the temperature to + 50 ^{O}C had a negligible effect on the yield of the reaction (**Table 13 experiment 10**). Decreasing the temperature had a more significant effect; there was a substantial decrease in selectivity for benzyl chloride (**4a**) at the lower temperature, with the polychlorinated products being favoured - **Table 13 experiment 11**. This may be due to more chlorine dissolving into the reaction solution at these low temperatures, as gases are more soluble in liquids at lower temperatures due to entropic effects. Whilst it is interesting to note, as polychlorinated products can be useful, the focus was the monochlorination of toluene. Therefore, low temperature reactions were not investigated further, but it could be beneficial to future studies.

The subsequent set of reactions investigated the effect of different sized flasks on the yield of the reaction – (**Table 13 experiment 12 and 13**). The reason for this was that a large flask would have a greater gas-liquid contact surface area which would improve the mass transport of chlorine from gas to solution. When this was tested it was observed that the large flask had little effect on the yield of **4a** but the use of a smaller flask reduced yield of the reaction, possibly because there was less chlorine in the flask.

The final point investigated was reducing the concentration of toluene by dissolving it in chloroform - **Table 13 experiment 14 and 15**. All previous reactions were carried out with neat toluene to avoid the waste of added additional solvent. By diluting the toluene in chloroform, the conversion of toluene increased to nearly 100 %; however, the selectivity of the desired product **4a** did not increase significantly compared to the reaction where the neat toluene was taken to full conversion - **Table 13 experiment 9**. This may be due to the statistical production of each product meaning that,

without additional influencing factors, this may be the highest level of selectivity for **4a** achievable in this system.

These experiments provided a set of conditions which were then used to investigate more synthetically interesting and useful chemical compounds. However, before describing these experimental results for other compounds, it is worth comparing the ChloroVap with the other photochlorination methods. Whilst not the highest yield generated, the use of neat toluene allowed the generation of **4a** (2.7g, 46 % -**Table 13 reaction 2**) in a reaction time of 2.5 mins and this gives a very approximate productivity level of 65 g/h (1.5 kg/day) for benzyl chloride (**4a**) in the ChloroVap in a batch process. Whilst this value is greater than close literature examples (e.g. Kappe and co-workers[2] 42 g/h), the work in the ChloroVap has been done under batch conditions whereas Kappe was using a flow system, meaning that automating would be required keep the ChloroVap working and producing product. However this issue could be addressed, as previous work has shown that the PhotoVap can be used to produce a semi-continuous processing reactor.[14] This can be achieved by controlling the rotatory evaporator, lamps and a number of regent/product pumps through a computer allowing the system to become automated.

To summarise the answers to the questions posed at the start of this section:

- The optimal irradiation time for these studies was found to be 2.5 minutes.

- 1 L of chlorine (3 g) was shown to give the best results when working with neat reagents and provided an excess of chlorine when dilute regents were tested.

- Increase temperature at the beginning of the reaction appeared to make little difference on the yield of the reaction however, lowering the temperature increased the selectivity for polychlorinated products. Therefore, a starting temperature of 25 °C (room temperature) was used for subsequent reactions.

- The flask size which was used in follow up experiments was 1 L as larger flasks did not increase the yield and smaller flasks gave reduced yield.

- Whilst using neat toluene gave the highest amount of **4a** produced, when toluene was
  diluted in chloroform the highest conversion was achieved.

Effect of electron donating and withdrawing groups

Following the experiments of toluene, the electronic and steric effects of substituents on the

aromatic ring were investigated - **Figure 31**.

i) X = CH$_3$, Y = H, Z = H
ii) X = H, Y = H, Z = CH$_3$
iii) X = H, Y = CH$_3$, Z = H

i) X = CH$_2$Cl, Y = H, Z = H, **4b** = 7 %
ii) X = H, Y = H, Z = CH$_2$Cl, **4c** = 31 %
iii) X = H, Y = CH$_2$Cl, Z = H, **4d** = 74 %
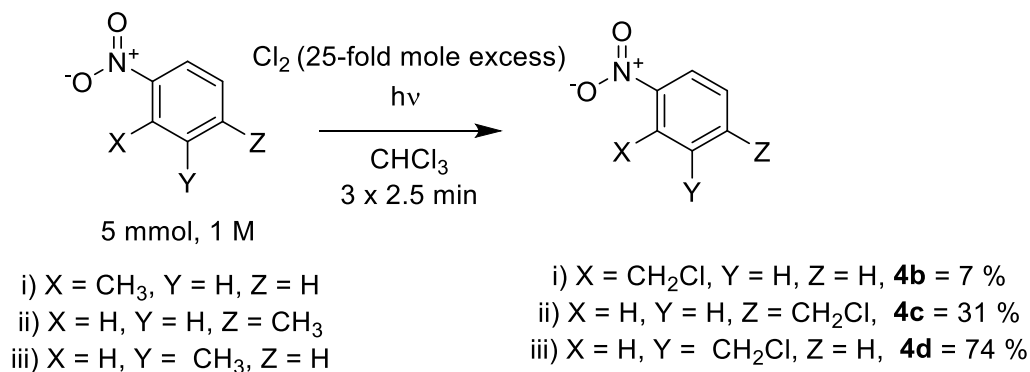
Figure 31: Isolated yield of a number of mono chlorinated substituted toluene species. Each nitrotoluene solution (1M) was irradiated for 3 x 2.5 min whereby the chlorine gas (3 g) was replenished for each round of irradiation.

Firstly, various nitro- species were looked at. In the first instance, the *ortho* species initially reacted

with a single round of photochlorination (2.5 min total); however, this gave little to no conversion of

the starting material. In a similar process to that described earlier, **Table 13 – experiment 9 – 11**, the

chlorine was replenished and the photochlorination process was repeated a further two times (3 x

2.5 min, 7.5 min total) which resulted in a modest yield of the *meso* substituted product **4b** (7 %)

alongside the unreacted starting materials.

When this same three-round photochlorination method was applied to the other two isomers of

nitrotoluene, the *meta* substituted variant yielded the greatest percentage of product (**4d** = 74 %)

whilst the *para* substituted isomer only achieved a yield of 31 %. This range in yield could be due to

the combination of a selection of possible factors.

These results can be rationalized by a combination of steric and electronic effects taking place

between the aromatic ring and the chloride radical. An alternative rationalisation for the low yield of

the *ortho* nitrotoluene was that it could have undergone a photochemically induced proton transfer.

93

This reaction was recently explored by Gilch and co-workers[15] who showed that a tautomerization is caused by irradiating *ortho*-nitrotoluene with UV light (250 nm) and results in the formation of an *aci*-nitro species then an alcohol - **Scheme 24**.
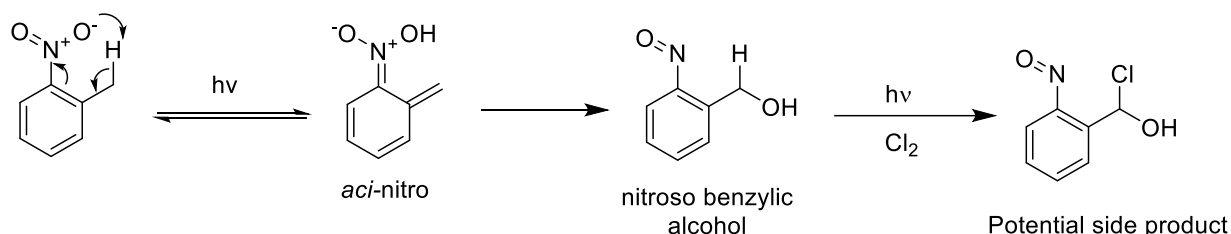
Scheme 24: Potential side reaction which *ortho*-nitrotoluene could undergo, based on the work of Gilch and co-workers.[15]

There was the possibility that this *aci*-nitro species could undergo photochlorination to form similar but unwanted products, thus reducing the efficiency of the reaction. However, none of these side products were observed in the mass spectrum or NMR data. This could be a result of the use of borosilicate glassware which stops the transmission of light below 300 nm, preventing the formation of the *aci*-nitro intermediate.

After this set of nitro species was investigated the corresponding methoxy species were photochlorinated with a single round of chlorine (2.5 min total). Unfortunately, none of these anisole compounds produced the desired monochlorinated products. The reasons for this were not investigated further.

Once the chemical reactivity of these substituted compounds had been explored, some industrially more relevant compounds were tested in the ChloroVap.

2-Chlorotoluene

The next example tried was the mono chlorination of 2-chlorotoluene (**Scheme 25**).
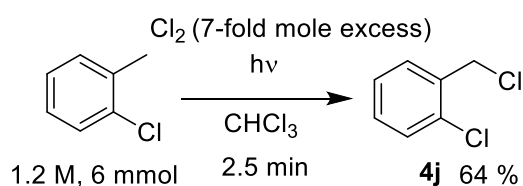
Scheme 25: Monochlorination of 2-chlorotoluene (1.2 M) to form 4j in with 2.5 min of irradiation.

This resulted in a good yield of **4j** (64 %) in a single round (2.5 mins) of photochlorination in the ChloroVap. This is a good result as the product of this reaction **4j** is a useful product that can be found in a few different commercial compounds - **Figure 32**. In fact, when this photochlorination reaction was conducted a good resulting yield (**4j** = 64 %) was achieved when using the ChloroVap method. This is a particularly interesting result when the time scale of the reaction is considered (2.5 min). As the reaction time is quick, the productivity of the reaction is high (15 g/h). Therefore, large amounts of this useful intermediate can be produced with minimal time consumption. Later in this chapter of the thesis, crude **4j** produced using the ChloroVap was used to synthesise an active pharmaceutical compound (API).

Viminol (analgesic)   Clobenzorex (stimulant)   Prothioconazole (fungicide)
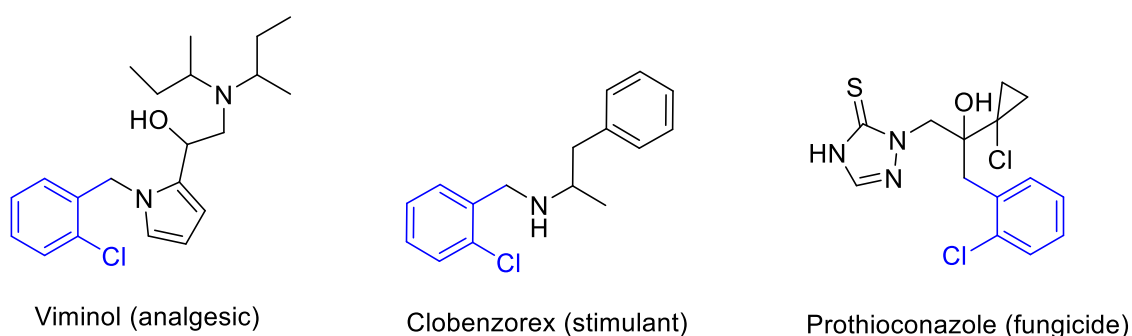
Figure 32: A selection of biologically active compounds which contain structures that could be derived from, 4j, can be found are shown.

2-Chlorophenyl acetic acid

The next compound to be investigated was the monochlorination of 2-chlorophenyl acetic acid (2CPA) - **Scheme 26**. This compound was chosen due to 2CPA being structurally similarity to 2 chlorotoluene with the addition of a carboxylic acid group and **4h** is another key intermediate to several APIs. But it was unclear whether the carboxylic acid (an electron withdrawing group) would aid in the mono chlorination of the 2CPA or hinder it.
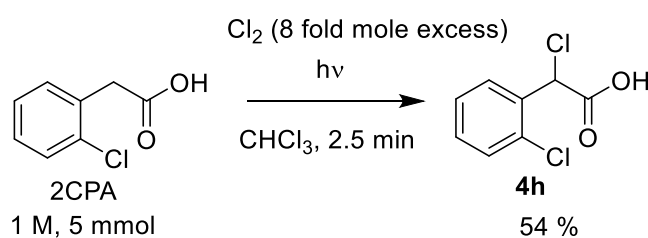
Scheme 26: Monochlorination of 2 chlorophenylacetic acid (1M, 2.5 min) to form 4h

The photochlorination (2.5 min, single round) of this 2CPA (1M) resulted in the production of the desired compound **4h** in good unoptimized yield (54%) - **Scheme 26**, showing that the additional carboxylic acid does not greatly affect the yield of the reaction. Whilst this unoptimized yield is not high, the starting material it is derived from is inexpensive so this may still make this synthesis useful.

As with the previous example, **4h** can be found in several APIs, shown in **Figure 33**.

Angiotension antagonist   Vasoconstrictor
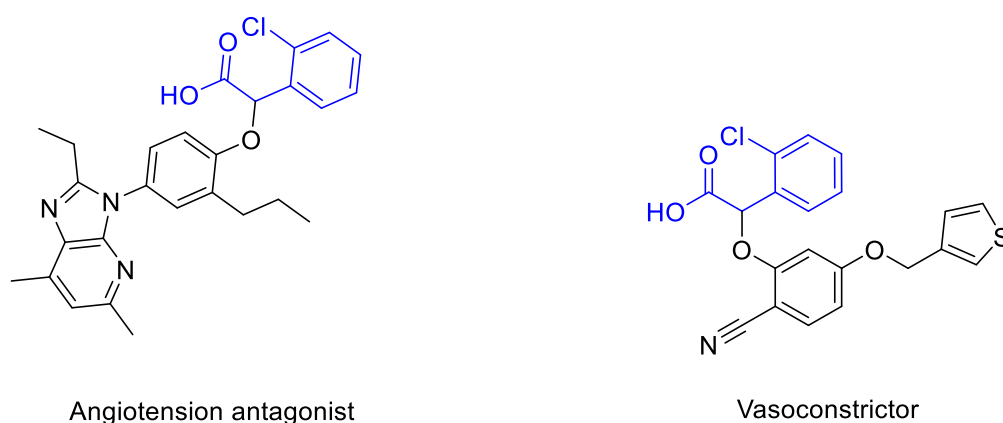
Figure 33: Two examples of APIs which contain structures that could be derived from 4h moiety.[16, 17]

A further derivative of 2CPA is the methyl ester of this compound **4l**. This is an interesting compound as it is a key intermediate in the synthesis of Plavix, an anticoagulant drug which has annual sales of approximately $6.4 billon - **Figure 34**.[18]

2CPA   **4l**   **4i**   Plavix (Clopidogrel)
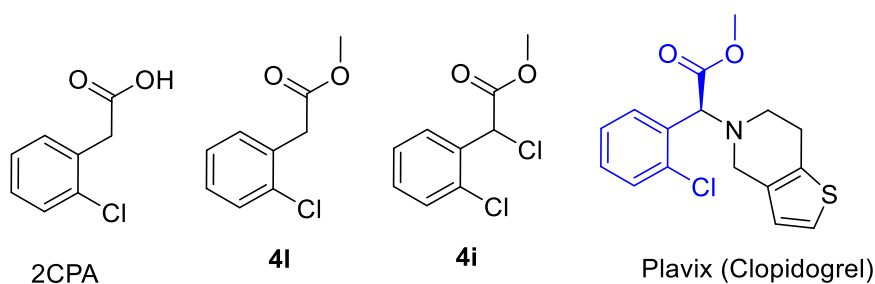
Figure 34: Key intermediates in the synthesis of Plavix – sales of $6.4 billion yearly.[18]

The original synthesis of this compound by Sanofi started from 2-Chloromandelic acid (2CMA) which underwent an initial esterification before the chlorination using thionyl chloride. This resulted in the key intermediate **4i**. The final step in the original synthesis was a coupling reaction using **4i** to make the Plavix - **Scheme 27**.
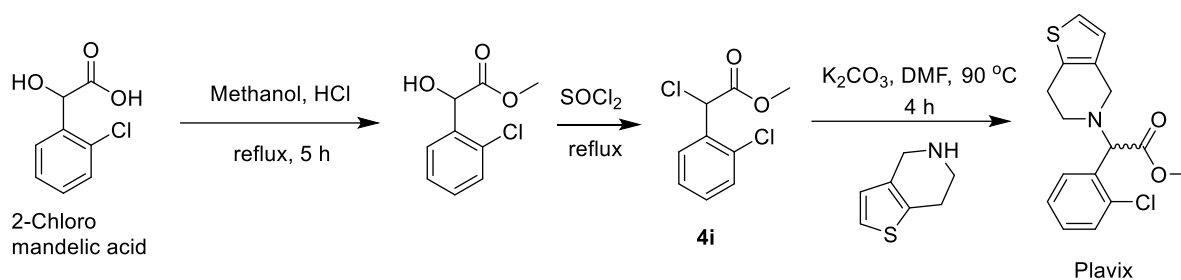
Scheme 27: Original synthesis of Plavix by Sanofi.[19,20]

An attempt to produce the intermediate **4i** was carried out using the ChloroVap. Whilst there is a formal description in the **Experimental** section, a brief summary of the experimental method is useful at this point. The 2CPA was dissolved in chloroform and photochlorinated in the usual fashion, to produce a yellow oil, to which methanol was added. This was exposed to chlorine gas and irradiated again. A biphasic solution was produced; the denser layer was found to contain the desired compound **4i** in good yield (86 %) - **Scheme 28**.
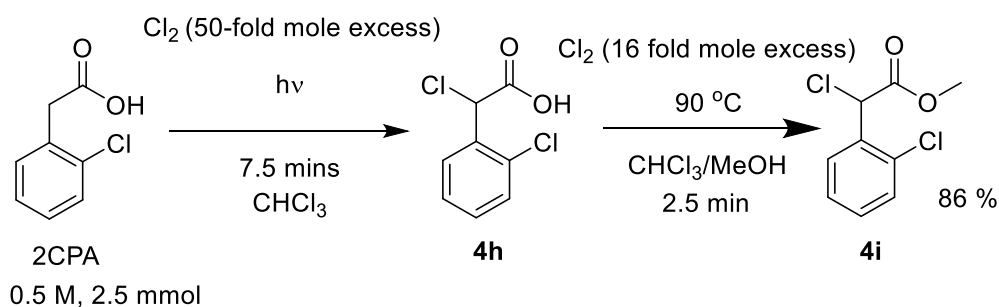
Scheme 28: This work synthesis of Plavix intermediate in 10 min at 0.5 M

Whilst this method may not be as elegant as other alternative routes,[21] it is an improvement on the original synthesis. It reduced the reaction time and allowed for the utilisation of a cheaper starting materials (2CPA 6-fold cheaper than 2CMA , Sigma Aldrich, 20/09/2019). Additionally, this route reduced the level of purification needed as the product formed a biphasic system, one phase of which contained only the desired product **4i**.

To determine whether this reaction could be conducted in a single step, chlorine was photolysed in the presence of 2CPA whilst dissolved in a solution of methanol to determine whether **4i** could be synthesised - **Scheme 29**.
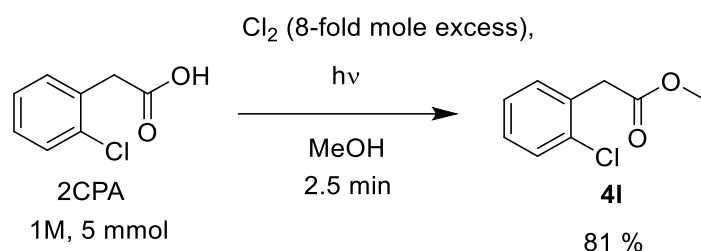
Scheme 29: Esterification of 2 chlorophenyl acetic acid (2CPA) (2.5 min, 1M) to form 4l

Surprisingly, the result of this reaction was not the desired product but the methyl ester product, **4l**, which was produced in good yield (81 %) and, curiously, formed a similar biphasic mixture within the methanol solvent – making separation and purification straightforward. Whilst this was not the intended product of the reaction, it did suggest that esterification reactions could be conducted using the ChloroVap. This unexpected reaction required further study to determine whether the esterification reaction was photochemical or thermal in nature. To better understand this esterification reaction several control reactions were conducted - **Table 14**.

Table 14: Control experiments for the esterification of 2 chlorophenylacetic acid
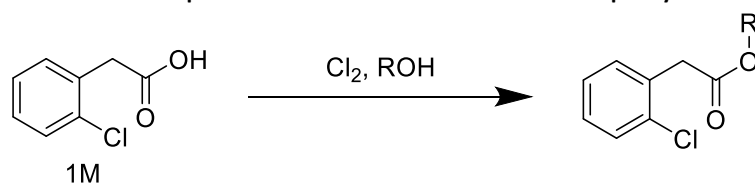
Experiment number	Solvent	Light	Starting Temperature (^{o}C)	Cl$_2$ (gas)	Product
1	Methanol	Y	25	Y	Y
2	Ethanol	Y	25	Y	Y
3	Methanol	N	90	Y	Y
4	Methanol	Y	25	N	N
5	Methanol	Y	25	Conc HCl	N
6	Methanol	N	25	Y	N
7	Methanol	N	90	N	N
8	CHCl$_3$	N	90	Y	N

Firstly, the alcohol was varied to determine if other alcohols would yield the corresponding products, which proved fruitful - **Table 14 experiment 1 and 2**. This showed that the esterification was possible with other alcohols and that the reaction was not reliant of the use of methanol.

Next the light was removed but the solution was heated to 90 ^{o}C in the dark - **Table 14 experiment 3**. The reason for use of this high temperature is that this is the temperature typically recorded

within the flask following 2.5 mins of irradiation. This reaction produced the methyl ester **4l**. This was strong evidence that the reaction was not proceeding via a photochemical process but rather by a thermal method due the reaction taking place in the absence of light.

Following on from this the solution was irradiated without the addition of chlorine gas. **Table 14 – experiment 4** unsurprisingly, it did not give the desired product, and this would support the need for chlorine in the reaction for it to take place. This is further supported by the utilisation of hydrochloric acid in many thermal esterification reactions[3] and the absence of this key reagent would significantly hamper the reaction process.

Next, the reaction was repeated in the presence of concentrated hydrochloric acid as the source of chlorine - **Table 14 experiment 5**. In this example, the reaction solution was irradiated with the same light source, for the same period as previous reactions. Intriguingly, this variant did not give any desired product. This could be due to the hydrochloric acid being in insufficient quantities to catalyse the reaction fast enough to produce **4l** in this reaction time. This suggests that the high quantities of chlorine used in this reaction system and high temperatures allowed the esterification to take place rapidly.

In **Table 14 experiments 6, 7 and 8** the experiment was conducted in the absence of heat, chlorine, or methanol, respectively. In each of these examples the desired product was not produced, suggesting the process was not photochemical in nature but purely thermal.

The results shown in **Table 14** suggested that the esterification reaction was a thermal process (heat from the lamp, reaching 90 $^\circ$C following irradiation) which was being accelerated by the presence of excess of hydrochloric acid (a product of the addition of chlorine to water) – which is used to catalyse the esterification of many carboxylic acids.

APIs synthesis

As discussed in previous sections, several key intermediates, **4i** and **j**, had been synthesised in the ChloroVap - **Figure 35**. The next test was to see whether these intermediates could be used to synthesise their respective biologically active compounds.

4i　　　　　**4j**　　　　　Plavix　　　　　Ticlopidine
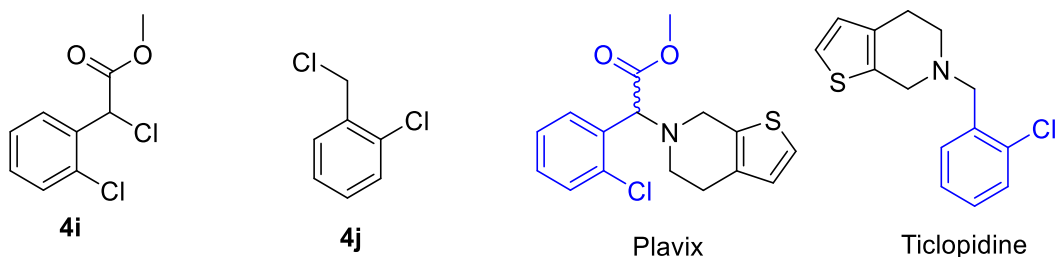
Figure 35: Left: key intermediates for APIs synthesis in the ChloroVap, Right: Corresponding active compounds.

The two target molecules of focus were Plavix and Ticlopidine. Both Plavix and Ticlopidine are

anticoagulant compounds which are prescribed to millions of people each year. This experiment was

conducted to determine whether the ChloroVap could be used to synthesise these types of

compounds. The first trial was the synthesis of Plavix. Using the same method described earlier,

2CPA was dissolved in chloroform, photochlorinated then an esterification reaction was conducted

resulting in a biphasic mixture - **Scheme 30**. After this 10-minute synthesis, the denser phase of the

biphasic mixture was separated and dried under *vacuo* and was then used in the coupling reaction

conducted to produce crude Plavix. Unfortunately, time did not allow for this compound to be fully

isolated, but this could be the target of future work.
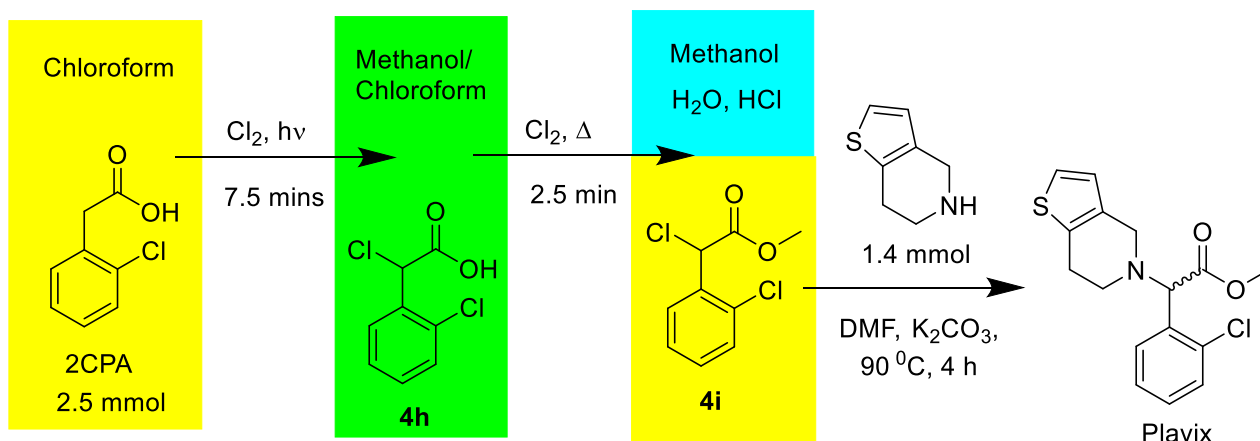
Scheme 30: Synthesis of Plavix using the ChloroVap

A similar approach was used to synthesize Ticlopidine. However, in this instance there was no

biphasic purification and the crude product **4j** was used to produce the crude API product which

again could not be fully isolated due to time constraints - **Scheme 31**.
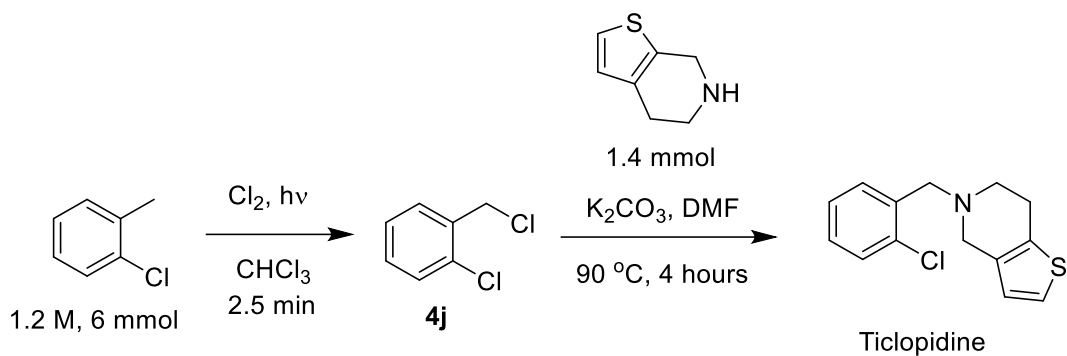
Scheme 31: Coupling reactions of crude Key intermediates made in the ChloroVap to make the active pharmaceutical ingredients Ticlopidine.

If this process for production of Plavix is compared with the Sanofi method several positive factors can be observed - **Scheme 32**.
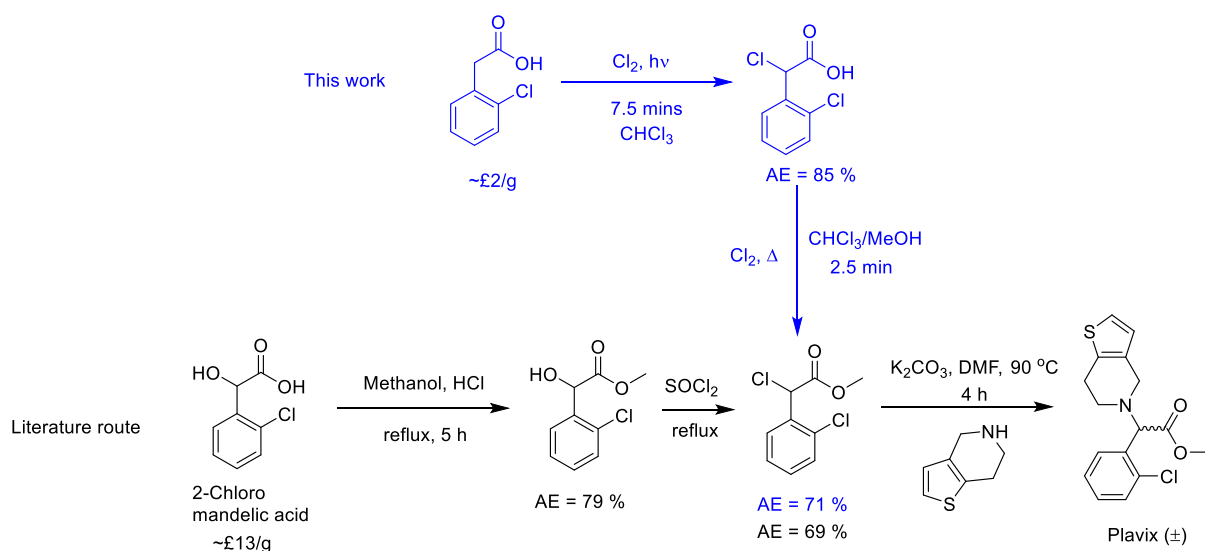
Scheme 32: Literature reported Plavix synthesis and compared with this method. This includes atom efficiency (AE) comparison of each process.

Firstly, there has been a large reduction in reaction time, from >5 hours to 10 mins to reach **4i**. By reducing the reaction time, the overall throughput of the reaction could be increased, allowing for more final product to be produced, in the same period. The second point is that the starting material of this method (2CPA) is cheaper than the original method (6-fold cheaper, Sigma Aldrich, 20/09/2019) which could mean that the method could operate at reduced overall cost compared to Sanofi's process. Additionally, as **4i** can be produced as a biphasic mixture this means that the process of purification of this product is reduced when compared to the original synthesis. Alongside this, the atom efficiency (AE) is higher in each step of the reaction conducted in the ChloroVap when

compared with the literature method – see **Appendix**. Interestingly, if atom efficiency of the two chlorination steps is compared, the method which uses thionyl chloride is significantly lower than this method (69 % vs. 85 % respectively). This could suggest that this route produces less waste than the Sanofi method, however AE does not always give the truest reflection of the effectiveness of a chemical reaction, therefore alternative methods of comparison should also be applied.

Whilst the E-factor to produce **4i** is not reported in the original synthesis of Plavix it is likely to be high (typical pharmaceutical compound E-factor = 25 -100).[22] Whilst the E-factor of the ChloroVap process cannot be precisely calculated, it is clear that the scavenging of HCl and excess chlorine with NaOH to form waste NaCl will impact significantly on the E-Factor (see **Appendix**). However, most if not all of this NaCl waste could, in principle, be avoided if chlorine gas could be regenerated from the sodium chloride solution by electrolysis (see following Section).

In summary, these preliminary experiments yielded the desired active compounds showing that, with the appropriate optimisation, this could be a potentially viable route for the synthesis of compounds in a more environmentally benign and rapid fashion than the original synthesis. This could be the focus of future work.

Electrolytic production of chlorine

As discussed above, much of the reaction waste comes from excess chlorine, and HCl generated as a by-product during the reaction. In the ChloroVap, the excess chlorine gas is passed through an alkaline solution to prevent the release of harmful hydrochloric acid. This reaction forms sodium chloride solution which could be recycled by electrolysis to reform chlorine gas - **Scheme 33.** Through this method the E-factor of chlorination reactions could be greatly reduced.
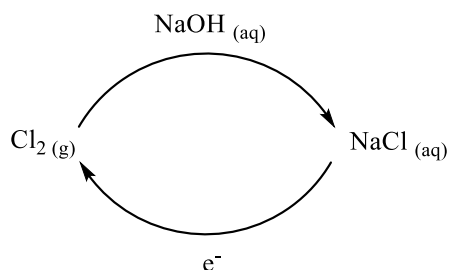
Scheme 33: Potential method for recycling chlorine gas, thus reducing waste.

In a brief proof of concept study, brine (~250g NaCl in 1L deionised water) was made in the lab and electrolysed in a Hoffmann Voltameter. Using this brine, it was possible to produce moderate quantities of chlorine gas (110 mL/h) on demand. The chlorine gas generated via this method (110 mL) was utilised for the photochlorination of toluene (1M, 5 mL) to generate the benzyl chloride, **4a**, in a low yield (10%) - **Scheme 34**. Whilst this yield is not as high as the reaction which used bottled chlorine gas, this method did show that this is viable for small scale photochlorination reactions to be conducted using chlorine produced from the electrolysis of brine.
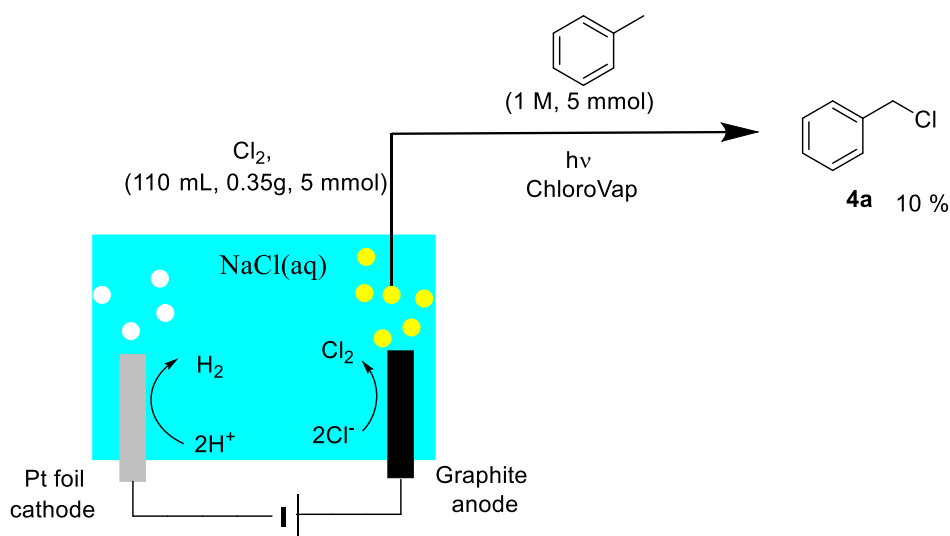
Scheme 34: Electrochemical production of chlorine gas from brine and use in a photochemical reaction to produce 4a

For amusement, seawater (100 mL, Skegness) was collected and electrolysed to assess the production rate of chlorine gas. Using seawater as the chloride source a small amount of chlorine gas was produced (5 mL in 20 mins). The reason for the lower quantity of chlorine being produced from seawater (15 mL/h) compared to that of brine (110 mL/h) is possibly due to seawater having a lower concentration of salt dissolved than in brine (~3.5 % vs. 25 % respectively).

This work showed that this method, whilst not perfect, has the potential to enable the laboratory chlorination of reagents in a controlled manner from safe and cheap starting material, brine. In this proof of principle study, it was possible to show that, with further optimisation, this may be a more atom efficient method of chlorination rather than using thionyl chloride and could be imagined in an analogous system to Thales Nano H-cube used to electrochemically generate hydrogen.

Conclusions

The focus of this work has been the development of a reactor which can easily perform photochlorination reactions on a laboratory scale. Once developed this "ChloroVap" reactor was used to conduct several test reactions on toluene. Following the synthesis of this test compound more complex starting materials were investigated. A highlight of this work was the rapid production of a key intermediate to the pharmaceutical compound of Plavix via an alternative method to the original synthesis. This was continued into the full synthesis of Plavix; however further work is needed to optimise the purification step of this API synthesis.

Once the key aims of the work had been achieved and demonstrated, the *in-situ* generation of chlorine was investigated though the electrolysis of brine. This was shown to be possible and gave the desired product when this chlorine was used in the ChloroVap to photochlorinate toluene, however the current equipment available was not able to generate chlorine at a high enough rate to be able to replace the chlorine cylinder in this system. This set up may be applicable to smaller scale systems or used in a flow process to utilise the chlorine as soon as it is made, similar to the work of Kappe and co-workers.

Bibliography

1.   Cantillo, D. & Kappe, C. O. Halogenation of organic compounds using continuous flow and microreactor technology. *React. Chem. Eng.* **2**, 7–19 (2017).
2.   Strauss, F. J., Cantillo, D., Guerra, J. & Kappe, C. O. A laboratory-scale continuous flow chlorine generator for organic synthesis. *React. Chem. Eng.* **1**, 472–476 (2016).
3.   Clayden, J., Warren, S. & Greeves, N. *Organic Chemistry*. (OUP, 2012).
4.   Oelgemöller, M. & Shvydkiv, O. Recent advances in microflow photochemistry. *Molecules* **16**, 7522–7550 (2011).
5.   Liu, S. *et al.* Highly selective halogenation of unactivated C(sp3)-H with NaX under co-catalysis

of visible light and Ag@AgX. *Green Chem.* **20**, 4729–4737 (2018).

6. Combe, S. H., Hosseini, A., Parra, A. & Schreiner, P. R. Mild Aliphatic and Benzylic Hydrocarbon C-H Bond Chlorination Using Trichloroisocyanuric Acid. *J. Org. Chem.* **82**, 2407–2413 (2017).

7. Zhang, L. & Hu, X. Room temperature C(sp2)-H oxidative chlorination: Via photoredox catalysis. *Chem. Sci.* **8**, 7009–7013 (2017).

8. Cox, R. A. & Swallow, A. J. The Chlorination and Bromination of Hydrocarbons under Infulence of High-energy Radiation and Other Initiating Agents. *J. Chem. Soc* 3727–3729 (1958).

9. Kharasch, M. S. & Brown, H. C. Chlorinations with Sulfuryl Chloride. I. The Peroxide-Catalyzed Chlorination of Hydrocarbons. *J. Am. Chem. Soc.* **61**, 2142–2150 (1939).

10. Borukhova, S., Noël, T. & Hessel, V. Hydrogen Chloride Gas in Solvent-Free Continuous Conversion of Alcohols to Chlorides in Microflow. *Org. Process Res. Dev.* **20**, 568–573 (2016).

11. Ehrich, H., Linke, D., Morgenschweis, K., Baerns, M. & Jähnisch, K. Application of microstructured reactor technology for the photochemical chlorination of alkylaromatics. *Chimia (Aarau).* **56**, 647–653 (2002).

12. Fukuyama, T., Tokizane, M., Matsui, A. & Ryu, I. A greener process for flow C-H chlorination of cyclic alkanes using: In situ generation and on-site consumption of chlorine gas. *React. Chem. Eng.* **1**, 613–615 (2016).

13. Clark, C. A., Lee, D. S., Pickering, S. J., Poliakoff, M. & George, M. W. UV PhotoVap: Demonstrating How a Simple and Versatile Reactor Based on a Conventional Rotary Evaporator Can Be Used for UV Photochemistry. *Org. Process Res. Dev.* **22**, 595–599 (2018).

14. Clark, C. A., Lee, D. S., Pickering, S. J., Poliakoff, M. & George, M. W. A Simple and Versatile Reactor for Photochemistry. *Org. Process Res. Dev.* **20**, 1792–1798 (2016).

15. Schmierer, T. *et al.* Femtosecond spectroscopy on the photochemistry of ortho-nitrotoluene. *Phys. Chem. Chem. Phys.* **12**, 15653–15664 (2010).

16. Greenlee *et al.* US5240938 (1993).

17. Astles, P. C. *et al.* Selective ET(A) antagonists. 5. Discovery and structure-activity relationships of phenoxyphenylacetic acid derivatives. *J. Med. Chem.* **43**, 900–910 (2000).

18. Saeed, A. *et al.* Developments in the synthesis of the antiplatelet and antithrombotic drug (S)-clopidogrel. *Chirality* **29**, 684–707 (2017).

19. Johnson, Sliskovic & Roth. *Contemporary drug synthesis.* (John Wiley & Sons, 2004).

20. Aubert & Maffrand. Thieno [3,2-c] pyridine derivatives and their therapeutic application. (1982).

21. Evans, R. W., Zbieg, J. R., Zhu, S., Li, W. & Macmillan, D. W. C. Simple catalytic mechanism for the direct coupling of α-carbonyls with functionalized amines: A one-step synthesis of plavix. *J. Am. Chem. Soc.* **135**, 16074–16077 (2013).

22. Sheldon, R. A. The: E factor 25 years on: The rise of green chemistry and sustainability. *Green Chem.* **19**, 18–43 (2017).

23. Ajvazi, N. & Stavber, S. Direct halogenation of alcohols with halosilanes under catalyst- and organic solvent-free reaction conditions. *Tetrahedron Lett.* **57**, 2430–2433 (2016).

24. Ding, R. *et al.* Treatment of alcohols with tosyl chloride does not always lead to the formation of tosylates. *Molecules* **16**, 5665–5673 (2011).

25. OoK, H. S. & Ho, C. S. T WO2007126258 (2007).

26. Li, Z. H. *et al.* N -Hydroxyphthalimide/benzoquinone-catalyzed chlorination of hydrocarbon C-H bond using N -chlorosuccinimide. *Org. Biomol. Chem.* **17**, 3403–3408 (2019).

27. Łażewska, D. *et al.* The computer-aided discovery of novel family of the 5-HT6 serotonin receptor ligands among derivatives of 4-benzyl-1,3,5-triazine. *Eur. J. Med. Chem.* **135**, 117–124 (2017).

28. Boddy, A. J. *et al.* Rapid Assembly of Saturated Nitrogen Heterocycles in One-Pot: Diazo-Heterocycle "Stitching" by N–H Insertion and Cyclization. *Angew. Chemie Int. Ed.* **58**, 1458–

1462 (2019).

29. Isabelle, A., Haurena, C., Gall, E. Le, Martens, T. & Ricci, G. 2-Chlorophenyl zinc bromide: A convenient nucleophile for the mannich-related multicomponent synthesis of clopidogrel and ticlopidine. *Molecules* **15**, 8144–8155 (2010).

Experimental

Experiment section content

Equipment and chemicals

All chemicals were purchased from commercial sources and used without further purification unless otherwise stated. The GC used was a Shimadzu GC-2010 fitted with a Supleco SPB70, 30 m length, 0.25 mm diameter, 0.25 μm particle size max temperature = 350 ^{o}C, GC column. The GC method used in this system was started at 50 °C which was increased to 300 °C over 10 mins and kept this temperature for a 5 mins.

The carrier gas: Helium at a flow rate of 40 ml/min H_2 flow = 40ml/min, Air flow = 400 ml/min.

Flash chromatography purification was typically conducted using a Teledyne ISCO Combiflash Rf flash chromatography system.

Electrolysis conducted using a Hoffmann Voltameter attached to digimess Concept series DC power supply HY3010.

Lamp UV/vis spectra was measured using a calibrated UV-Vis spectrometer (Ocean Optics) fitted with a cosine probe. NMR data was collected on a 400 MHz Bruker spectrometer and NMR data was processed using MestraNova software and the values are reported in ppm.

Reactor optimisation

General procedure for use for the ChloroVap

More detail is given in the SOP (see **Appendix**).

Toluene (5 mL, d = 0.867 g/mL, 47 mmol) was placed in a round bottom flask (1 L). This was attached

to the ChloroVap and chlorine gas (3 g, d = 3.2 g/L, 43 mmol) was added. This mixture was rotated at

150 RPM and then irradiated for 2.5 min using a 2 kW Mercury arc lamp. Following this the excess

chlorine was removed through the use of a water aspirator and by flowing nitrogen through the flask

for approx. 5 min. The product of this was filtered through $NaHCO_3$ then put onto GC and yield

calculated using a calibrated method against a commercial example of benzyl chloride. The

photochlorination process was repeated 1,2 or 3 times.

The temperature was initially controlled using a water bath at room temperature or heat to 50 °C.

To cool to – 50 °C the water in the bath was replaced with a dry ice/acetone mixture.

It was noted that prior to the photolysis the temperature was usually 20 °C however upon irradiation

for 2.5 min the temperature usually increased to approximately 90 °C.

Optimisation variations

A number of different parameters were varied using slight variations of the general procedure

described above. The variations made were:

- Irradiation time (1, 2.5, 5 or 10 mins).

- Variation quantities of chlorine added (1 g (14 mmol), 3 g (43 mmol) or 10 g (142 mmol))

- Summation of repeated chlorination (i.e., chlorine added, photolysis take place, excess

  chlorine removed – repeated up to three times).

- Flask size: 0.5 L, 1 L, or 3 L

- Water bath temperature (room temperature, 50 °C or – 50 °C)

- Concentration of toluene (neat (d = 0.867 g/mL, 47 mmol), 1M (5 mmol d = 0.867 g/mL, 0.53

  mL in 5 ml chloroform), 0.1M (0.5 mmol, d = 0.867 g/ml, 0.05 mL, in 5 mL chloroform)

Electrolysis of brine and use of chlorine for the photochlorination of toluene

A Hoffmann Voltameter (100 mL, graphite cathode, platinum foil anode) was filled with brine (NaCl saturated deionised water, ~36g/100 ml). This solution was electrolysis (0.5 A, 30 V, Direct current) for 1 hour to produce 110 mL (d = 3.2 g/L, 5 mmol) of chlorine gas. This gas was allowed to flow into the ChloroVap reactor, in the 1 L round bottom flask was toluene (0.32 mL, d = 0.867 g/mL, 3 mmol) dissolved in chloroform (5 mL). This was rotated at 150 RPM and then irradiated for 2.5 mins in the usual fashion. The resulting solution was analysed by GC.

Photochlorination reactions

4a - (chloromethyl)benzene
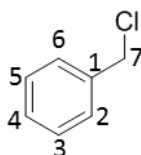
Following the general procedure, a mixture of toluene (0.42 mL, 0.36 g, d = 0.867 g/mL, 4 mmol, 1 M) and chloroform (4 mL) was reacted with chlorine gas (3 g, d = 3.2 g/L, 43 mmol). The crude reaction mixture has the excess solvent removed under *vacuo*. The crude mix was then dry loaded onto silica gel and purified using flash chromatography (petroleum ether: ethyl acetate 95:5). This gave an off-yellow oil of the desired product (0.2644 g, 52%).

^{1}H NMR (400 MHz, Chloroform-*d*) δ 7.45 − 7.29 (m, 5H (2-6)), 4.60 (s, 2H (7)).

^{13}C NMR (101 MHz, Chloroform-*d*) δ 137.6 (1), 128.9 (6/2), 128.7 (5/3), 128.6 (4), 46.43 (7)

GCMS [C_7H_7Cl] calc: 126.0, found: 126.1 and [C_7H_7]$^+$ calc: 91.0, found 91.2.

This matched with data reported by reference 23.

4b - 1-(chloromethyl)-2-nitrobenzene
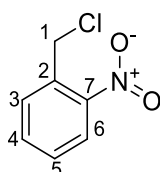
The general procedure was followed with 2-nitrotoluene (0.6 mL, d = 1.163 g/mL, 5 mmol) was dissolved in chloroform (5 mL) and reacted with chlorine gas (3 g, d = 3.2 g/L, 43 mmol). This chlorination step was repeated a further two times. Next, the reaction mixture had the excess solvent removed under *vacuo*. The crude mix was then dry loaded onto silica gel and purified using flash chromatography (cyclohexane: dichloromethane 95:5). This gave an off-yellow oil of the desired product (0.0615 g, 7%).

¹H NMR (400 MHz, Chloroform-*d*) δ 8.06 (dd, *J* = 8.2, 1.3 Hz, 1H (4)), 7.75 – 7.57 (m, 2H (3/5)), 7.51 (m, 1H (6)), 4.98 (s, 2H (1)).

¹³C NMR (101 MHz, Chloroform-*d*) δ 133.9 (4), 132.6 (7), 131.7 (3), 129.6 (5), 125.4 (6), 125.4 (2), 42.9 (1).

ESI MS: [$C_7H_8ClNO_2$]⁺ calc: 173.0, found: 173.0.

This matched with data reported by reference 24.

4c - 1-(chloromethyl)-4-nitrobenzene
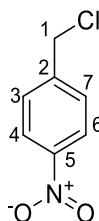
4-nitrotoluene (0.706 g, 5 mmol) was dissolved in chloroform (5 mL) and the process described above was repeated to give a white solid of the desired product (0.264g, 31%).

¹H NMR (400 MHz, Chloroform-*d*) δ 8.26 – 8.20 (m, 2H (4/6)), 7.60 – 7.54 (m, 2H (3/7)), 4.65 (s, 2H, (1)).

¹³C NMR (101 MHz, Chloroform-*d*) δ 144.4 (5/2), 129.5 (3/7), 124.1 (4/6), 44.7 (1).

ESI MS: [C_7H_7ClNO]⁺ calc: 156.0, found: 156.1.

This NMR matched with data reported by reference 24. The MS data varies slightly, possibly due to the difference in fragmentation of the ion during the ionisation processes.

4d - 1-(chloromethyl)-3-nitrobenzene
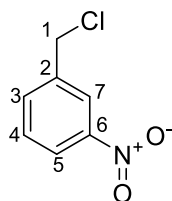
Similarly, to the previous two examples, 3-nitrotoluene (0.6 mL, d = 1.157 g/mL, 5 mmol) was dissolved in chloroform (5 mL) and photochlorinated in the ChloroVap and purified as before to give an off-yellow oil of the desired product (0.6407g, 74 %).
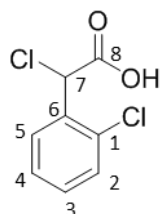
¹H NMR (400 MHz, Chloroform-*d*) δ 8.28 (s, 1H (7)), 8.20 (d, *J* = 7.8 Hz, 1H (5)), 7.74 (d, *J* = 7.7 Hz, 1H (3)), 7.56 (t, *J* = 7.9 Hz, 1H (4)), 4.67 (s, 2H (1)).

¹³C NMR (101 MHz, Chloroform-*d*) δ 148.5 (6), 139.5 (2), 134.6 (3), 129.9 (4), 123.6 (7), 123.5 (5), 44.7 (1).

ESI MS: $[C_7H_8ClNO_2]^+$ calc: 173.0, found: 173.0.

This NMR matched with data reported by reference 24.

4h - 2-chloro-2-(2-chlorophenyl)acetic acid

In this reaction 2-chlorophenyl acetic acid (0.862 g, 5 mmol) was dissolved in chloroform (5 mL) an exposed to chlorine gas (3 g, d = 3.2 g/L, 43 mmol) as described in the general procedure, with a threefold repetition in the chlorination step. The crude mix was then dry loaded onto silica gel and purified using flash chromatography (Hexane: ethyl acetate 25:75). This gave an off-yellow oil of the desired product (0.5525 g, 54%).

¹H NMR (400 MHz, Chloroform-*d*) δ 7.69 – 7.63 (m, 1H, (2)), 7.44 – 7.37 (m, 1H (5)), 7.35 – 7.29 (m, 2H (3/4)), 5.92 (s, 1H (7)).

^{13}C NMR (101 MHz, Chloroform-*d*) δ 171.9 (8), 133.6 (6), 133.5 (1), 130.7 (5), 129.9 (3/4), 127.7 (2), 55.3 (7).

ESI HRMS: $[C_8H_6Cl_2O_2Na]^+$ calc: 226.9877, found: 226.9623.

4i- methyl 2-chloro-2-(2-chlorophenyl)acetate
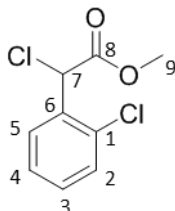
As above, 2-chlorophenyl acetic acid (0.445 g, 2.5 mmol) was dissolved in chloroform (5 mL) and reacted with chlorine gas (3 g, d = 3.2 g/L, 43 mmol) following the general procedure and this chlorination step was repeated a further two times.

Following this, methanol (5 mL) was added and further chlorine (3 g, d = 3.2 g/L, 43 mmol) was added and subsequently irradiated in the same manner as before. This formed a by-phasic mixture. The organic phase was extracted (chloroform 3 x 5 mL) and dried *under vacuo*.

The crude mix was then dry loaded onto silica gel and purified using flash chromatography (Hexane: ethyl acetate 90:10). This gave an off-yellow oil of the desired product (0.469 g, 86%).

^{1}H NMR (400 MHz, Chloroform-*d*) δ 7.66 – 7.60 (m, 1H (2)), 7.43 – 7.38 (m, 1H (5)), 7.35 – 7.28 (m, 2H (3/4)), 5.89 (s, 1H (7)), 3.80 (s, 3H (9)).

^{13}C NMR (101 MHz, Chloroform-*d*) δ 168.5 (8), 133.9 (6), 133.5 (1), 130.6 (5), 129.9 (3/4), 127.7 (2), 55.5 (7), 53.6 (9).

ESI HRMS: $[C_9H_9Cl_2O_2]^+$ calc: 218.9979, found: 218.9969.

This matched with data reported by ref 25.

4j - 1-chloro-2-(chloromethyl)benzene
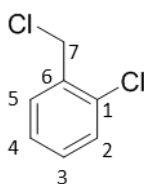
2-Chlorobenzene (0.63 mL, d = 1.11 g/mL, 6 mmol) was dissolved in chloroform (5 mL) and reacted with chlorine gas (3 g, d = 3.2 g/L, 43 mmol) in accordance with the general procedure. This gave the desired product (0.6132 g, 64 %) which was used for further reactions.

¹H NMR (400 MHz, Chloroform-*d*) δ 7.47 (dd, *J* = 5.8, 3.6 Hz, 1H (5)), 7.41 (dd, *J* = 5.6, 3.7 Hz, 1H (2)), 7.28 (dd, *J* = 5.9, 3.5 Hz, 2H (4/3)), 4.71 (s, 2H (7)).

¹³C NMR (101 MHz, Chloroform-*d*) δ 135.2 (1), 134.2 (6), 131.0 (5), 130.0 (2), 129.9 (3), 127.3 (4), 43.7 (7).

HMRS: $[C_7H_5Cl_2]^+$ calc: 158.9768 found:158.9641

This matched with data reported by reference 26.

Esterification reactions

Control experiments

2-chlorophenyl acetic acid (0.862 g, 5 mmol) was placed in a round bottom flask (1 L) and this was dissolved in various solvents (5 mL). This was attached to the ChloroVap and to this mix either chlorine gas (3 g, d = 3.2 g/L, 43 mmol) or hydrochloric acid (37 %, 1 mL, 12 mmol). This mixture was rotated at 150 RPM and then irradiated for either 0 or 2.5 mins using a 2 kW Mercury arc lamp. Following this the excess chlorine was removed through the use of a water aspirator and by flowing nitrogen through the flask for approx. 5 min.

In the examples where light was not used the temperature that the reaction was carried out at was initially room temperature in the other cases the reaction was conducted for 3 mins at 90 °C.

4l - methyl 2-(2-chlorophenyl)acetate
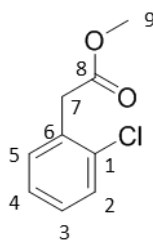
2-chlorophenyl acetic acid (0.862 g, 5 mmol) was dissolved in methanol (5 mL, d = 0.792 g/mL, 123 mmol) and exposed to chlorine gas (3 g, d = 3.2 g/L, 43 mmol) and then the general procedure was followed.

This formed a by-phasic mixture; the organic layer was seen to be a yellow oil of the desired product (0.741 g, 81%).
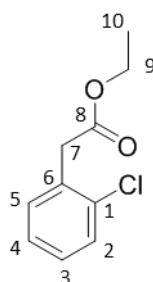
**^{1}H NMR** (400 MHz, Chloroform-*d*) δ 7.42 – 7.35 (m, 1H (5)), 7.29 (m, 1H (2)), 7.25 – 7.19 (m, 2H (3/4), 3.79 (s, 2H (7)), 3.72 (s, 3H (9)).

^{13}C NMR (101 MHz, Chloroform-*d*) δ 171.04 (8), 134.5 (1), 132.4 (6), 131.5 (5), 129.5 (2), 128.7 (4), 126.9 (3), 52.3 (9), 38.9 (7).

ESI HRMS: $[C_9H_{10}O_2Cl]^+$ calc: 185.0369, found: 185.0361.

This matched with data reported by reference 27.

4m- ethyl 2-(2-chlorophenyl)acetate

As with the previous example, 2-chlorophenyl acetic acid (0.862 g, 5 mmol) was dissolved in ethanol (5 mL, d = 0.789 g/mL, 85 mmol) and the previous method repeated.

This formed a by-phasic mixture; the organic layer was seen to be a yellow oil of the desired product (0.6878 g, 69%).

¹H NMR (400 MHz, Chloroform-*d*) δ 7.41 (m, 1H (5)), 7.32 (m, 1H (2)), 7.26 (m, 2H (3/4)), 4.22 (s, 2H (9)), 3.80 (s, 2H (7)), 1.30 (s, 3H (10)).

¹³C NMR (101 MHz, Chloroform-*d*) δ 170.8 (8), 134.5 (1), 132.4 (6), 131.7 (5), 129.4 (2), 128.7 (4), 126.9 (3), 61.5 (9), 39.6 (7), 14.3 (10).

This matched with data reported by reference 28.

Coupling reactions

Plavix - methyl 2-(2-chlorophenyl)-2-(6,7-dihydrothieno[3,2-c]pyridin-5(4H)-yl)acetate
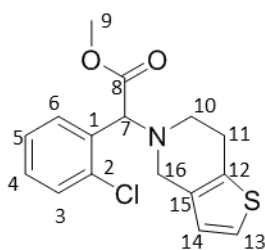
2-chlorophenyl acetic acid (0.445 g, 2.5 mmol) was dissolved in chloroform (5 mL) and reacted with chlorine gas (3 g, d = 3.2 g/L, 43 mmol) by following the general procedure. The chlorination step was repeated a further two times.

Following this, methanol (5 mL, d = 0.792 g/mL, 123 mmol) was added and further chlorine (3 g, d = 3.2 g/L, 43 mmol) was added and subsequently irradiated in the same manner as before. This formed a by-phasic mixture. The organic phase was extracted (chloroform 3 x 5 mL) and dried *under vacuo*.

This crude yellow oil was dissolved in dimethylformamide (5 mL) and potassium carbonate (0.75 g, 5 mmol) and 4,5,6,7-tetrahydrothieno[3,2-c]pyridine (250 mg, 1.4 mmol) was added. This solution was heated to 90 °C for 4 hours. Then water (10 mL) and dichloromethane (10 mL) were added and the organic layer separated. The organic layer was washed with water (10 ml x 5) and the organic mixture was dried over sodium sulphate. The orange solution was filtered and dried under *vacuo*. This gave a dark red oil which contained the crude product (328 mg).

¹H NMR (400 MHz, Chloroform-*d*) δ 7.73 (dd, *J* = 7.4, 2.2 Hz, 1H (3)), 7.43 (dd, *J* = 7.3, 2.1 Hz, 1H (6)), 7.30 (td, *J* = 7.1, 2.0 Hz, 2H, (4/5)), 7.07 (d, *J* = 5.1 Hz, 1H (13)), 6.69 (d, *J* = 5.1 Hz, 1H (14)), 4.95 (s, 1H (7)), 3.81 (d, *J* = 3.5 Hz, 1H (16)), 3.75 (s, 3H, (9)), 3.69 – 3.63 (m, 1H, (16)), 2.91 (s, 4H (10/11)).

¹³C NMR (101 MHz, Chloroform-*d*) δ 171.3 (8), 134.7 (1), 133.9 (2), 133.3 (12), 133.3 (15), 130.0 (3), 129.8 (4), 129.5 (5), 127.2 (6), 125.3 (13), 122.8 (14), 67.9 (7), 52.19 (9), 50.7 (10), 48.3 (16), 25.6 (11).

ESI HRMS: $[C_{16}H_{17}ClNO_2S]^+$ calc: 322.0668, found: 322.0679.

This matched with data reported by reference 21.

Ticlopidine - 5-(2-chlorobenzyl)-4,5,6,7-tetrahydrothieno[3,2-c]pyridine
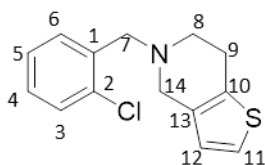
2-Chlorobenzene (0.63 mL, d = 1.11 g/mL, 6 mmol) was dissolved in chloroform (5 mL) and exposed to chlorine gas (3 g, d = 3.2 g/L, 43 mmol) in accordance with the general procedure.

The resulting crude yellow oil was dissolved in dimethylformamide (5 mL) and potassium carbonate (0.75 g, 5 mmol) and 4,5,6,7-tetrahydrothieno[3,2-c]pyridine (250 mg, 1.4 mmol) was added. This solution was heated to 90 °C for 4 hours. Then water (10 mL) and dichloromethane (10 mL) were added and the organic layer separated. The organic layer was washed with water (10 ml x 5) and the organic mixture was dried over sodium sulphate. The orange solution was filtered and dried under *vacuo*. This gave a dark red oil which contained the crude product (403 mg).

¹H NMR (400 MHz, Chloroform-*d*) δ 7.97 - 7.33 (m, 4H (3-6)), 7.08 (d, *J* = 5.1 Hz, 1H (11)), 6.72 (d, *J* = 5.2 Hz, 1H (12)), 3.83 (s, 2H (7)), 3.65 (s, 2H (14)), 2.95 – 2.84 (m, 4H (8/9)).

¹³C NMR (101 MHz, Chloroform-*d*) δ 136.3 (1), 134.0 (13), 133.6 (10), 131.1 (2), 130.7 (6), 129.6 (4), 128.4 (3), 126.9 (5) 125.4 (11), 122.8 (12), 58.6 (7), 53.3 (14), 50.9 (8), 25.7 (9).

ESI HRMS: $[C_{16}H_{17}ClNO_2S]^+$ calc: 264.0613, found: 264.0622.

This matched closely with data reported by ref 29.

Appendix

Chlorovap Standard operating procedure

<u>Modified rotary evaporator for photochemical chlorination Standard Operating Procedure</u>

<u>Introduction</u>

A standard rotary evaporator has been modified to allow the photochemical chlorination reactions to be carried out. This new device has been termed the "ChloroVap" and is shown below.
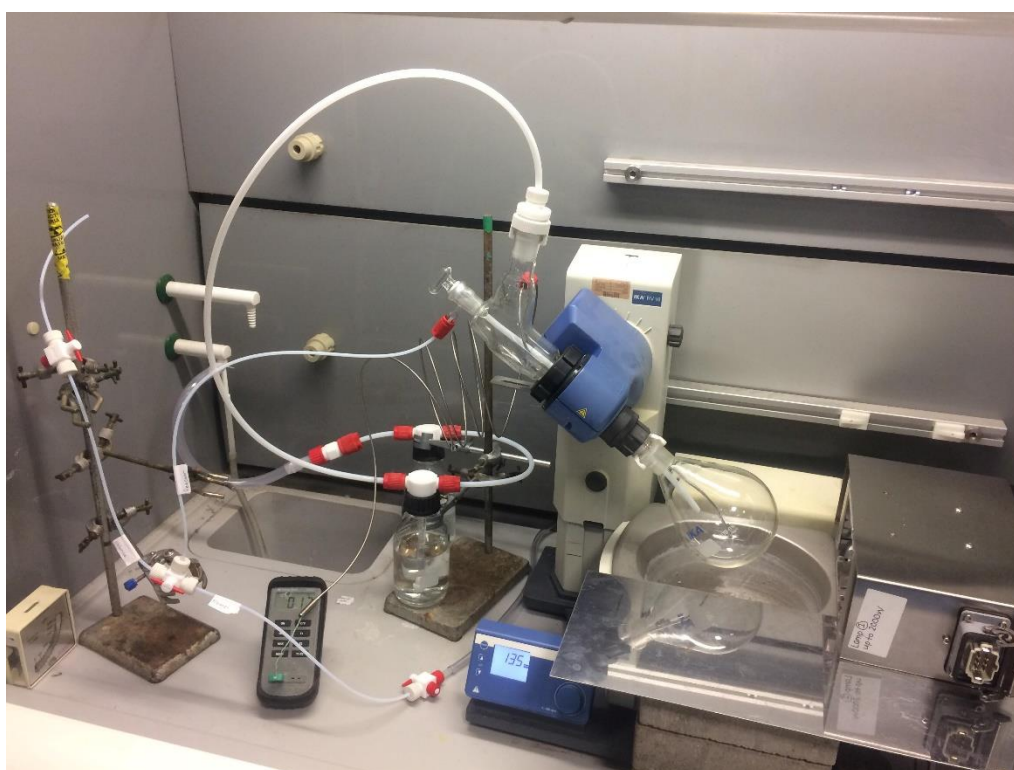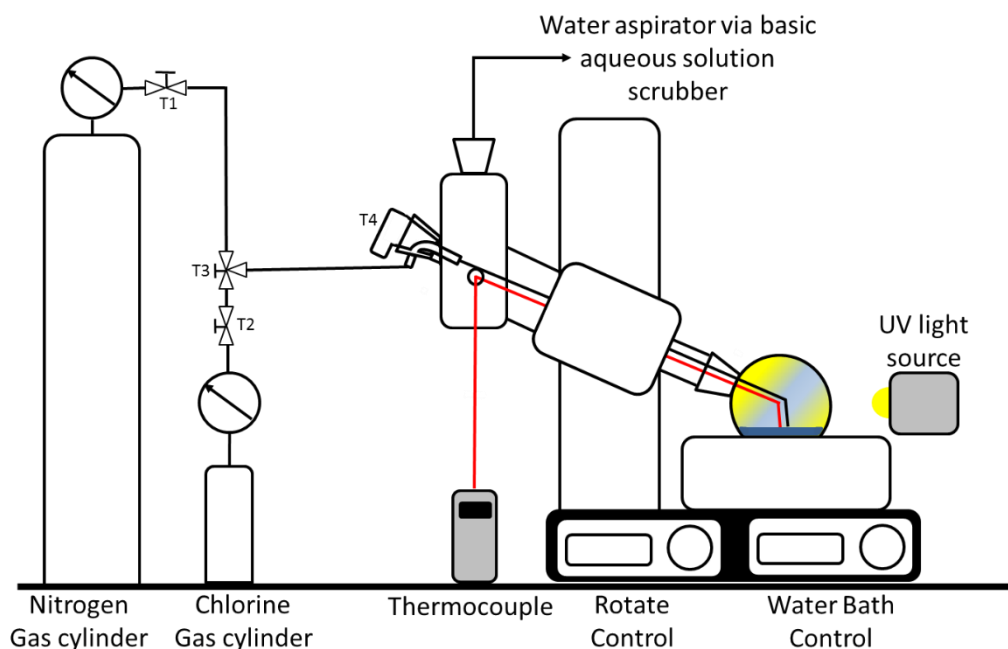

Figure 36: Image of ChloroVap

Figure 37: Schematic diagram of ChloroVap

Use of ChloroVap

BEFORE STARTING EXPERIMENT CHECK FUMEHOOD IS WORKING CORRECTLY AND THERE

ARE NO NOTICES RELATING TO THE POTENTIAL RELEASE OF TOXIC CHEMCIALS

Pre reaction work

1. Fill in all safety forms and read all relevant documents.
2. Fill water bath with deionised water.
3. Check scrubber bottles are filled with basic solution (0.1 N potassium hydroxide solution) with the addition of universal indicator to determine the pH of the solution.
4. Pressure and vacuum test all joints and taps (using snoop or a bucket of water).
5. Test Thermocouple and temperature monitor to check they are working.
6. Check Nitrogen gas pressure levels.
7. Fill round bottom flask with desired quantity of reaction reagents and attach using an PTFE coated steel clip.
8. Check thermocouple is inside reaction solution.
9. Open all stop cocks and taps (T1, T2 and T4).
10. Set the three-way valve (T3) to only allow chlorine into the reactor (follow impressions on tap).
11. Place the gas cylinder onto a balance and record the mass of the cylinder before the experiment.
12. Attach high powered Mercury arc lamps to power supply (see UV PhotoVap HAZOP).
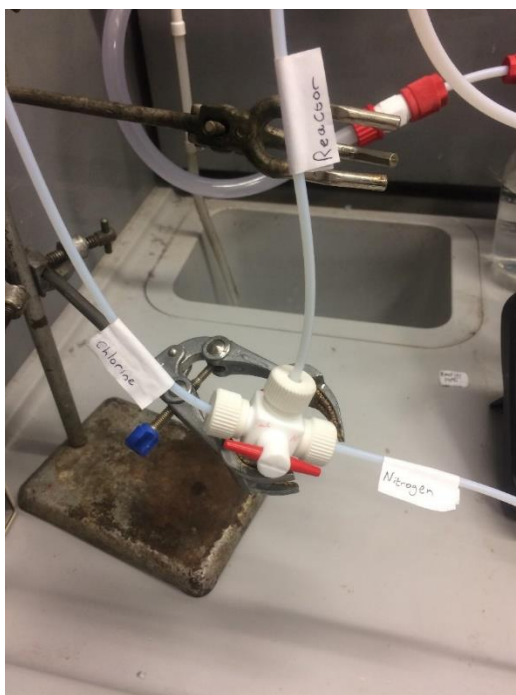
Reaction

1. Turn or rotary device of rotary evaporator to desired revolution per min rate (150 RPM).
2. Check all taps and stop cocks are open and the three-way valve is set to allow chlorine into the reactor.
3. **Slowly**, open chlorine regulator to allow chlorine gas into reactor.
4. Allow round bottom flask to fill to desired level with chlorine gas (chlorine mass can be determined by difference in cylinder weight).
5. Close chlorine regulator to allow no more chlorine into the reactor.
6. Place red plastic sheeting in place.
7. Turn on UV light source (UV PhotoVap HAZOP).
8. Allow reaction to occur.
9. Turn off UV light source (UV PhotoVap HAZOP).

Post reaction work

1. Remove red plastic sheeting.
2. Turn on water aspirator to remove excess chlorine gas.
3. Once most of the chlorine gas appears to have been removed, turn three way tap to allow nitrogen into the reactor alone and turn on nitrogen flow.
4. Repeat process until all excess chlorine gas has been removed.
5. Once all chorine gas been removed turn off nitrogen flow and water aspirator.
6. **Carefully** remove clip and round bottom flask to collect product.
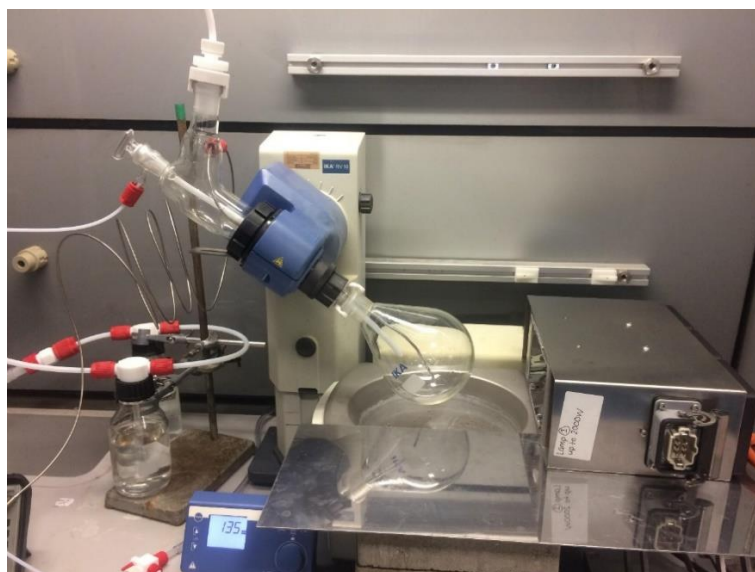
In case of emergency

Turn off power to light source but leave water aspirator on.

If there is a small chlorine leak turn off gas flow at regulator and wait until gas has dissipated before

fixing issue.

If there is a large chlorine leak close fume hood door and leave until all gas has dissipated.
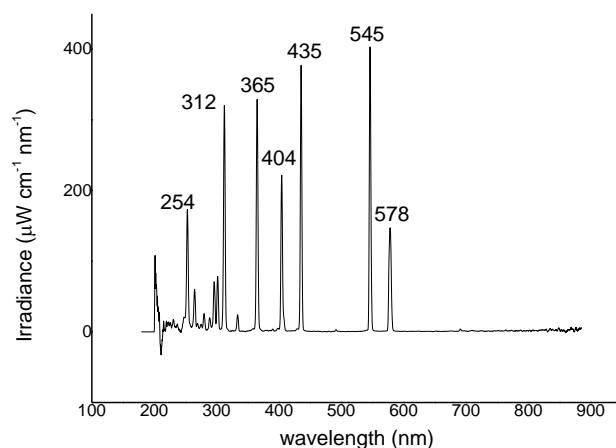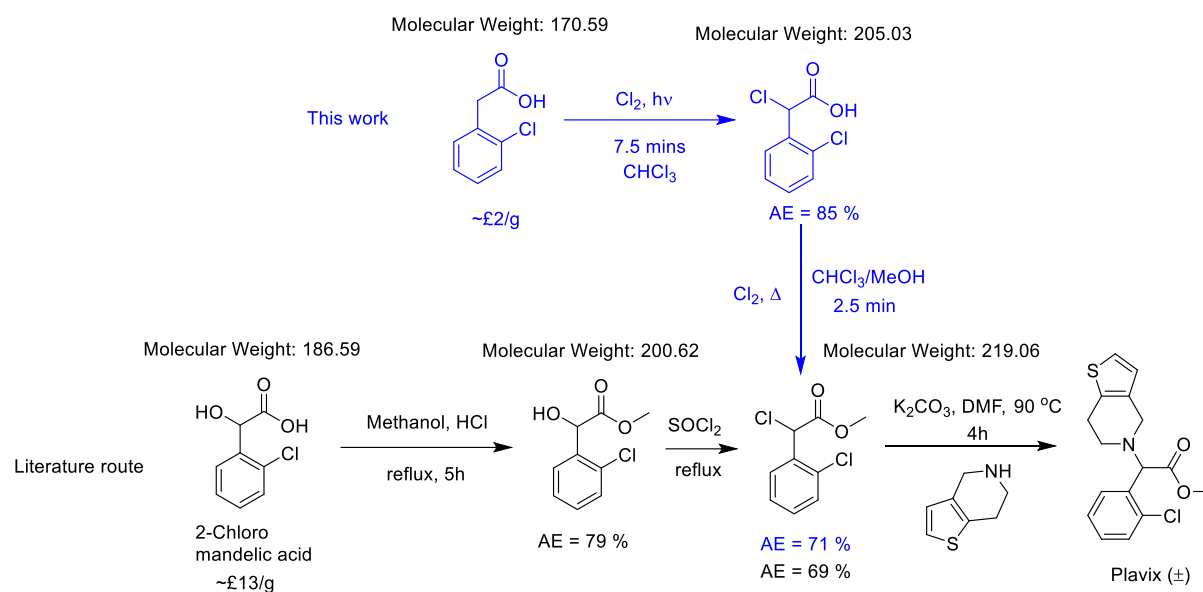
ChloroVap Lamp output spectrum

Figure 38: UV/vis spectrum of (2kW) medium pressure mercury arc lamp (at 20 % power) left for 30 seconds to reach equilibrium, measured using a calibrated UV-Vis spectrometer (Ocean Optics) fitted with a cosine probe, 20 cm from lamp.

Metric calculations

Atom efficiency calculations of 4i

Atom efficiency of this work:

Step 1:

$$AE\ (\%) = \frac{205}{171 + 71} x\ 100 = 85\ \%$$

Step 2:

$$AE\ (\%) = \frac{219}{205 + 71 + 32} x\ 100 = 71\ \%$$
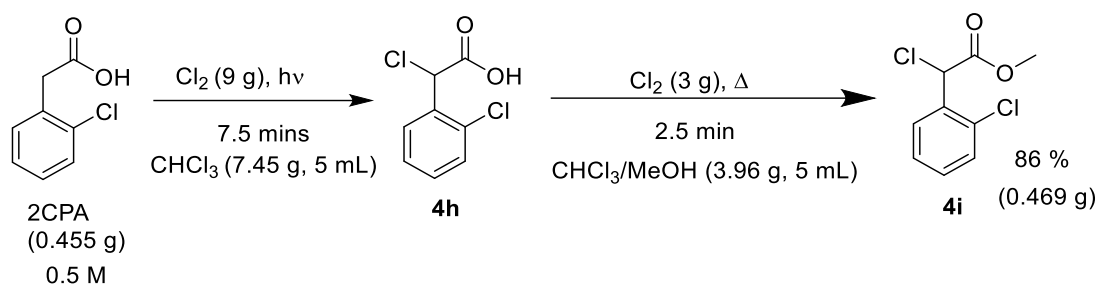
Atom efficiency of literature process:

Step 1:

$$AE\ (\%) = \frac{201}{187 + 36 + 32} x\ 100 = 79\ \%$$

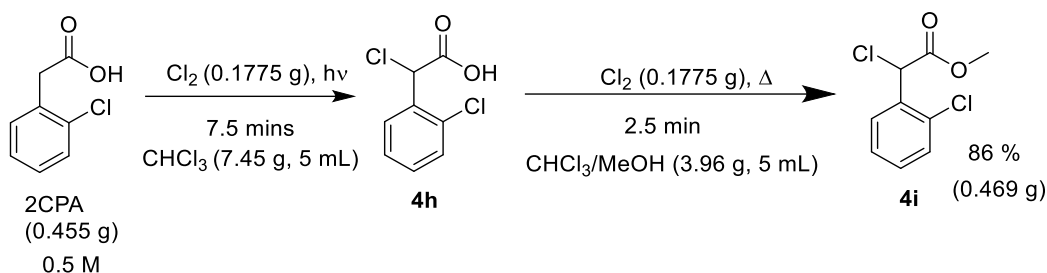Step 2:

$$AE\ (\%) = \frac{219}{201 + 119} x\ 100 = 69\ \%$$

E-factor of 4i

$$E - factor\ (with\ chorine\ gas) = \frac{((9 + 3 + 7.45 + 3.96 + 0.455) - 0.469)}{0.469}$$

$$E - factor\ (with\ chorine\ gas) = \frac{23.4}{0.469}$$

$$E - factor\ (with\ chlorine\ gas) = 49.88$$

$$E - factor\ (with\ chorine\ gas\ recycling) = \frac{((7.45 + 3.96 + 0.455 + (0.1775\ x\ 2)) - 0.469)}{0.469}$$

$$E - factor\ (with\ chorine\ gas\ recycling) = \frac{11.75}{0.469}$$

$$E - factor\ (with\ chorine\ gas\ recycling) = 25.1$$

Chapter 4- Bioderived solvents applied to photochemical reactions

Introduction

Current reserves of fossil fuels are diminishing but, for the last 50 years, the chemical industry has been heavily reliant on these resources for raw materials, particularly for solvents to conduct reactions.[1,2] One possible option for greater sustainability is for these processes to be conducted with an increased use of biologically derived materials[1-4]– see **Figure 39**.
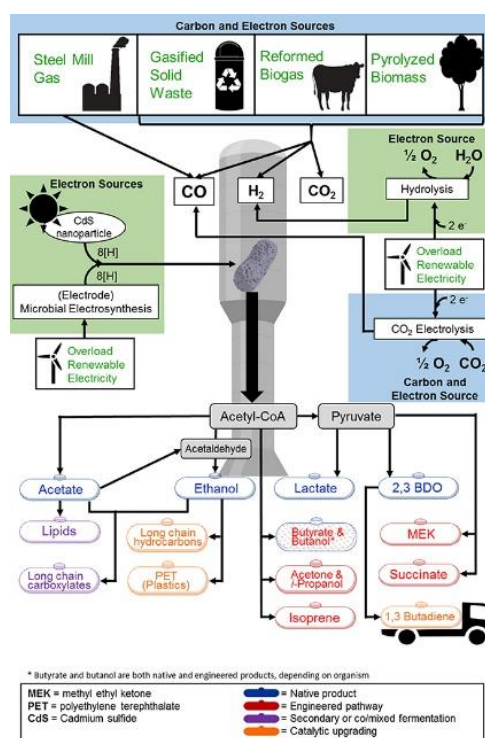

Figure 39: Simple diagram depicting the pathways by which key chemical building blocks can be synthesised from biological sources. The large array of potential chemical feedstocks is noteworthy in this image. Image taken from Reference 3

An area of research interest, for the production of pharmaceutical ingredients, is the replacement of fossil fuel-based solvents with more benign alternatives.[5] As solvents typically constitute approximately 90% of the non-aqueous mass required to make a drug[5,6] there is great industrial

interest in solvent choice. This is further exemplified by the number of greener solvent guides produced by leading pharmaceutical companies such as: GSK[5], AstraZeneca[7] and Pfizer[8]. By combining the industrially led desire for the use of less harmful solvents, with biologically derived options, a significant impact could be achieved by moving away from the continued use of fossil fuel focused resources.

There are many possible biologically derived solvent options available for chemical reactions - **Figure 40**.[1,3,4,9] However, when applied to photochemical reactions there are a number of specific factors which must be considered in addition to solubility. The first is that the solvent should not absorb the light required to conduct the photochemical reaction. This is easily ascertained by measuring the UV/vis absorption spectrum of the new bioderived solvent. Next, is that the solvent should not react with either the starting material, excited states, transition states or products of the chosen photochemical reaction. These two factors render a number of these biologically derived solvents unsuitable for photochemical reactions but do present several options which can be explored. Furthermore, if a specific bioderived solvent does not provide the desired characteristics, it might be possible to use a mixture of two or more solvents to meet the necessary requirements. Recently, Inomata *et al.* proposed using more benign solvent mixtures to solubilise Active Pharmaceutical Ingredients (API) and allow safer downstream processing.[10] In their work, they discuss utilising the Kamlet-Taft parameters to obtain solvent mixtures which mimic the solubility properties of standard solvents. This opens the possibility of utilising their approach to identify an array of solvent combinations, where individual solvents may be unsuitable to be used by themselves for photochemical reactions but together are able to meet the desired requirements.

So, could comparing the Kamlet-Taft parameters be a suitable method for guiding researchers to replacements of conventional solvents by bioderived alternatives?
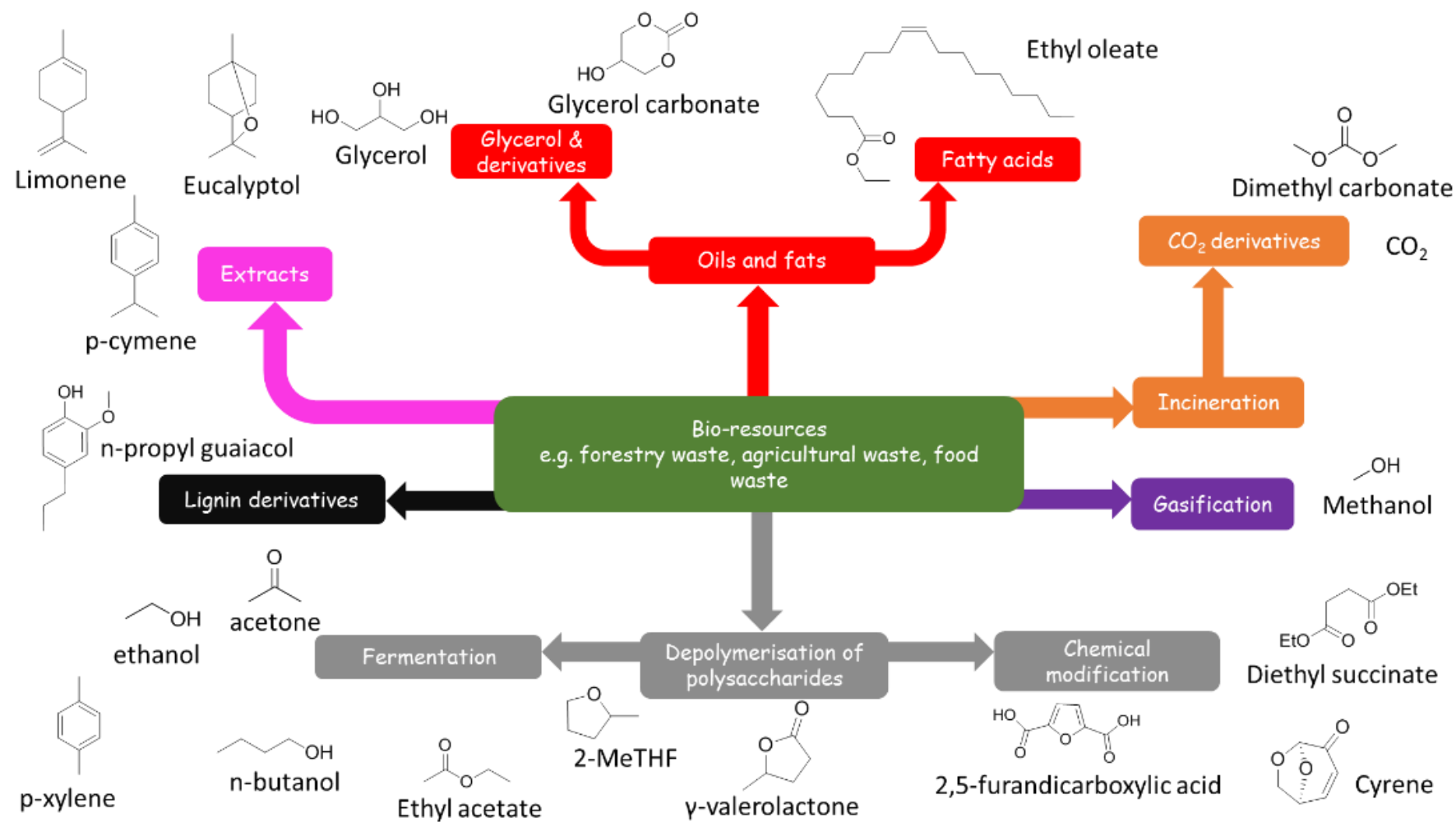
Figure 40: A selection of bioderived solvents which could be used in chemical reactions. Whilst there are a vast number of solvents available, this is constrained by the requirements of photochemical reactions solubility of the reagents and products. Adapted from Reference 8.

Kamlet-Taft Parameters

When comparing solvents there are a large number of scales which could be employed.[10,11] Some of

these scales can be measured physically such as boiling point, dielectric constant and density. This

has resulted in a large library of data for pure solvents being available.[11] However, when

investigating novel solvent mixtures, for which there is little data available, the scale proposed by

Kamlet and Taft can be easily applied. The Kamlet-Taft parameters are a comprehensive solvent

scale which quantify a solvent's dipolarity/polarizability (π^*), hydrogen bonding acceptor ability (β)

and hydrogen bonding donor ability (α).[12–16] The Kamlet-Taft values quantify the interactions

between solvent and solute by using a spectroscopic probe to measure the effect of that solvent on

the probe, with reference to a solvent which does not affect the probe.[13] In essence, the Kamlet-Taft

parameters measure the solvatochromic effect of a solvent on a probe through hydrogen bonding or

polarizability of the solvent. At the start of the work in this Thesis, the Kamlet-Taft parameters were

not known for the desired bioderived solvent mixtures; therefore, these were measured, using a

number of spectroscopic probes – see **Appendix** for details.

A more complex comparison method, Linear Solvation Energy Relationship (LSER), may also hold

promise.

Linear solvation energy relationship (LSER)

$$Log\ K = Log\ K_o + p\pi^* + a\alpha + b\beta + h(\delta_H)$$

Equation 4: Linear solvation energy relationship (LSER) equation. K = rate constant, π^* = polarizability, α = ability of solvent to donate a proton, β = ability of solvent to accept a proton, δ_H = Hildebrand solubility parameter. K_o, a, s, b, h = solvent independent coefficients characteristic of the process and indicative of the rate constant.

Linear solvation energy relationship (LSER), **Equation 4**, was first suggested by Kamlet, Taft and

Abboud in 1977[16] and then developed further by them throughout the 1980s.[17,18] Since that time,

LSER has been applied to a number of cases to aid in the explanation of solvent effects on the rates

of chemical reactions.[19–21] In their work, Kamlet and Taft, suggest that the rate of a particular reaction is heavily reliant on the solute-solvent relationship. They go on to propose that the rate of a chemical reaction is highly dependent on associated factors (K_o, p, a, b, h) of each characteristic solvent parameter (π^*, α, β, δ_H) of a solvent – **Equation 4**. This implies that, once these associated factors (K_o, p, a, b, h) have been determined, the rates of chemical reactions, in any solvent where the Kamlet-Taft parameters are already known, can be readily predicted by the LSER approach.

In addition to the π^*, β and α values already discussed LSER includes the Hildebrand solubility parameter, δ_H, which is a measure of the solvent-solute interactions that are interrupted in creating a solute cavity in the solvent – **Equation 5**. [19, 22] This adds a further consideration to Kamlet and Taft's LSER work beyond the hydrogen bonding nature and polarizability of the solvent by including a consideration of the energy required to reorganise the solvent cage around the solute necessary to allow a reaction to occur.

$$\delta_H = \sqrt{\frac{\Delta H_V - RT}{V_m}}$$

Equation 5: Hildebrand solubility parameter calculation ΔH_v = enthalpy of vaporisation, R = ideal gas constant, T = Temperature, V_m = molar volume.

In the case of binary mixtures of solvents, δ_H is relatively easily calculated,[22] by the summation of the two δ_H of the solvent in proportion to the volume fraction – **Equation 6**.

$$^{i,j}\delta = \frac{^i\emptyset \; ^i\delta + \; ^j\emptyset \; ^j\delta}{^i\emptyset + \; ^j\emptyset}$$

Equation 6: Hildebrand-Scathard equation of Binary mixtures, $^i\Phi$ = volume fraction of solvent i, $^i\delta$ = Hildebrand parameter of solvent i.

LSER has been applied to a number of photochemical reactions. Bensasson *et al.* utilised LSER to investigate the [4+2]-cycloaddition of photogenerated singlet oxygen with 1,4-Dimethylnaphthalene.[19] In that work they showed that the use of LSER for their reaction across 28 different solvents resulted in high levels of agreement between the logarithm of the experimentally derived rate constant and the calculated rate constant - **Figure 41**. More recently Gutiérez showed

that LSER was a useful technique when considering the quenching of the excited singlet state of oxygen by a range of *p*-quinones in an array of solvents (methanol, ethanol, n-butanol, acetone, benzene etc.).[21]
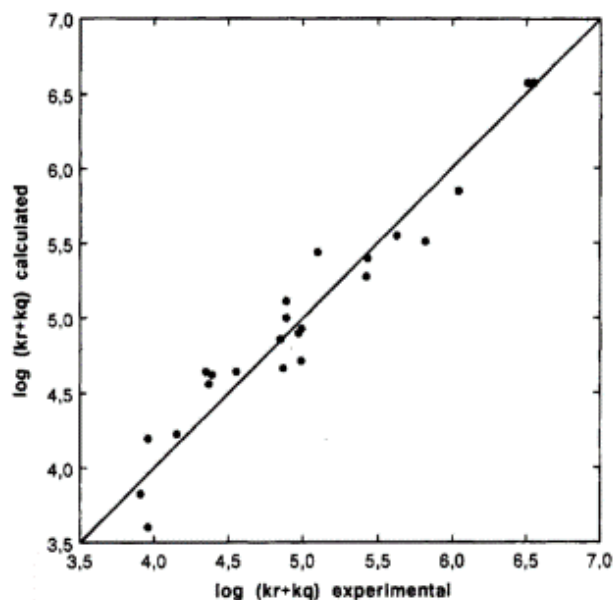

Figure 41: Double-logarithmic plot of reactions rate constants (calculated vs. experimental) of singlet oxygen with 1,4-Dimethylnaphthalene in various solvents to make the endoperoxide product using LSER. Taken from Reference 19.

Aims

The first aim of this work is to determine whether photochemical reactions can be conducted in bioderived solvents (BDS) and, if so, how this compares to the same reaction conducted in crude oil-based solvents (COBS). Following this, the second aim will be to assess whether the Kamlet-Taft (KT) parameters could be used to identify a BDS capable of mimicking a COBS and be used as a replacement, resulting in similar yield/rate of reaction. The third aim will be to probe binary mixtures of BDS to assess whether any have the correct properties to potentially replace COBS for photochemical reactions. The fourth and final aim is to explore whether LSER can be applied to the data collected and be able to predict the rate of photochemical reactions within an untested bioderived solvent(s).

Strategy

Strategy to answer Aim 1:

Identify a number of well-studied photochemical reactions and conduct them in COBS (e.g., acetonitrile, dichloromethane etc.) then repeat the same conditions in a selection of BDS (e.g., xylene, ethanol, dimethyl carbonate). The results will be used to compare and contrast between the reactions run in COBS and BDS to identify any potential replacements.

Strategy to answer Aim 2:

Conduct a literature search of known Kamlet Taft solvents in use, measure the KT values which are not known. Compare the reactions already run in COBS with reaction run in BDS with similar KT parameters, if necessary/possible conduct further reactions in BDS with the similar KT values. Use these values to assess the use of KT values as a solvent replacement method.

Strategy to answer Aim 3:

Repeat strategy applied to aim 2 however in this instance using binary mixtures of BDS.

Strategy to answer Aim 4:

Use the reaction rates determined in several previously conducted photochemical reactions to calculate LSER predetermined factors and apply these factors to the same reaction enabling the prediction of reaction rates in untested solvents. Then repeat the reaction in a selection of untested solvents to check the validity of the LSER method.

Results and Discussion

Single component system: *Intramolecular [2+2] photocyclisation*

100 mM
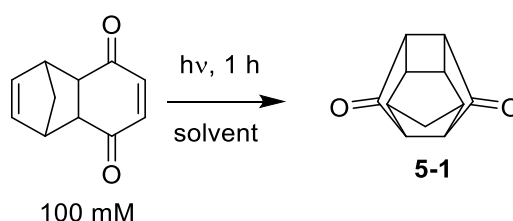
Scheme 35: Photochemical [2+2] photocyclisation of Cookson's Dione.

128

The first reaction that these parameters were applied to was the intramolecular photochemical reaction to form Cookson's dione – **Scheme 35**. This reaction was chosen as it is a simple intramolecular [2+2] photochemical reaction which has been studied within the Nottingham group. Additionally, the reaction produces a single product which can be easily identified through the use of NMR spectroscopy, allowing the reaction to be monitored through the use of this technique – a method previously used by Clark et al.[23]

The reaction set up, in this first solvent reaction study, was in an immersion well reactor and the solution was irradiated using a mercury arc lamp. To allow the reaction rate to be monitored (1 mL) samples were collected every 10 mins over the course of the experiment (1-hour, total reaction volume = 100 mL).
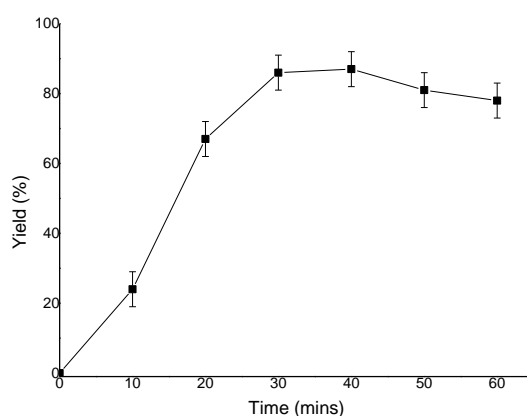

Figure 42: Reaction yield of the photocyclization of Cookson's Dione conducted in dichloromethane.

Looking at **Figure 42**, it is possible to see that there is an initial lag phase over the first 10 mins for the curve, as the lamp warms up, then the reaction progressed in a more linear manner, and finally reaches a plateau. The final point is that towards the end of the experiment the reaction yield begins to drop. This may be due to a small amount of photodegradation of the product taking place as the solution was irradiated for an extended period. The evidence for this was the formation of a thin film of reactor fouling seen on the reactor flask after the reaction.

The reaction was then repeated in another COBS, acetonitrile, and two BDS, dimethyl carbonate and
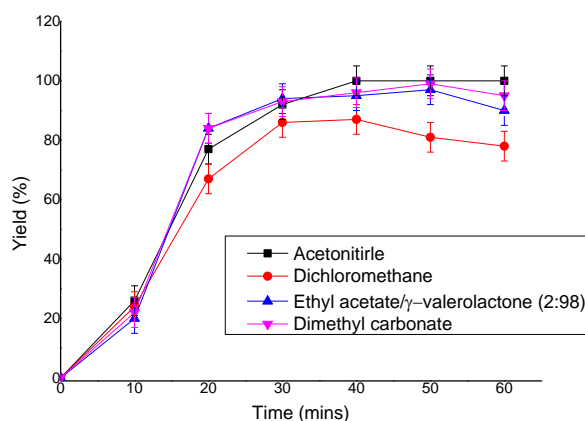
γ-valerlactone/ethyl acetate, see **Figure 43**.

It is clear from **Figure 43** that the rates of the reaction in all four solvents are broadly similar. The

first part of each reaction was approximately linear, as might be expected for a zero-order reaction

where the rate of reaction depends on the intensity of the light rather than the concentration of the

reactant, an effect which has been observed in other photochemical reactions.[24] This allows a very

approximate value for the rate of the reaction to be obtained as indicated in the reaction in
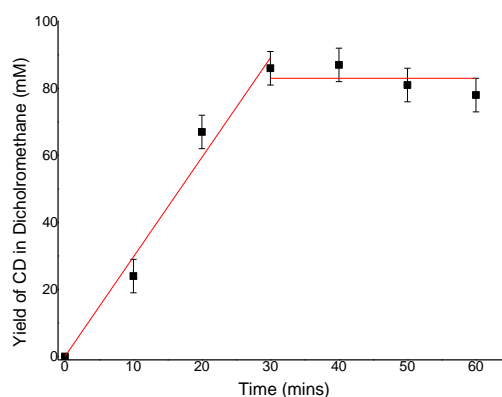
dichloromethane.

Figure 44: Photocyclization of Cookson's Dione conducted in dichloromethane with linear increase (left) and plateau section (right).

A similar analysis can be applied to the other solvents, **Figure 45** and the values are summarised in

Table 1, which also shows the Kamlet-Taft parameters for the solvents. Two key points emerge from

this Table.

1. The reaction can be carried out equally successfully in the bio-derived and conventional

   solvents.

2. There is no obvious correlation between the rates of the reaction in the four solvents which

   are essentially identical, and the Kamlet-Taft parameters of those solvents which are
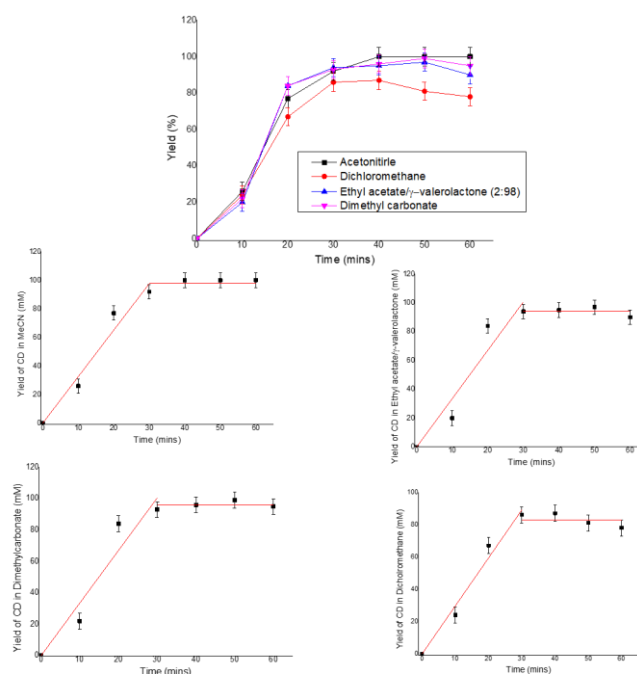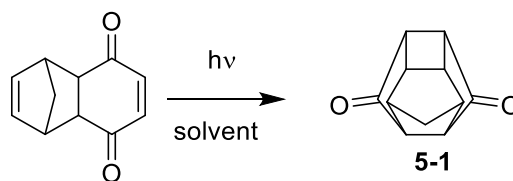
   significantly different.

Figure 45: Linear analysis of Cookson's dione production

Table 15: Comparison of KT parameters and reaction rates for the intramolecular [2+2] reaction of Cookson's Dione in various solvents.


Solvent	π^*	B	α	Reaction rate[#] (mM/min)
Dichloromethane	0.82	0.1	0.13	3 ± 0.2
Dimethyl carbonate	0.51	0.43	0.13	3 ± 0.3
γ-valerlactone/Ethyl Acetate (2:98)	0.82	0.45	0	3 ± 0.3
Acetonitrile	0.66	0.4	0.19	3 ± 0.2

[#]average taken over the first 30 mins of the reaction

This lack of correlation between reaction rate and Kamlet-Taft parameters may be due to the fact that this reaction is intramolecular, meaning that the influence of the solvent may be small. As mentioned above, the dominant factor in determining the rate is likely to be the intensity of the lamp. However, these experiments are encouraging in that they indicate the viability of bio-derived solvents for at least some photochemical reactions. It was then decided that a more complex reaction was needed to be tested. To this end, an intermolecular [2+2] photochemical reaction was selected, as it was believed that the rate of such a reaction might be more strongly influenced by the nature of the solvent.

Two component system: *Intermolecular [2+2] photocycloaddition*

The [2+2] photocycloaddition of tetrahydrophthalic acid anhydride (THPAA) and propargyl alcohol was investigated. - **Scheme 36**.
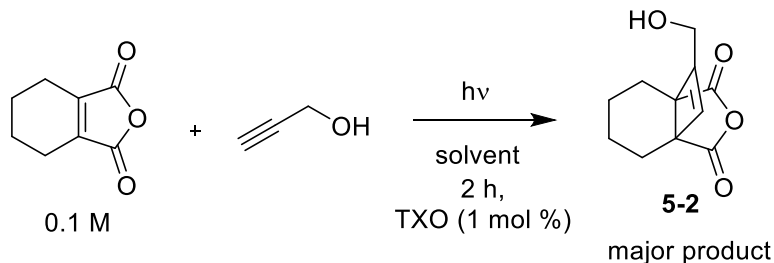
Scheme 36: Intermolecular [2+2] photocycloaddition of THPAA and propargyl alcohol to a bridged product (5-2)

Acetonitrile was chosen as the conventional solvent to benchmark the rate. Next, the reaction was repeated in three pure solvents or binary solvent mixtures which could be bioderived and have Kamlet-Taft parameters close to those of acetonitrile. The results from these experiments are shown in **Figure 46** and the reaction rates, derived from an analysis similar to that described previously, are summarised in **Table 16**. In a similar fashion to the intramolecular reaction above, this reaction also appears to show approximately zero order kinetics, even though it might be expected that there would be some influence on the reaction rate from differences in diffusion rates in the solvent due to differences in viscosity.
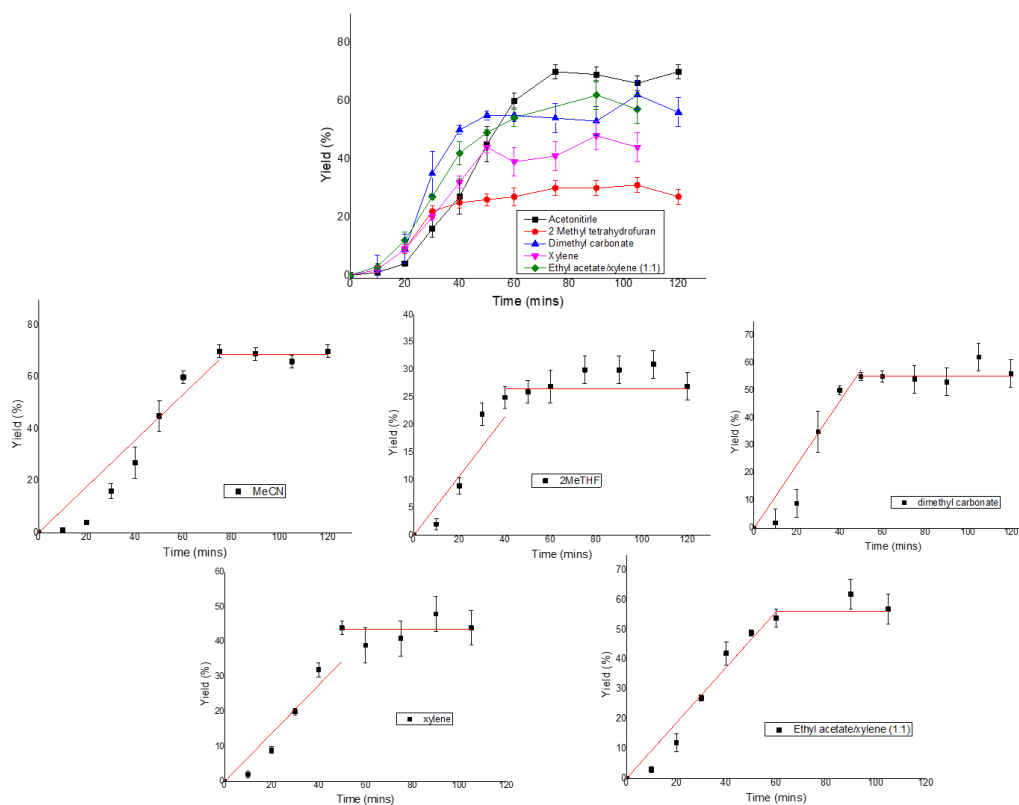
Figure 46: Linear analysis of bridged product

Table 16: Kamlet-Taft and Hildebrand parameters for each solvent used with the photochemical reaction of THPAA and propargyl alcohol along with linear section reaction rate.
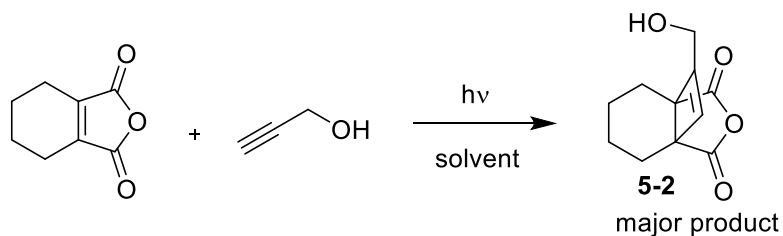
Solvent	π*	β	α	Reaction rate (mM/min)
Acetonitrile	0.66	0.4	0.19	1.0 ± 0.1
Ethyl Acetate/Xylene (1:1)	0.6	0.4	0	1.0 ± 0.1
Dimethyl carbonate	0.51	0.49	0.13	1.2 ± 0.1
2 Methyl tetrahydrofuran	0.48	0.48	0	0.5 ± 0.1
Xylene	0.51	0.1	0	0.7 ± 0.1

The first bioderived solvent was a blend of ethyl acetate and xylene in a 1:1 (v/v) mixture. This was done because this blend had been measured to have Kamlet-Taft π* and β values (See **Appendix**) very similar to that of acetonitrile (0.6, 0.4 vs. 0.66, 0.4 respectively). The data in **Table 16** and **Figure 46** indicate that the reaction in a mixture of ethyl acetate/xylene (1:1), gave similar results to acetonitrile. This result may be showing that the Kamlet-Taft parameters could be used as a guide for the replacement of COBS with BDS without significant impact on the reaction rate.

Following this reaction, the experiment was repeated in dimethyl carbonate. This solvent also has π*, β and α values close to acetonitrile (0.51, 0.49, 0.13 vs. 0.66, 0.4, 0.19 respectively). However, there was a modest increase in the reaction rate. This suggests that the small difference between the Kamlet-Taft parameters of the two solvents may be enough to affect the reaction rate.

The reaction was then performed in xylene and 2 methyl tetrahydrofuran (2MeTHF). These were chosen because their Kamlet-Taft parameters are somewhat different from those of acetonitrile. Both of these BDS had lower rate of reaction to acetonitrile. This could be the result of these two solvents having very different Kamlet-Taft values and could support the use of the Kamlet-Taft parameters as a solvent replacement method. However, caution should be taken when analysing these results. Xylene has a strong absorption band (λ_{max} = 280 nm) and may be reducing the amount of UV light being absorbed by the substate and hence reducing the reaction rate. The reason why the reaction run in 2MeTHF had a surprisingly low yield, could also be due to absorption of UV, although 2MeTHF does not itself absorb strongly. However, it does contain a stabiliser butylated hydroxytoluene (BHT) which is added to the 2MeTHF to prevent free radical formation. This stabiliser could be absorbing UV or directly interfering in the free radical mechanism of the reaction. From this set of experiments, two points became apparent:

- Conducting the reaction in two solvents with very similar Kamlet-Taft parameters resulted in very similar reactions rates.

- Reactions performed in solvents where the Kamlet-Taft parameters are significantly different gave dissimilar reaction rates, although there are several possible explanations for the differences.

As an intermolecular photochemical reaction had been examined and an apparent solvent exchange identified (acetonitrile for ethyl acetate/xylene (1:1)) the reaction complexity was increased once again to look at an intermolecular reaction which included a gaseous component.

Three component system: *Photooxidation of citronellol*

The system examined next was the photooxidation of citronellol. The reaction has been studied extensively within the Nottingham group[24,25] because it is one of the industrial methods for the production of Rose oxide - a high value fragrance molecule.[26] This reaction is still frequently studied due to the production of several different peroxide isomers which give rise to unwanted side products, and there is interest in improving the selectivity of this reaction.

This reaction begins with the photosensitiser absorbing light and becoming excited. After intersystem crossing to the triplet state, the energy is transferred from the photosensitiser to oxygen causing it to change from the triplet ground state to singlet oxygen, $^1O_2$ – a highly reactive species – **Figure 47**.
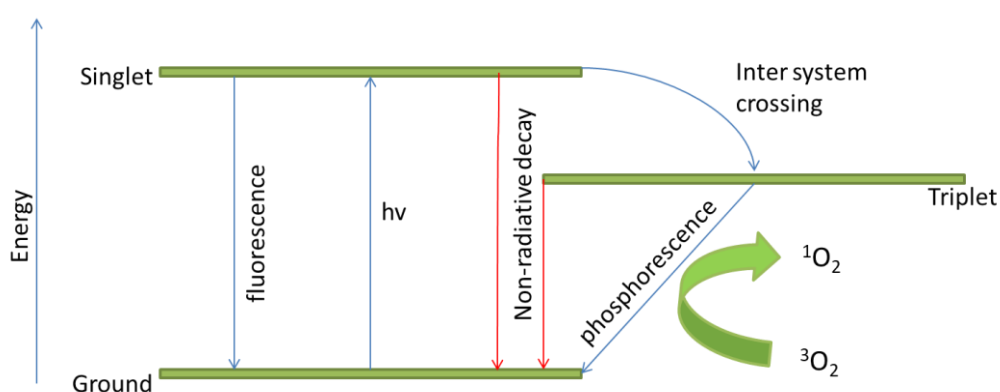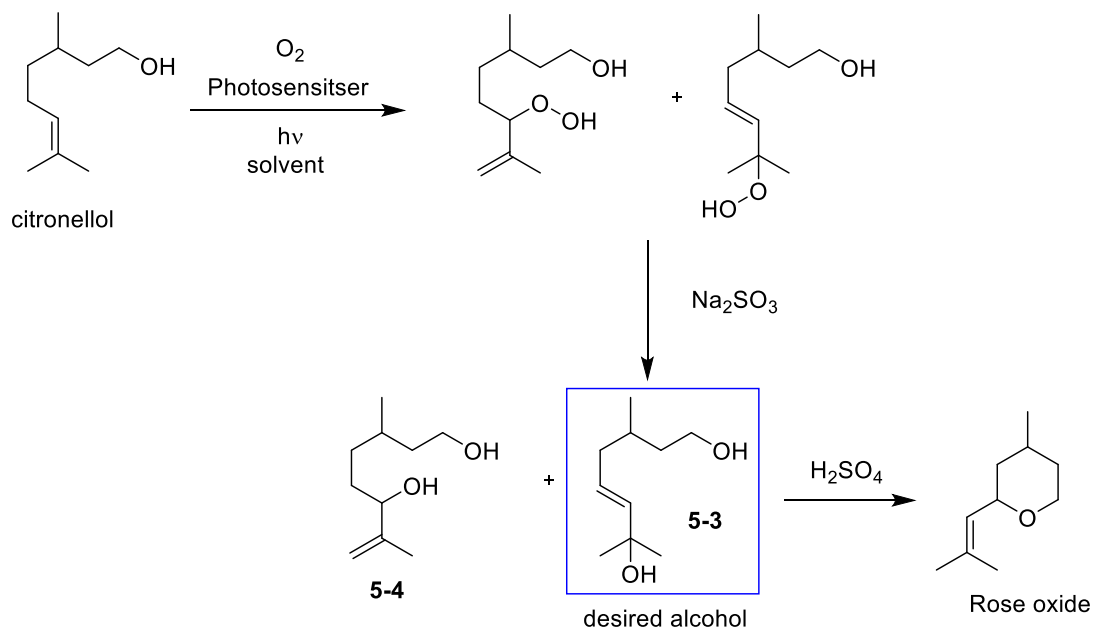

Figure 47: Simplified Jablonski diagram showing the production of singlet oxygen using a photosensitiser.

136

The $^1O_2$ then reacts thermally with citronellol to from a hydroperoxide species which can be reduced to form an alcohol. One of these alcohol species, **5-3**, can form Rose oxide through an acid catalysed ring closure - **Scheme 37**.

Scheme 37: Photo oxidation of citronellol to form Rose oxide

This reaction was chosen for this work because it requires the combination of different factors to come together - **Table 17**. Firstly, the gaseous O_2 needs to be present in the solution to allow the reaction to progress, and there are different solubility levels of the gas in each solvent. Alongside this, all the reagents need to be soluble in the chosen solvent. Once all the components are present in the solution, the oxygen needs to be excited by the photosensitiser and the $^1O_2$ can react with the citronellol to form the two peroxides. The situation is further complicated by the variation of singlet oxygen lifetimes in each of these solvents since the lifetime of singlet oxygen varies between solvents - **Table 17**.

Table 17: Various factors which need to be considered when conducting the photooxidation of citronellol in a number of different solvents.

Solvent	Lifetime of singlet oxygen (µs)[a]	Dielectric constant [b, d]	Solubility of oxygen, (mol fraction) [e]	π^{*c}	β^c	α^c
CCl$_4$	59,000	2.23[d]	-	0.21	0.1	0
CHCl$_3$	229	4.81[d]	-	0.58	0.1	0.20
Dichloromethane	99	9.08[d]	7.09 x 10^{-4}	0.82	0.1	0.13
Acetonitrile	81	37.5[b]	-	0.66	0.40	0.19
Acetone	46	20.7[b]	8.71 x 10^{-4}	0.62	0.48	0.08
Ethyl Acetate	45	6.02[b]	-	0.45	0.45	0
Benzene	30	2.27[b]	8.20 x 10^{-4}	0.55	0.1	0
Toluene	30	2.38[b]	9.81 x 10^{-4}	0.49	0.1	0
o-Xylene	23	2.57[d]		0.51	0.1	0
Methanol	10	32.6[b]	4.15 x 10^{-4}	0.67	0.69	1.07
Water	3	78.5[b]	-	1.20	0.47	1.17

[a] Lifetime calculated by dividing 1 by the rate constant for the decay of $^1O_2$ in air saturated solvent , rate constants at 293 K from References 27,28,29 [b] at 25 °C from Reference 11, [c] from Reference 9, [d] at 20 °C from Reference 11, [e] At 293K and 101 MPa from Reference 30.

The reason behind the variation in lifetime of $^1O_2$ is the rate of transfer of energy from $^1O_2$ to the vibrational energy of the solvent. The higher the vibrational energy (e.g. due to OH bonds (3500 cm^{-1}), the faster the energy transfer.[31] Therefore in a solvent which contains O-H bonds the $^1O_2$ is rapidly quenched. This means that the longest $^1O_2$ lifetimes are often observed in solvents, which contain neither C-H nor O-H bonds, for example carbon tetrachloride and deuterated solvents -

Table 17. Since the lifetime of singlet oxygen varies significantly, a control experiment was conducted to test whether differences in the lifetime of singlet oxygen would affect the proposed experiments with bio-derived solvents. The two solvents selected were chosen because $^1O_2$ has very different lifetimes in them. In deuterated chloroform, the lifetime is long (>230 µs) because this solvent contains neither O-H nor C-H bonds, and, in ethanol the lifetime is only ~10 µs. Unfortunately, some compromises had to be made in the control experiment because the same photosensitiser could not be used as neither of the available photosensitisers was soluble in both solvents. However, as can be seen, this turned out not to be a problem. For each solvent, the reaction was followed for 10 minutes taking samples at roughly 2-minute intervals. The results are shown in **Figure 48** and **Table 18** and it is clear from the figure that:

(i)   Both reactions reach completion within 10 minutes.

(ii)   The reaction in *d*-chloroform was slightly faster even though the lifetime of $^1O_2$ is ca. x20

longer than in ethanol, presumably because the rate of reaction of $^1O_2$ with the

citronellol at these concentrations is faster than the rate of deactivation of the $^1O_2$.

(iii)   The difference in photosensitiser does not seem to have a big effect on the reaction

rate.

(iv)   Therefore, differences in the solubility of O_2, lifetime of $^1O_2$ and the nature of the

photosensitiser can probably be ignored, at least for preliminary experiments with
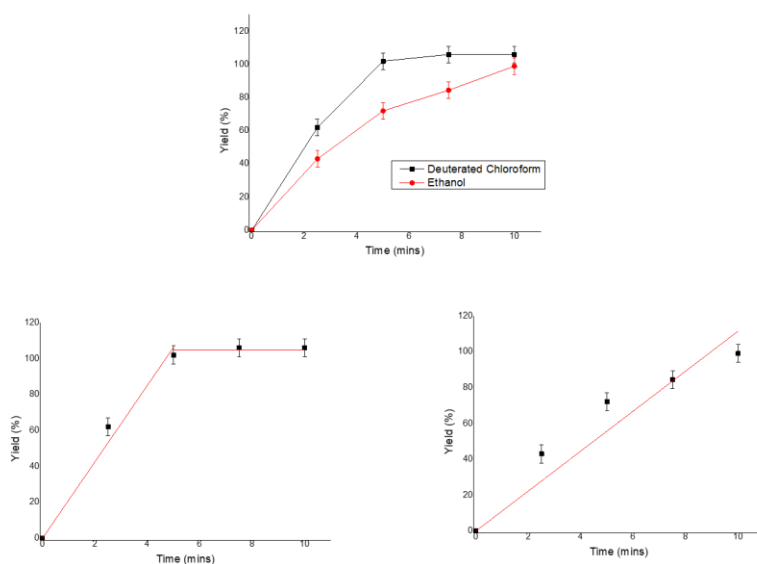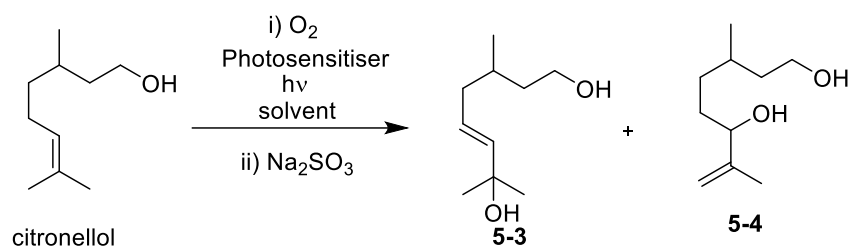
bioderived solvents.

Figure 48: Photooxidation of citronellol in *d*-chloroform and ethanol solvents to yield 5-3 and 5-4.

Table 18: Results of the control experiment used to study the rate of the photooxidation reaction when conducted in solvents where the singlet oxygen lifetime varied significantly.

Solvent Mix	Photosensitiser	Reaction rate (mM/min)	Yield of 5-3 and 5-4 (%) at 10 mins
d-chloroform	TPP	21.2 ± 1.2	100
Ethanol	RB	11.2 ± 0.9	99

Following the control experiment above, the oxidation of citronellol with photo-generated $^1O_2$ was repeated in a number of different BDS. To allow a greater range of solvents to be explored, two different photosensitisers were employed to ensure that the chosen photosensitiser was fully dissolved in each solution.

The first set of experiments shown was to examine the photooxidation of citronellol (with Rose Bengal as the photosensitiser) in acetonitrile and a number of bioderived solvent replacements which had shown promise (e.g. ethyl acetate/xylene, 1:1) in the previous section. The results are shown in **Figure 49** and were analysed in the same manner as the previous two experiments, with the data showing zero order kinetics. However, as this system utilised visible light (white LEDs, Asynt PhotoVap, λ_{max} = 450 nm) as the light source there was no initial lag phase due to warm up period of the lamp as seen in the previous examples. The different reaction rates for the photooxidation of citronellol and the Kamlet-Taft parameters for the chosen solvents are shown in **Table 19**.
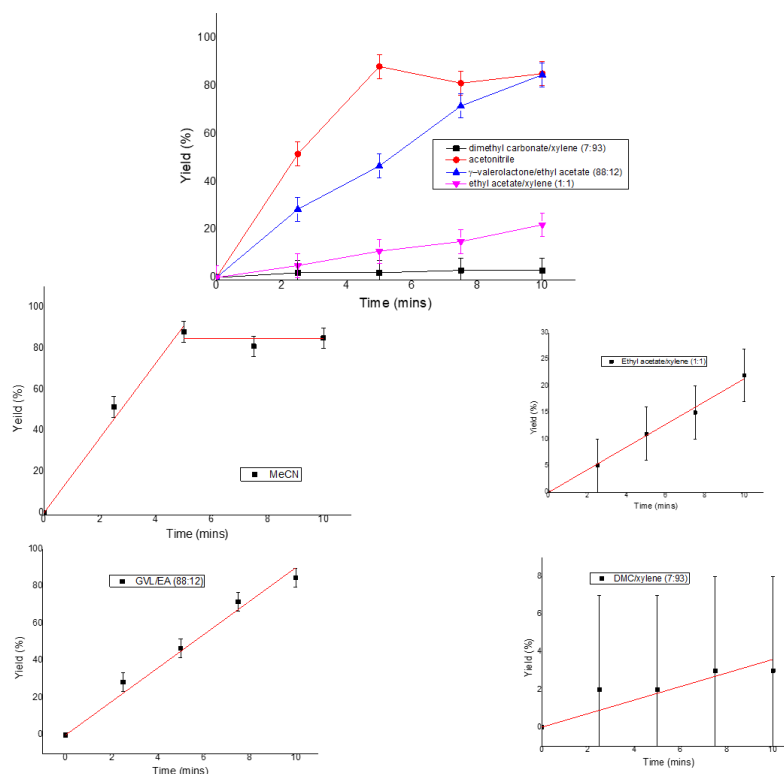
Figure 49: Photooxidation of citronellol in various different solvents using Rose bengal (RB) as a photosensitiser to yield 5-3 and 5-4.

Table 19: Results showing a number of attempts to find a mimic solvent for acetonitirle the photooxidation of citronellol using rose bengal as the photosenstiser to yeild 5-3 and 5-4
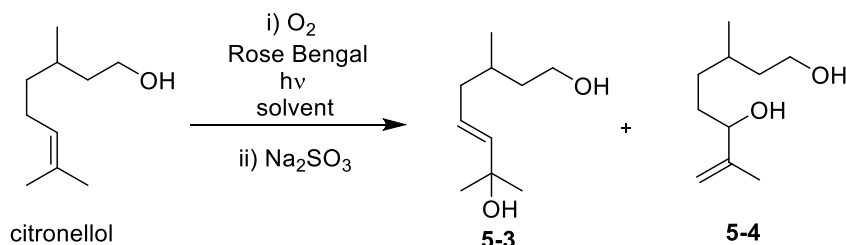
Solvent Mix	π*	β	α	Yield of 5-3 and 5-4 (%) at 10 mins	Reaction rate (mM/min)
Acetonitrile	0.66	0.4	0.19	85	18.2 ± 0.8
Ethyl Acetate/Xylene (1:1)	0.6	0.4	0	22	2.2 ± 0.1
γ-valerolactone /Ethyl Acetate (88:12)	0.66	0.16	0	84.5	9.0 ± 0.3
Dimethyl carbonate/Xylene (7:93)	0.47	0.4	0	3	0.4 ± 0.1

As before, acetonitrile was used as a benchmark COBS to compare with the BDS. The

photooxidation of citronellol was conducted in ethyl acetate/xylene (1:1), the solvent which had

shown the most promise in the study of [2+2] photocycloaddition of propargyl alcohol to THPAA

above. Surprisingly, this time there was a significant difference between the reactions rates in the

acetonitrile and the ethyl acetate/xylene mixture with almost a 10-fold difference between the two

reaction rates, **Table 19**.

To explore this effect further, the reaction was repeated in γ-valerolactone /ethyl acetate (88:12)

and dimethyl carbonate/xylene (7:93). The reason these solvent mixtures were chosen was that

each of these had a Kamlet-Taft parameter which matched that of acetonitrile. However, neither of

these solvents came close to the reaction rate observed when using the acetonitrile itself. These

results show that using Kamlet-Taft parameters alone cannot predict the outcome of this reaction in

these solvents. This could be a result of some of the factors previously mentioned such as oxygen

solubility, photosensitiser, singlet oxygen lifetime or could also be related to differences in viscosity

of the solvent.

One of these possible factors could be related to the photosensitiser used in the previous reactions

having different yields of singlet oxygen in these solvents. So, the photosensitiser was replaced, and

the reaction was rerun in another collection of bioderived solvents - **Figure 50**.

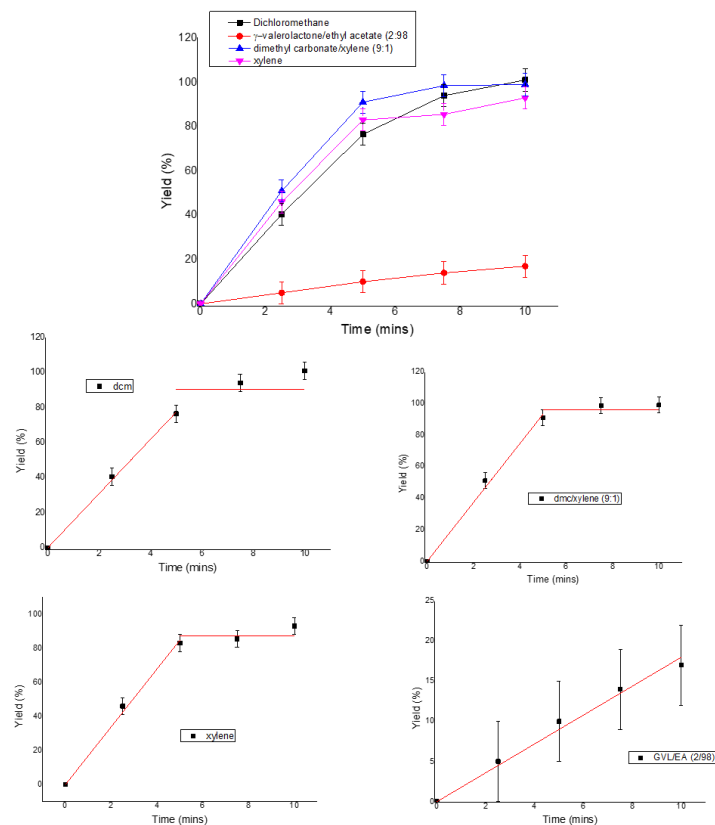**Figure 50: Photooxidation of citronellol in various different solvents using tetraphenylporphrin (TPP) as a photosensitiser to yield 5-3 and 5-4.**

Table 20: Results showing a number of attempts to find a mimic solvent for dichloromethane the photooxidation of citronellol, using tetraphenylphorin (TPP) as the photosensitiser to yeild 5-3 and 5-4.
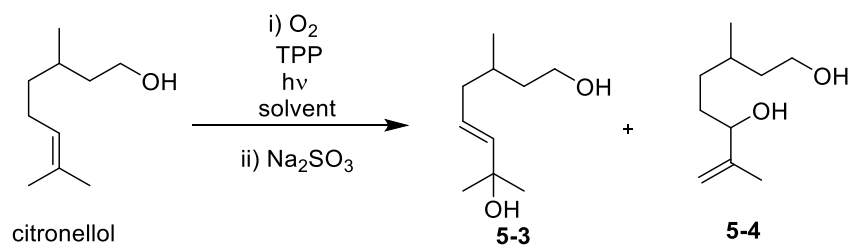
Solvent Mix	π*	β	α	Yield of 5-3 and 5-4 (%) at 10 mins	Reaction rate (mM/min)
Dichloromethane	0.82	0.1	0.13	100	15.4 ± 0.3
Xylene	0.51	0.1	0	93	17.0 ± 0.5
Dimethyl carbonate/Xylene (9:1)	0.51	0.48	0.12	99	18.6 ± 0.6
γ-valerolactone /Ethyl acetate (2:98)	0.82	0.45	0	17	1.8 ± 0.1

143

In this set of reactions, the benchmark solvent chosen was dichloromethane and a different photosensitiser which makes it distinct from the previous experiments. The solvents chosen in this reaction set were selected as each had a single matching Kamlet-Taft parameter with that of the benchmark solvent.

In xylene and dimethyl carbonate/xylene (9:1, v/v) the rates were very close to the rate in dichloromethane (**Table 20**). These solvents were chosen as xylene had the same Kamlet-Taft β value as dichloromethane and dimethyl carbonate/xylene (9:1) had an α value similar to that of dichloromethane. This is an interesting finding as it shows that even in a complex reaction mixture it is possible to replace a COBS with a BDS alternative without negatively affecting the rate of the reaction.

However, in the system with a matching π^* value, γ-valerolactone /ethyl acetate (2:98), there was a significant deviation from the reaction rate of the benchmark solvent. This set of experiments could possibly indicate that the Kamlet-Taft parameters with the greatest impact on the reaction rate are β and α parameters.

The results shown in **Table 19** combined with **Table 20** suggest that the Kamlet-Taft parameters may not be the only factors which need to be considered when determining whether conversional solvents can be replaced with bioderived alternatives in this three component reaction system. Therefore, the next section describes how a different approach was examined to see whether it worked better.

Linear solvation energy relationship studies

As discussed in the Introduction, following their initial reporting of the first parameters the team of Kamlet and Taft used these values to develop a method for the prediction of the rate of chemical reaction based on the Kamlet-Taft values – known as the Linear Solvation Energy Relationship (LSER). They showed this to work well with some reactions involving singlet oxygen – see **Equation 7**.

$$Log\ K = Log\ K_o + p\pi^* + a\alpha + b\beta + h(\delta_H)$$

Equation 7: Linear solvation energy relationships (LSER) equation. π*, α and β (The Kamlet-Taft parameters), δ_H (Hildebrand value), (K) rate constant, reaction contact (K_o). *p, a, b and h* are experimentally determined values.

There have been a number of reported studies which show a strong correlation between the LSER calculated reaction rates and experimentally derived values. [19, 20, 21] If this method could be applied to photochemical reactions, it could greatly reduce the amount of solvent wasted by trial and error attempts to find the optimum solvent mixture to conduct such reactions in. In this section, the LSER method is applied to some of the reactions described above to determine the utility of this method for future reactions. When the method of LSER was applied to the case of the photooxidation of citronellol in CH$_3$CN (see **Appendix** for calculation details) and other similar solvents, good agreement was observed between predicted and experimentally measured rates - **Table 21**.

Table 21: Results showing a number of attempts to find a mimic solvent for acetonitirle the photooxidation of citronellol
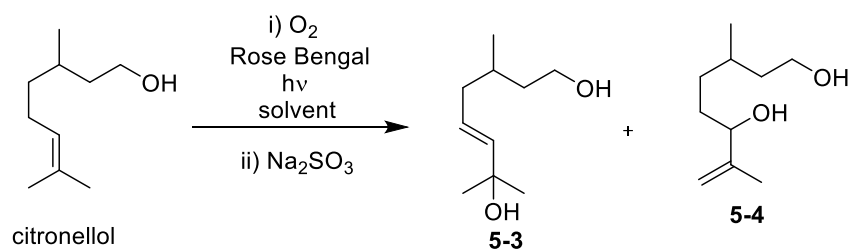
Solvent Mix	π*	β	α	δ_H	Reaction rate (mM/min)	LSER predicted reaction rates (mM/min)
MeCN	0.66	0.4	0.19	24.4	18.2 ± 0.8	17.8
γ-valerolactone /Ethyl Acetate (88:12)	0.66	0.16	0	20.9	9.0 ± 0.3	8.7
DMC/Xylene (7:93)	0.47	0.4	0	18.2	0.4 ± 0.1	0.39
Ethyl Acetate/Xylene (1:1)	0.6	0.4	0	18.3	2.2 ± 0.1	2.15
Ethanol	0.6	0.78	0.9	26.5	11.2 ± 0.9	12.5
Ethyl acetate	0.45	0.45	0	18.2	1.8 ± 0.1	0.29

LSER values used for Equation 1, calculated to be: Log K$_0$ = -4.7, p = 5.6, a =0.04, b = -0.12, h = 0.09.

If the Kamlet-Taft parameters (π*, α and β), Hildebrand value (δ$_H$) and rate constant (K) for a number of different reactions are known, they can be applied to solve Error! Reference source not found..

Using multiple simulations equations (Gaussian elimination) the other factors (K_o, p, a, b and h) can be determined and, assuming they remain constant for each solvent used to predict reaction rates in untested solvents where the Kamlet-Taft and Hildebrand parameters are known. In **Table 21** the data obtained in the first five entries was used to predict the reaction rate in ethyl acetate (see **Appendix** for graph).

In ethyl acetate there was some general agreement between the predicted LSER result of this method and the experimentally determined reaction rate for this reaction. However, the results did not appear to provide an accurate predictive method for the reaction rate.

The reason for the inconsistency between the predicted and experimentally considered systems could be the result of additional factors (e.g. dielectric constant) having a greater impact on the reaction rate than initially considered. Thus, this lack of consideration of these factors in the LSER calculations may be causing the lack of correlation between calculated and experimentally collected results. These attempts to use the LSER approach seem to have little predictive value for these reactions and therefore are probably not worth pursuing further.

Conclusion

The research described in this chapter has not been uniformly successful. However, it has produced some results which may prove useful to future workers in this area. The primary aim of this chapter was to investigate whether photochemical reactions could be conducted in bioderived solvents (BDS) instead of crude oil-based solvents (COBS). This investigation was successful. Three example reactions were tested, (intramolecular [2+2] photocyclization of Cookson's dione, intermolecular [2+2] photocycloaddition of THPAA and propargyl alcohol and the photo oxidation of citronellol). In each case, at least one BDS was identified as being a suitable alternative for conducting the photochemical reaction without negatively affecting either the reaction rate or the yield. These alternatives were: (a) dimethyl carbonate for the Cookson's dione reaction, (b) ethyl acetate/xylene (1:1) for [2+2] photocycloaddition of THPAA and propargyl alcohol and (c) xylene for the photooxidation of citronellol.

The next stage of the work was to test whether the Kamlet-Taft (KT) parameters could be used to identify which BDS might be capable of mimicking a particular COBS and, hence, to be used as a replacement for that COBS. The result was only moderately successful. In the intramolecular reaction of Cookson's dione, varying the KT values appeared to have limited impact on the reaction rate. For the [2+2] photocycloaddition of THPAA and propargyl alcohol by contrast, reactions conducted in solvents with similar KT values resulted in very similar reaction rates. Thus, the use of binary mixtures of BDS allowed KT parameter space to be explored and led to the identification of a biologically derived alternative for acetonitrile in the [2+2] photocycloaddition reaction.

By contrast, when the photooxidation of citronellol by photogenerated singlet oxygen was carried out in these apparently similar solvents, substantially dissimilar reaction rates were observed.

Finally, linear solvation energy relationships (LSER) methodology was probed to determine whether this could be used (in conjunction with KT parameter) to predict the rate of photochemical reactions in untested BDS. Sadly, within the small range of reactions tested, this approach proved to be unreliable in the predictions and it is probably not useful to pursue for this application.

Experimental

Chemicals and equipment

All chemicals were purchased from commercial sources and used without further purification unless otherwise stated. The Tetrahydrophthalic acid anhydride was supplied by the Brooker-Milburn group of Bristol University and used without further purification.

NMR data was collected on a 400 MHz Bruker spectrometer and NMR data was processed using MestraNova software and the values are reported in ppm. UV/vis spectra were collected using an Ocean OpticsUSB 2000+ UV/vis spectrometer.

Kamlet-Taft measurements

This majority of the Kamlet-Taft parameters were performed by C. Forrest, a Master's student in the Nottingham Group, under the supervision of the author.

α value measurements

Reichardt's dye (~3 mg) was dissolved in the desired solvent (25 mL). The UV/vis spectrum of the mixture was taken and the λ_{max} determined which was used to determine the Kamlet-Taft α parameter – see **Appendix**.

β value measurements

4-nitrophenol (~3 mg) was dissolved in the desired solvent (25 mL). The UV/vis spectrum of the mixture was taken and the λ_{max} determined which was used to determine the Kamlet-Taft β parameter – see **Appendix**.

π* value measurements

4-nitroanisole (~3 mg) was dissolved in the desired solvent (25 mL). The UV/vis spectrum of the mixture was taken and the λ_{max} determined which was used to determine the Kamlet-Taft π* parameter – see **Appendix**.

Cookson's Dione

Cookson's dione (1.74 g, 0.01 mol, 0.1 M) was dissolved in the chosen solvent (100 mL total). This was put into a glass immersion well reactor and irradiated using a mercury arc lamp (medium pressure 125 W) for 1 hour. Samples (1 mL) were collected every 10 mins and analysed by NMR with the addition of an external standard (biphenyl). NMR data agreed with reference 23.

Tetrahydrophthalic acid anhydride and propargyl alcohol

Tetrahydrophthalic acid anhydride (1.52 g, 0.01 mol, 0.1 M), propargyl alcohol (0.87 mL, d = 0.972 g/mL, 0.015 mol, 0.15 M) and thioxanthone (24 mg, 0.1 mmol, 1 mol %) were dissolved in the solvent of choice (100 mL). This was placed into a glass immersion well and irradiated with a mercury arc lamp (medium pressure, 125 W) for 1 hour. Samples (1 mL) were taken every 10 mins. These were added to biphenyl external standards and analysed by NMR. NMR data agreed with reference [32] – see **Appendix** for worked example.

Citronellol photooxidation

Citronellol (0.55 mL, 0.855 g/mL, 3 mmol, 0.1 M) was dissolved in the chosen solvent (30 mL total). To this mixture tetraphenylporphyrin (TPP, 9 mg, 0.014 mmol) or Rose Bengal (6 mg, 0.006 mmol) was added. This reaction mixture was placed into a 1 L glass round bottom flask and it was attached to the PhotoVap. This solution was rotated at 150 RPM and irradiated with white LEDs for 10 mins. Samples were collected every 2.5 mins. The samples (1 mL) were quenched with triphenylphosphine (0.8 g, in diethyl ether) and an external standard of biphenyl was added before NMR analysis. NMR data agreed with reference 25.

Bibliography

1. Xu, Y., Hanna, M. A. & Isom, L. "Green" Chemicals from Renewable Agricultural Biomass - A Mini Review. *Open Agric. J.* **2**, 54–61 (2008).
2. Narodoslawsky, M., Niederl-Schmidinger, A. & Halasz, L. Utilising renewable resources economically: new challenges and chances for process development. *J. Clean. Prod.* **16**, 164–170 (2008).
3. Liew, F. M. *et al.* Gas Fermentation-A flexible platform for commercial scale production of low-carbon-fuels and chemicals from waste and renewable feedstocks. *Front. Microbiol.* **7**, (2016).
4. Biddy, M. J., Scarlata, C. J. & Kinchin, C. M. Chemicals from biomass: A market assessment of bioproducts with near-term potential. *NREL Rep.* (2016) doi:10.2172/1244312.
5. Henderson, R. K. *et al.* Expanding GSK's solvent selection guide – embedding sustainability into solvent selection starting at medicinal chemistry. *Green Chem.* **13**, 854–862 (2011).
6. Constable, D. J. C. *et al.* Key green chemistry research areas—a perspective from pharmaceutical manufacturers. *Green Chem.* **9**, 411–42 (2007).
7. Diorazio, L. J., Hose, D. R. J. & Adlington, N. K. Toward a More Holistic Framework for Solvent Selection. *Org. Process Res. Dev.* **20**, 760–773 (2016).
8. Prat, D. *et al.* CHEM21 selection guide of classical- and less classical-solvents. *Green Chem.* **18**,

288–296 (2015).

9.   Gu, Y. & Jérôme, F. Bio-based solvents: An emerging generation of fluids for the design of eco-efficient processes in catalysis and organic chemistry. *Chem. Soc. Rev.* **42**, 9550–9570 (2013).

10. Duereh, A., Sato, Y., Smith, R. L. & Inomata, H. Methodology for replacing dipolar aprotic solvents used in API processing with safe hydrogen-bond donor and acceptor solvent-pair mixtures. *Org. Process Res. Dev.* **21**, 114–124 (2017).

11. Haynes, W. M. & Lide, D. R. *CRC Handbook of chemistry and physics: a ready-reference book of chemical and physcial data*. (2011).

12. Laurence, C. & Gal, J.-F. *Lewis Basicity and affinity scales, data and measurements.* (2010).

13. Lagalante, A. F., Abdulagatov, A. & Bruno, T. J. Kamlet-Taft thermosolvatochromic parameters of hydrofluoroethers and hydrofluoroether azeotropic mixtures. *J. Chem. Eng. Data* **47**, 47–51 (2002).

14. Kamlet, M. J. & Taft, R. W. The Solvatochromic Comparison Method. I. The β-Scale Of Solvent Hydrogen-Bond Acceptor (HBA) Basicities. *J. Am. Chem. Soc.* **98**, 377–383 (1976).

15. Taft, R. W. & Kamlet, M. J. The Solvatochromic Comparison Method. 2. The α-Scale of Solvent Hydrogen-Bond Donor (HBD) Acidities. *J. Am. Chem. Soc.* **98**, 2886–2894 (1976).

16. Kamlet, M. J., Abboud, J. L. & Taft, R. W. The Solvatochromic Comparison Method. 6. The π* Scale of Solvent Polarities1. *J. Am. Chem. Soc.* **99**, 6027–6038 (1977).

17. Abraham, M. H., Taft, R. W., Kamlet, M. J. & Doherty, R. M. *Chem. Brit.* **22**, 551–554 (1986).

18. Kamlet, M. J., Abboud, J. L. M., Abraham, M. H. & Taft, R. W. Linear Solvation Energy Relationships. 23. A Comprehensive Collection of the Solvatochromic Parameters, π, α, and β, and Some Methods for Simplifying the Generalized Solvatochromic Equation. *J. Org. Chem.* **48**, 2877–2887 (1983).

19. Aubry, J. M., Mandard-Cazin, B., Rougee, M. & Bensasson, R. V. Kinetic Studies of Singlet Oxygen [4 + 2]-Cycloadditions with Cyclic 1,3-Dienes in 28 Solvents. *J. Am. Chem. Soc.* **117**, 9159–9164 (1995).

20. Uslu, H. Linear Solvation Energy Relationship (LSER) modeling and kinetic studies on propionic acid reactive extraction using alamine 336 in a toluene solution. *Ind. Eng. Chem. Res.* **45**, 5788–5795 (2006).

21. Gutiérrez, M. I. Solvent effect on the physical quenching of singlet molecular oxygen by p-quinones. *Photochem. Photobiol. Sci.* **7**, 480–484 (2008).

22. Barton, A. F. M. *CRC Handbook of solubility parameters and other cohesion parameters*. (CRC Press LLC, 1991).

23. Clark, C. A., Lee, D. S., Pickering, S. J., Poliakoff, M. & George, M. W. UV PhotoVap: Demonstrating How a Simple and Versatile Reactor Based on a Conventional Rotary Evaporator Can Be Used for UV Photochemistry. *Org. Process Res. Dev.* **22**, 595–599 (2018).

24. Bourne, R. A. *et al.* Homogeneous photochemical oxidation via singlet O2 in supercritical CO2. *Chem. Commun.* 4457–4459 (2008).

25. Clark, C. A., Lee, D. S., Pickering, S. J., Poliakoff, M. & George, M. W. A Simple and Versatile Reactor for Photochemistry. *Org. Process Res. Dev.* **20**, 1792–1798 (2016).

26. Alsters, P. L., Jary, W., Nardello-Rataj, V. & Aubry, J. M. Dark singlet oxygenation of β-citronellol: A key step in the manufacture of rose oxide. *Org. Process Res. Dev.* **14**, 259–262 (2010).

27. Rodgers, M. A. J. Solvent-Induced Deactivation of Singlet Oxygen: Additivity Relationships in Nonaromatic Solvents. *J. Am. Chem. Soc.* **105**, 6201–6205 (1983).

28. Schweitzer, C. & Schmidt, R. Physical mechanisms of generation and deactivation of singlet oxygen. *Chem. Rev.* **103**, 1685–1757 (2003).

29. Bregnhøj, M., Westberg, M., Jensen, F. & Ogilby, P. R. Solvent-dependent singlet oxygen lifetimes: Temperature effects implicate tunneling and charge-transfer interactions. *Phys. Chem. Chem. Phys.* **18**, 22946–22961 (2016).

30. Sato, T., Hamada, Y., Sumikawa, M., Araki, S. & Yamamoto, H. Solubility of oxygen in organic solvents and calculation of the Hansen solubility parameters of oxygen. *Ind. Eng. Chem. Res.* **53**, 19331–19337 (2014).

31. Hurst, J. R. & Schuster, G. B. Nonradiative Relaxation of Singlet Oxygen in Solution. *J. Am. Chem. Soc.* **105**, 5756–5760 (1983).

32. Booker-Milburn, K. I., Cowell, J. K., Delgado Jiménez, F., Sharpe, A. & White, A. J. Stereoselective intermolecular [2+2] photocycloaddition reactions of tetrahydrophthalic anhydride and derivatives with alkenols and alkynols. *Tetrahedron* **55**, 5875–5888 (1999).

33. Laurence, C., Nicolet, P. & Helbert, M. Polarity and basicity of solvents Part 2. Solvatochromic hydrogen-bonding shifts as basicity parameters. *J. Chem. Soc. Perkin Trans. 2* 1081–1090 (1986)

Chapter 5 Conclusions

Introduction

To conclude this Thesis, we revisit the Aims set out in the Introduction and assess the progress made.

Thesis Aims

- The first aim of the thesis was to explore an industrially relevant photo-redox reaction, an amide bond synthesis. This type of reaction was chosen as, explained in Chapter 2, it has not been extensively explored from a Green Chemistry perspective. Alongside the photochemistry work, the application of biology (in the form of enzyme catalysed transformations) was to be explored to control the chirality within the product, potentially reducing the complexity of the reaction sequence needed to produce the desired product.

- The second aim was to develop a reactor which was capable of safely conducting photochlorination reactions using chlorine gas. Once built and tested, the reactor was to be used to synthesize several compounds which could be of interest for larger scale production. Photochlorination was chosen for further exploration as there are only a limited number of published methods for conducting chlorination with chlorine gas and as described in Chapter 3, the unique properties of the PhotoVap could solve several long-standing issues.

- The final aim of the Thesis was to study the application of bio-derived solvents for use in photochemical reactions, beginning with binary and then ternary solvent mixtures to achieve the desired solvent properties for successful photochemical reactions.

Conclusions

Aim 1

Starting from the small scale photoredox reactions reported, the first task was to investigate how readily the process could be scaled up. Indeed, Chapter 2 shows that it was possible to achieve a 500-fold increase in productivity through the application of the reactors available at Nottingham. This was an important first step in a potential green chemistry assessment process because, if a reaction only works at a very small scale, then it cannot be used to manufacture required amounts of compounds. In addition, this gives a benchmark set of conditions which can be used to compare the "green-ness" of competing routes to amide bond formation.

Following the successful scale up, the possibility of replacing the iridium photocatalyst with an organic photocatalyst was explored. This was identified as a key aspect of the reaction as the iridium photocatalyst was prohibitively expensive for further scale-up of the reaction. These experiments showed that the compound chosen, was not very efficient at catalysing the amide bond formation but did highlight the possibility of conducting the reaction electrochemically.

The electrochemical synthesis of route was then investigated through a small number of exploratory reactions which culminated in the production of one desired amide by this method, showing the validity of this approach. The electrochemical method appears to be much more rapid than the photochemical route (25 mins vs. 600 mins) and the productivity of early-stage reaction was shown to be much higher in comparison to the photochemical reaction (1.58 g/day vs. 0.024 g/day). The decrease in reaction time and absence of an expensive catalyst makes this reaction highly attractive for further investigation.

As the research progressed, it became apparent that an area with little exploration of this type of reaction was the use of chiral amines. The control of chirality within the photochemical reaction has been challenging in the production of pharmaceutical compounds. The use of enzymes to produce chiral amines in a flow reactor followed by a photochemical transformation to an amide was the

ambitious end goal of the work. Whilst this goal was only partially achieved, progress was significant. This work reported the production of the desired amide in a two-step batch process (enzymatic then photochemical). The drawback was that the yield was lower when no purification took place after the enzymatic reaction. Fortunately, when the amine was extracted from the enzymatic mixture and then used in a photochemical reaction the yield was greatly improved. This could be an opportunity for in-line separation to be applied to a future flow method enabling the enzymatic and photochemical routes to be combined into a single process.

Aim 2

The second Thesis aim was to develop a reactor based on the PhotoVap capable of handling chlorine gas for photochlorination reactions. This was achieved by the creation of the ChloroVap. Once built, the ChloroVap was optimised using the photochlorination of toluene as a test case. The resulting system had a productivity of 1.5 kg/day of benzyl chloride, approaching the levels required for small-scale production of APIs.

Then several photochlorination reactions were successfully carried out on other compounds including a key intermediate to the medicine Plavix. This photochlorination route has an atom efficiency that appears to be higher than that of the original synthesis of Plavix. The extra steps needed in the synthesis of Plavix were attempted and a crude product mixture was obtained; sadly, time did not allow the API to be fully isolated.

One long-standing issue with photochlorination reactions has been the source of chlorine gas. This Thesis reports having successfully demonstrated that chlorine gas could be generated *in-situ* from brine using electrolysis and then used in the ChloroVap to produce benzyl chloride. Whilst this electrolysis method was not optimised and the yields were therefore rather low, the potential advantage of this approach is that the waste HCl trapped in the NaOH scrubber could be recycled giving a much more efficient utilisation of the chlorine atoms. Therefore, it might be worth pursuing this work further.

The third aim was to investigate whether photochemical reactions could be conducted in bioderived solvents (BDS) instead of crude oil-based solvents (COBS). This part of the research was successful. In all three example photochemical reactions tested, at least one BDS was identified as being a suitable alternative for conducting the photochemical reaction without negatively affecting either the reaction rate or the yield. These alternatives were: (a) dimethyl carbonate for the Cookson's dione reaction, (b) ethyl acetate/xylene (1:1) for [2+2] photocycloaddition of THPAA and propargyl alcohol and (c) xylene for the photooxidation of citronellol.

The next stage of the work was to test whether the Kamlet-Taft (KT) parameters could be used to identify which BDS might be capable of mimicking a particular COBS and, hence, to choose a BDS that could be used as a replacement for that COBS. The results were only moderately successful. In the intramolecular reaction of Cookson's dione, varying the KT values appeared to have limited impact on the reaction rate. For the [2+2] photocycloaddition of THPAA and propargyl alcohol by contrast, reactions conducted in solvents with similar KT values resulted in very similar reaction rates. Thus, the use of binary mixtures of BDS allowed KT parameter space to be explored and led to the identification of a biologically derived alternative for acetonitrile in the [2+2] photocycloaddition reaction.

Finally, linear solvation energy relationships (LSER) were probed to determine whether they could be used (in conjunction with KT parameter) to predict the rate of photochemical reactions in untested BDS. Sadly, within the small range of reactions tested, this approach proved to be unreliable in the predictions and it is probably not useful to pursue for this application.

Future work

In each of the areas of research there are some additional points which could be the focus of future efforts.

In the amide bond formation study, it might be interesting to expand the scope of the amide production through a combination of enzymatic and photochemical process, in a single continuous

process. This could be coupled with exploration of the electrochemical route and attempt to couple the enzymatic and electrochemical route into a single process.

The ChloroVap, developed within this project could be used to explore the chemical space around photochlorination of molecules of interest. In particular, this could include the production of polychlorinated compounds which were not studied in this Thesis. Beyond this, the ChloroVap concept could be altered to enable the other gas-liquid photochemical reactions to be studied such as the Reed reaction for the production of sulfonyl chloride compounds.

Finally, the learning from Aim 3 could be applied to amide bond formation and to photochlorination to enable these photochemical reactions to be performed in a more sustainable manner, for example, using some of the solvent mixtures identified in Chapter 5 to replace the acetonitrile (in the amide formation reaction) and chloroform (in the photochlorination reaction).

This Thesis has identified a number of future research areas and I wish the best of luck to anyone who follows on with any of the topics which have been explored here.

Appendix – Additional scientific contributions

In addition to the work described previous, the paper below has been summited for review to the Proceedings of National Academy of Science (PNAS). In this work, I conducted a number of the early Time Resolved InfraRed (TRIR) spectroscopy studies before this section of the project was concluded by Dr Surajit Kayal.

Integrated Multistep Photochemical and Thermal Continuous Flow Reactions; Production of Bicyclic Lactones with Kilogram Productivity.

Rowena A. Howie,[a] Luke D. Elliott,[b] Surajit Kayal,[a] Xue-Zhong Sun,[a] Magnus W. D Hanson-Heine,[a] Jonathan Hunter,[a] Charlotte A. Clark,[a] Ashley Love,[a] Christopher Wiseall,[a] Martyn Poliakoff,[a] Kevin I. Booker Milburn[b] and Michael W. George*[a,c]

[a]School of Chemistry, University of Nottingham, University Park, Nottingham, NG7 2RD, UK
[b]School of Chemistry, University of Bristol, Cantock's Close, Bristol, BS8 1TS, UK.
[c]Department of Chemical and Environmental Engineering, University of Nottingham Ningbo China, 199 Taikang East Road, Ningbo, 315100, China.
Emails: mike.george@nottingham.ac.uk

This PDF file includes:
 Main Text
 Schemes 1 to 2
 Figures 1 to 2
 Tables 1 to 2

Abstract

Combining continuous photochemistry and flow reactions in high temperature/high pressure water has enabled us to integrate a multi-step sequence into a single process with a reduction in reaction time to <10 min compared to >24 hr in batch. At the same time, applying this approach to different substrates has allowed us to increase previously low yields to levels high enough to make those reactions potentially useful for multi-stage synthesis. In this paper, we describe the [2+2] cycloaddition / fragmentation of 3,4,5,6-tetrahydrophthalic anhydride and propargyl alcohol and analogous compounds leading to bicyclic lactones to demonstrate how photochemistry and thermal chemistry can be combined using continuous flow techniques to create complex structures on a relatively large scale. We show how photochemical and high temperature water flow reactors can be used to carry out a three- step reaction sequence as a single integrated and continuous process. The reaction time has been reduced by exploiting the enhanced acidity of high temperature water/acetonitrile mixtures. The overall process is demonstrated on an equivalent productivity of a > 1 kg/day productivity using lab scale equipment. Our approach should be simple to scale-up in an appropriate factility, for larger scale production of chemicals. Process analytical technology and modelling were used to support the reaction development, while UV and IR time resolved spectroscopy have been used to provide a deeper understanding of the reaction mechanism.

Significance Statement

Continuous flow reactors can open up wider process windows than are available for traditional batch reactions in organic chemistry. We show how linking photochemical and high-pressure thermal reactors in a continuous sequence enables the exploitation of the enhanced acidity of high temperature water to transform the yield of previously low yielding reactions as well as significantly reducing the reaction time of an electrocyclic ring opening. Even on laboratory scale our approach can deliver compounds with kilogram productivity.

Introduction

There is increasing use of continuous chemical synthesis in both academia and industry. In this context, one unmet goal is the ability to efficiently integrate continuous flow photochemistry with thermal chemistry to construct complex molecules in a more sustainable manner particularly for pharmaceutical, specialty chemical, and flavor and fragrance applications (1). This need for integration has been driven by efficient and innovative syntheses and has been accompanied by developments in continuous flow reactors which simplify the problems of scaling up photochemical reactions. Whilst the recent explosion in the use of visible light mediated photoredox reactions has offered new pathways for cross coupling and late stage functionalization, the structures generated can often be accessed by traditional means. Excited state photochemistry on the other hand, offers rapid access to sp3 rich scaffolds often unobtainable by thermal and catalytic routes. Although the basic reactions have been known for many years, the products obtained are starting to be appreciated as novel scaffolds in their own right. The focus on photochemistry has, in part, been facilitated by the increasing application of continuous flow chemistry, Additionally, the unique reactivity of the often strained photochemical products can be exploited to further diversify the molecular space and complexity.

There is considerable interest in applying the release of strain within organic molecules to create versatile building blocks and complex scaffolds. This has proved to be a powerful and widely used approach in thermal chemistry, where releasing the high ring strain in, for example, cyclopropanes and cyclobutanes lead to many possibilities for ring-opening in synthesis (2,3). This interest in ring-opening has coincided with a renaissance in organic photochemistry, partly prompted by the ability of photochemistry to promote transformations that are not accessible by

158

more traditional synthetic routes (4), and particularly relevant to this paper, to easily introduce strain into organic molecules.

The scale-up problems of photochemistry are principally concerned with ensuring that every molecule in a large volume of reaction mixture is exposed to sufficient light to promote the desired transformation. Flow chemistry can be particularly useful for photochemistry because it enables reaction mixtures to be irradiated in a relatively narrow pathlength with much better light penetration than in a larger tank reactor. Such flow reactors can be used to produce kilogram quantities of compounds either by scaling out (i.e. several reactors in parallel) or by scaling up with highly efficient reactors in combination with high power light sources (5). Of course, continuous flow chemistry also offers advantages in thermal reactions, such as those that release ring strain mentioned above. These advantages include (i) improved temperature control because of enhanced heat transfer, (ii) the opportunity to link the separate stages of a multi-step synthesis into a single, cleaner process by 'daisy-chaining' a number of different reactors in series and (iii) access to new operating windows (e.g. operating with traditional solvents well above their boiling points) which can widen the scope of known transformations. Superheating of solvents has particularly striking effects in the case of water because, at higher temperatures, H-bonding is weakened with a drop in dielectric constant and increased solubility of organic compounds (e.g. at 300 °C, H_2O has solvent properties similar to those of acetone); at the same time, the ionic product of water increases giving enhanced concentrations of both $[H]^+$ and $[OH]^-$, opening up the possibility of acid catalysis in the *absence of added acid* (6).

Thus, there is a considerable attraction in the concept of creating a single continuous flow process to link photochemical and thermal reactors which first create strained structures and then release that strain to generate complex molecular architectures. The challenge, however, is how to match the productivity rates (g/h) of the photochemical and thermal processes so that the reactors can be successfully integrated into a single chain, smoothly converting starting materials into desired product(s) with high selectivity and good productivity.

Insert Scheme 1

In this paper we use the [2+2] cycloaddition / fragmentation of 3,4,5,6-tetrahydrophthalic anhydride (THPA, **1a**) and propargyl alcohol (**2a**) and analogous compounds as a case study to show how photochemistry and thermal chemistry can be combined using continuous flow techniques to create complex structures on a relatively large scale. We show how we have taken a series of photochemical and thermal reactions leading to a bicyclic lactone, **7a** in scheme 1, and have integrated them into a single process in continuous flow. The reaction was first reported over 25 years ago (7), and then used in model studies towards the natural product pachylactone (8) and to study the thermal electrocyclic ring opening scope (9). Together these papers established that the yields of the final ring-expanded product varied considerably with different sized rings; that is from 84% for **7a**, the 8/5 compound, to as little as 6% for the 7/5 analog and, as might be expected, the rate of converting the diester of **6a** to **7a** increased with temperature (e.g. maximum yield of **7a** was achieved in 28 hours in refluxing xylene (bp 139 °C) but only 7 hours in diglyme (bp 162 °C).

Although excellent yields of **7a** were obtained in these early studies, the ability to scale-up and hence to fully exploit the methodology was severely limited by the efficiency of the initial photochemical step and the sluggishness of the final thermal step. In this paper we demonstrate that to successfully address this challenge requires a combination of engineering, fundamental chemistry and reactor modelling, which results in a short reaction time in a flowing high-temperature water reactor to increase the productivity transforming a 24-hour acid reflux to a ca. 10-minute residence time. Our multi-faceted approach to this reaction has the following aims: (i) to study the photophysics of the reaction to gain greater insight into the excited state behavior of the substrate; (ii) to optimize the photochemical cycloaddition and thermal fragmentation for optimal productivity and sustainability and (iii) to combine- photochemical and thermal steps into a single streamlined continuous flow process. Our initial optimization focused on the parent

1a/2a reaction but we also demonstrate how other thermally fragmented products inaccessible by traditional means can be accessed using high temperature flow techniques. This study develops a multi-step approach to achieving productivities of kg/day. Our initial strategy was to study the photophysics of the photochemical reaction and hence to accelerate the reaction by use of a thioxanthone photosensitizer, then to identify a solvent that it is compatible with all the different reactions and lastly to optimize the process to maximize its productivity. The final process has enabled us to avoid a solvent change and, by exploiting the unusual acidity of solvent mixtures containing high temperature water, to eliminate the need for concentrated HCl as a catalyst, and, hence, to combine two reactions steps into one. Finally, we demonstrate that our approach can transform the yields of other substrates, e.g. **7b** and **7c**, where previous, more traditional batch processing has failed to give usable yields of the final product.

Results and Discussion

The initial photochemical reaction which ultimately leads to **7a** has been known for some years, but the overall productivity was somewhat low (8). The overall process starting from **1a** to the target lactone **7a** involves three stages, (see Scheme 1) (i) the initial [2+2] photochemical addition, (ii) hydrolysis of the resulting anhydride and (iii) a combined electrocyclic ring opening and lactonization, which itself occurs via several intermediates, to form **7a**. In the original publication these three steps were carried out in different solvents, which clearly would be problematic for a continuous integrated process.

In order to improve the efficiency of these reactions particularly targeted at scale-up we have investigated a range of photosensitisers (see ESI) and found that isopropylthioxanthone (ITX) to be an efficient triplet sensitizer giving ca. ~tenfold increase in productivity compared to the unsensitized reaction. We then screened a range of solvents and identified EtOAc as the optimal solvent for photochemistry in terms of productivity and yield (ESI) and sustainability. Using this solvent the photochemistry was scaled-up with the continuous flow Firefly reactor (5c) at 3 kW, (EtOAc, 0.5 M): 1 mole scale in 1.1 hrs, then 5 mole scale in 5.5 hrs with no reactor fouling.

Addition of water to ethyl acetate (EtOAc) allows the hydrolysis to be carried out rapidly as an emulsion and results in aqueous solution of **6a** after separation. The thermal electrocyclic ring opening of **6a** → **7a** was found to proceed slowly at reflux in H_2O (3 days) but could be catalyzed by 20 mol% HCl, reducing the time to 19 hrs. The resulting product could be isolated in high purity by filtration of the cooled reaction mixture, giving 510 g from a 5 mole photochemical reaction (see ESI). A 24 hour continuous run with the photochemical reactor would give over 2.2 kg of product but with this method would require the use of a 25 L batch reactor for the aqueous thermal reaction. These results, however, opened up the possibility of using flow chemistry to exploit the inherent acidity of superheated H_2O to eliminate the need for HCl with the added advantage of accelerating the reaction by running it at higher temperatures. Unfortunately, EtOAc is incompatible with H_2O at high temperatures as it hydrolyses rapidly. By contrast, acetonitrile (CH_3CN) only reacts slowly with H_2O even >300 °C (10-11). In order to implement a fully continuous process it is preferable to avoid solvent change or biphasic mixtures and, although EtOAc gave the highest productivity for the photochemical step, CH_3CN proved more desirable particularly as it has only marginally worse productivity for the photochemistry but is fully miscible with H_2O. Therefore, we decided to build the process around using aqueous CH_3CN for the subsequent steps i.e. carrying out the photochemistry in pure CH_3CN and then adding an equal volume of H_2O for the subsequent thermal stages since H_2O inhibits the photochemistry if added from the outset.

Insert Figure 1

Figure 1 summarizes the key data from a detailed Time Resolved IR (TRIR) study of the reaction of **1a** with **2a** in CD_3CN – the deuterated solvent was used to avoid IR bands of CH_3CN masking these regions of the spectrum. Initial experiments with **1a** in the absence of other reagents allowed us to identify the IR bands of the singlet and triplet excited states, [1]**[1a]** and [3]**[1a]**, Figure 1A and 1B. This experiment also showed that ca. 60% [1]**[1a]** decays back to the ground state of **1a** rather than to [3]**[1a]**, thereby confirming why direct excitation of **1a** is not the most efficient approach to promoting the reaction of [3]**[1a]** with **2a.** Similar experiments with solutions of the photosensitizer thioxanthone, TXO, (not illustrated) allowed the bands of the excited states of the TXO to be identified. Then, using **1a** and TXO together, the rate of energy transfer from [3][TXO] to **1a** was measured (Figure 1C and 1D). Finally, TRIR data from a mixture containing **1a**, **2a** and TXO confirmed, for the first time, the presence of proposed intermediate diradical **3a** and shows that there is no reformation of **1a**. This indicates that the quantum yield of formation of the diradical **3a** is considerably higher than in the absence of TXO. The spectra also showed that both of the photoproducts **4a** and **5a** are derived from the same intermediate, **3a**,

making it unlikely that one could easily change the ratio of **4a**: **5a** by simple variation of the reaction parameters.

The development of the integrated process was carried out in three stages. First, using a small autoclave, we studied the batch ring opening and lactonization reaction of **5a** to **7a** in high temperature water (see ESI) to check that (i) the ring opening did occur and (ii) hydrolysis of the lactone did not take place. These experiments were successful with optimal conditions of 200 °C for 10 mins. Transferring this reaction to a continuous pressurized flow reactor revealed a problem, namely that, although the reaction took place, the desired product **7a** precipitated when the water cooled down causing blockages, prior to the release of pressure. Fortunately, the lactone **7a** is soluble in aqueous CH_3CN, and the reaction still took place with near quantitative yield, when using the CH_3CN/H_2O mixture as the solvent, although, the optimal temperature required for maximum throughput (260 °C) was somewhat higher that than in the batch reaction in H_2O. Then to investigate whether the hydrolysis of **5a** could also be carried out in a high temperature aqueous CH_3CN, we pumped a solution of **5a** through thermal reactor and found that both reactions could be carried out as a combined process in a single reactor. The reaction worked equally well with a mixture of **4a** and **5a** obtained directly from the photochemical reaction, as opposed to pure **5a**, Thus, it was not necessary to separate the photoproducts **4a** and **5a** prior to hydrolysis. In addition, the reaction in CH_3CN/H_2O was carried out with a residence time of < 2.5 mins. These results opened the way for a single integrated process from **1a**→ **7a** based on aqueous CH_3CN.

Insert Figure 2

Figure 2 is a schematic diagram of our apparatus, broadly it consists of a fluorinated ethylenepropylene (FEP) tubular photoreactor with a 400 W mercury lamp, filtered by borosilicate glass. Then, after a reservoir to prevent any back pressure reaching the photochemical reactor, the solution is fed into a HPLC pump to generate the pressure needed for the thermal stage. A second pump delivers the H_2O and the resulting CH_3CN/H_2O reaction mixture passes directly into a heated coiled tubular reactor which serves as both preheater and reactor. This is followed by cooldown and pressure release, yielding a solution of the target product **7a**, the hydrolysis product of **4a** and residual ITXO. Evaporation of CH_3CN from this aqueous solution resulted in precipitation of **7a**, in high purity, which could be then separated by filtration from the solution of any remaining diacid **6a** and the hydrolysis products of **4a**.

Using this system, **1a** (0.1 M) with 1.5 eqs of **2a** and TXO (1 mol%) in CH_3CN were flowed through the photoreactor at 10 ml/min, giving greater than 95% conversion and a 68% yield of **5a**, 41 mmol/h (plus 15% **4a**). This solution was then mixed with water in a 1:1 ratio by volume to give a total flow rate of 20 ml/min and thermally treated at 240 to 260 °C, as summarized in Table 1. At the highest temperature, near quantitative yields of **7a** were obtained for the thermal steps, giving an overall yield of 67% for the daisy-chained process. This corresponds to a productivity of 39 mmol/hr and is a marked improvement over the 44% yield of **7a** obtained via separate batch processing, particularly considering the reduction in overall reaction time from greater than 24 hours to a residence time of just 10 minutes in flow.

Insert Table 1

From these results, it was clear that the maximum throughput of the combined reactor was being limited by the photochemical rather than the thermal reactors. Therefore, we installed two additional identical photoreactors in parallel with the first, thereby at least tripling the productivity of the photochemical reaction. Running these combined reactors together with small changes to the reaction conditions and an increased concentration of substrate to 0.5 M allowed the overall productivity of the daisy-chained sequence to be increased to 225 mmol/hr. For this test run the reactors were successfully held at the desired reaction conditions for 1 hour after equilibration with no evidence of reactor fouling or precipitation of reactants. Extrapolating from this 1 hr

period would give an equivalent rate of formation of **7a** of greater than 1.1 kg/day, using lab scale equipment.

Work using a novel tubular quartz reactor, with a 3 kW Hg lamp, gave very promising results for the further scale up of the photochemical step. This so-called *'Firefly'* reactor (5c) was used to carry out the photochemical step on 1 mole of **1a** at a 0.5 M concentration in ethyl acetate, using a 30 ml/min flow rate and a 3 kW lamp power. This resulted in full conversion, giving a 70% yield of **5a** at a productivity of 630 mmol/hr. This reaction was subsequently repeated on a 5 mole scale, over the course of 5 hours, with no evidence of fouling within the reactor. These results represent an approximately three-fold increase in productivity and flow rate over the parallel, triple 400 W FEP reactors, taking the photochemical productivity beyond the current capabilities of our thermal reactor. Process modelling of the thermal reactor using the Process Systems Enterprise (PSE) gPROMS software predicts 82% conversion using similar conditions as reported above in the current reactor, which rises to full conversion and >95% yield if the reactor volume were doubled (see ESI).

Construction of a larger scale reactor train was not carried out during this project, due to limitations in terms of space and equipment as well as the safety restrictions presented by a University research laboratory. Nevertheless, these results are very promising because they suggest that only a modest increase in scale for the thermal reactor would be required to match the output of the *Firefly* reactor and reach the equivalent of 1 tonne/year, an industrially relevant milestone/benchmark for many pharmaceutical products. Thermal flow chemistry is particularly suited to reactions involving challenging substrates which may decompose at conditions close to those required for their formation. Faster heating, compared to batch reactors of similar productivity, allows the desired conditions to be achieved rapidly, minimizing reaction times, while improved cooling rates help to avoid thermal degradation of unstable products. Therefore, the process intensification that we have achieved with **7a** suggests that we might be able to increase the previously reported low yields for related reactions to a more useful level, see examples in Scheme 1, because the yields for the photochemical stage of those reactions were similar to that in the **7a** system, with the loss of yield occurring mainly in the thermal steps. Thus, we have focused our investigations on thermal flow reactions, while performing the preceding photochemical steps in batch. Some of the starting materials required for these reactions are economically prohibitive for scale-up, so we decided to build a smaller scale thermal reactor, to reduce waste and to run these reactions at a reasonable cost. The performance of this smaller reactor was validated using the synthesis of **7a** and monitored in real time using Raman spectroscopy, Figure 2. (This allowed the scalability of the reaction to be investigated, with good agreement between results obtained previously in the larger reactor to those predicted from a gProms model developed using results from the small-scale reactor.

This smaller reactor is described in detail in the ESI but, in brief, it consists of a similar tubular heated reactor as used previously, but with a 1 mL heated volume, ca. 50 times smaller. The same aqueous CH_3CN was used as the solvent for these reactions. The thermal steps in reaction of **1a** with 3-butyn-1-ol (**2b**), have previously required longer reaction times due to less favored formation of the 6-membered lactone **7b** but, in our reactor, a 61% yield of the ring opened product, **7b**, was obtained after only a 2 min residence time at 250 °C. This contrasts favorably to the previously reported 36 hour reflux in xylene.

Insert Table 2

We then investigated the reaction sequence starting with **1c** and **2a** which ultimately leads to the 7/5 bicyclic ring-opened product **7c**, Scheme 1C. When this reaction was originally reported, the methyl ester of this analog was obtained via a series of batch processes over several days with an overall yield of just 4%. Again, good yields had been achieved for the photochemical and esterification steps, with the problem lying in the thermal ring opening steps (6% and later 25%), due to the increased strain in the 7-membered *cis-trans* diene intermediate and reduced stability of **7c**. With only modest optimization (see ESI), we increased the yield of the thermal stages up to

45% of **7c** plus 36% of **6c**, as shown in table 2. This represents a considerable improvement, especially considering the reduction in thermal reaction time from >24 hrs in batch to ca. 2 minutes in flow. Increasing the temperature of 300 °C gave up to 78% of **7c**, using an increased flow rate to shorten the residence time. However, as there was some evidence for the hydrolysis of CH_3CN under these conditions, an alternative solvent mixture would be required if this substrate were to be pursued further.

Reaction of **1a** with alcohol, **2d**, gave quite different results, because the steric bulk of the Me group in **2d** appears to seriously hinder the ring expansion sequence. Tolerance of such methyl groups has been shown for analogs containing a larger ring system, although in the case of **5d** batch processing was reported to lead to recovery of the starting material or decomposition. Reacting the photoproduct **5d** in our continuous flow reactor in aqueous CH_3CN led to the formation of the expected diacid **6d** up to 68% at 250 °C. Higher reaction temperatures appear to promote unusual further reactivity, leading to the formation of two novel compounds, **8** and **9**, were isolated in reasonable yields (12% and 34% respectively), Scheme 2. The formation of **8** and **9** could occur via a decarboxylation and subsequent cyclisation. Investigations are ongoing to confirm the proposed mechanism and to establish whether this unusual reactivity could be exploited to carry out a range of similar reactions in high temperature water.

Conclusions

We have successfully integrated photochemical and high temperature water flow reactors to carry out a three- step reaction sequence as a single integrated and continuous process. The addition of a thioxanthone photosensitizer and exploiting the enhanced acidity of high temperature water/acetonitrile mixtures has enabled the reaction time to be reduced from >24 hrs to 10 minutes. This reaction was demonstrated on the equivalent productivity of a > 1 kg/day productivity using lab scale equipment. Although we were operating at the maximum practical scale for a university laboratory, our approach should be simple to scale-up in an appropriate factility, for larger scale production of chemicals. Process analytical technology and modelling were used throughout to support the reaction development, while UV and IR time resolved spectroscopy have been used to provide a deeper understanding of the reaction mechanism. Extending the approach ot other substrates has allowed us to increase previously low yields to levels high enough to make those reactions potentially useful for multi-stage synthesis.

Materials and Methods

Futher experimental details are to be found in the ESI.

Acknowledgments

References

1. (a) M. Baumann, T. S. Moody, M. Smyth, S. Wharry, A Perspective on Continuous Flow Chemistry in the Pharmaceutical Industry. *Org. Process Res. Dev.* (2020) in press *doi.org/10.1021/acs.oprd.9b00524*; (b) C. Sambiagio, T. Noël, Flow photochemistry:

shine some light on those tubes! Trends Chem. 2, 92-106 (2020); (c) C. Badman, C. L. Cooney, A. Florence, K. Konstantinov, M. Krumme, S. Mascia, M. Nasr, B. L. Trout, Why We Need Continuous Pharmaceutical Manufacturing and How to Make It Happen. *J. Pharm. Sci.* 108, 3521-3523 (2019); (d) M. B. Plutschack, B. Pieber, K. Gilmore, P. H. Seeberger, The Hitchhiker's Guide to Flow Chemistry(II). *Chem. Rev.* 117, 11796-11893 (2017); (e) Adamo, R. L. Beingessner, M. Behnam, J. Chen, T. F. Jamison, K. F. Jensen, J.-C. M. Monbaliu, A. S. Myerson, E. M. Revalor, D. R. Snead, T. Stelzer, N. Weeranoppanant, S. Y. Wong, P. Zhang, On-demand continuous-flow production of pharmaceuticals in a compact, reconfigurable system. Science 2016, 352, 61-67;(f) B. Gutmann, D. Cantillo, C. O. Kappe, Continuous-Flow Technology A Tool for the Safe Manufacturing of Active Pharmaceutical Ingredients. *Angew. Chem. Int. Ed. 54,* 6688-6728 (2015).

2. H. N. C. Wong, M.-Y. Hon, C.-W. Tse, Y.-C. Yip, J. Tanko, T. Hudlicky, Use of cyclopropanes and their derivatives in organic synthesis. *Chem. Rev.* 89, 165-198 (1989).

3. C. Ebner, E. M. Carreira, Cyclopropanation Strategies in Recent Total Syntheses. *Chem. Rev.* 117, 11651-11679 (2017).

4. (a) F. Politano, G. Oksdath-Mansilla, Light on the Horizon: Current Research and Future Perspectives in Flow Photochemistry. *Org. Process Res. Dev.* 22, 1045-1062 (2018); (b) M. D. Kärkäs, J. A. Porco, C. R. J. Stephenson, Photochemical Approaches to Complex Chemotypes: Applications in Natural Product Synthesis. *Chem. Rev.* 116, 9683-9747 (2016); (c) D. Ravelli, S. Protti, M. Fagnoni, Carbon-Carbon Bond Forming Reactions via Photogenerated Intermediates. *Chem. Rev.* 116, 9850-9913 (2016); (d) S. Poplata, A. Tröster, Y.-Q. Zou, T. Bach, Recent Advances in the Synthesis of Cyclobutanes by Olefin [2+2] Photocycloaddition Reactions. *Chem. Rev.* 116, 9748-9815 (2016); (e) A. A. Ghogare, A. Greer, Using Singlet Oxygen to Synthesize Natural Products and Drugs. *Chem. Rev.* 116, 9994-10034 (2016); (f) D. Cambié, C. Bottecchia, N. J. W. Straathof, V. Hessel, T. Noël, Applications of Continuous-Flow Photochemistry in Organic Synthesis, Material Science, and Water Treatment. *Chem. Rev.* 116, 10276-10341 (2016); (g) D. Blanco-Ania, S. A. Gawade, L. J. L. Zwinkels, L. Maartense, M. G. Bolster, J. C. J. Benningshof, F. P. J. T. Rutjes, Rapid and Scalable Access into Strained Scaffolds through Continuous Flow Photochemistry. *Org. Process Res. Dev.* 20, 409-413 (2016).

5. (a) D. S. Lee, M. Sharabi, R. Jefferson-Loveday, S. J. Pickering, M. Poliakoff, M. W. George, Scalable Continuous Vortex Reactor for Gram to Kilo Scale for UV and Visible Photochemistry. *Org. Process Res. Dev.* 24, 201-206 (2020); (b) C. A. Clark, D. S. Lee, S. J. Pickering, M. Poliakoff, M. W. George, UV PhotoVap: Demonstrating How a Simple and Versatile Reactor Based on a Conventional Rotary Evaporator Can Be Used for UV Photochemistry. *Org. Process Res. Dev.* 22, 595-599 (2018); (c) L. D. Elliott, M. Berry, B. Harji, D. Klauber, J. Leonard, K. I. Booker-Milburn, A Small-Footprint, High-Capacity Flow Reactor for UV Photochemical Synthesis on the Kilogram Scale *Org. Process Res. Dev.* 20, 1806-1811 (2016); (d) Y. Su, K. Kuijpers, V. Hessel, T. Noël, A convenient numbering-up strategy for the scale-up of gas-liquid photoredox catalysis in flow. *React. Chem. Eng.* 1, 73-81 (2016); (e) J. W. Beatty, J. J. Douglas, R. Miller, R. C. McAtee, K. P. Cole, C. R. J. Stephenson, Photochemical Perfluoroalkylation with Pyridine N-Oxides: Mechanistic Insights and Performance on a Kilogram Scale. *Chem.* 1, 456-472 (2016); (f) K. C. Harper, E. G. Moschetta, S. V. Bordawekar, S. J. Wittenberger, A Laser Driven Flow Chemistry Platform for Scaling Photochemical Reactions with Visible Light. *ACS Cent. Sci.* 5, 109-115 (2019).

6. (a) P. E. Savage, A perspective on catalysis in sub- and supercritical water. *J. Supercrit. Fluids* 47, 407-414 (2009); (b) N. Akiya, P. E. Savage, Roles of water for chemical reactions in high-temperature water. *Chem. Rev.* 102, 2725-2750 (2002); (c) A. A. Galkin, V. V. Lunin, Subcritical and supercritical water: a universal medium for chemical reactions. *Russ. Chem. Rev.* 74, 21-35 (2005); (d) J. An, L. Bagnell, T. Cablewski, C. R. Strauss, R. W. Trainor, Applications of high-temperature aqueous media for synthetic organic reactions. *J. Org. Chem.* 62, 2505-2511 (1997); (e) N. S. Kus, Organic reactions in subcritical and supercritical water.*Tetrahedron* 68, 949-958 (2012).

7. K. I. Booker-Milburn, J. K. Cowell, L. J. Harris, Model studies towards the total synthesis of asteriscanolide. *Tetrahedron Lett.* 35, 3883-3886 (1994).

8. (a) K. I. Booker-Milburn, F. Delgado Jiménez, A. Sharpe, Sequential ring-opening/cyclisation reactions of bicyclo[4.2.0]oct-7-enes for the synthesis of cyclooctadiene fused lactones: Model studies towards the total synthesis of pachylactone Tetrahedron 55, 5889-5902 (1999); (b) K. I. Booker-Milburn, J. K. Cowell, F. Delgado Jiménez, A. Sharpe, A. J. White, Stereoselective intermolecular [2+2] photocycloaddition reactions of tetrahydrophthalic anhydride and derivatives with alkenols and alkynols. Tetrahedron 55, 5875-5888 (1999).

9. (a) K. I. Booker-Milburn, J. K. Cowell, A. Sharpe, F. D. Jiménez, Tetrahydrophthalic anhydride and imide: Remarkably efficient partners in photochemical [2+2] cycloaddition reactions with alkenols and alkynols Chem. Commun. 249-251 (1996); (b) M. J. Ralph, D. C. Harrowven, S. Gaulier, S. Ng, K. I. Booker-Milburn, The Profound Effect of the Ring Size in the Electrocyclic Opening of Cyclobutene-Fused Bicyclic Systems *Angew. Chem. Int. Ed.* 54, 1527-1531 (2015).

10. (a) E. Venardou, E. Garcia-Verdugo, S. J. Barlow, Y. E. Gorbaty, M. Poliakoff, On-line monitoring of the hydrolysis of acetonitrile in near-critical water using Raman spectroscopy. *Vib. Spectrosc.* 35, 103-109 (2004); (b) P. Krammer, H. Vogel, Hydrolysis of esters in subcritical and supercritical water. *J. Supercrit. Fluid* 16, 189-206 (2000).

11. Care must be taken when carrying out reactions using high temperature water and acetonitrile due to the possible hydrolysis of acetonitrile via acetamide to acetic acid and ammonia. However, except where noted, no evidence of this hydrolysis was found under the reaction conditions studied

12. (a) M. K. Kuimova, W. Z. Alsindi, J. Dyer, D. C. Grills, O. S. Jina, P. Matousek, A. W. Parker, P. Portius, X. Zhong Sun, M. Towrie, C. Wilson, J. Yang, M. W. George, Using picosecond and nanosecond time-resolved infrared spectroscopy for the investigation of excited states and reaction intermediates of inorganic systems. *Dalton Trans.* 3996-4006 (2003); (b) M. Towrie, D. C. Grills, J. Dyer, J. A. Weinstein, P. Matousek, R. Barton, P. D. Bailey, N. Subramaniam, W. M. Kwok, C. Ma, D. Phillips, A. W. Parker, M. W. George,

Development of a broadband picosecond infrared spectrometer and its incorporation into an existing ultrafast time-resolved resonance Raman, UV/Visible, and fluorescence spectroscopic apparatus. *Appl. Spectr.* 57, 367-380 (2003).

13. The ps-TRIR spectra obtained 1 ps following direct irradiation of **1a** at 266 nm clearly show the parent bands are bleached and a new transient produced with bands at 1763 cm^{-1} which is assigned to $^1n\pi^*$ excited state of **1a**, Figure1. The presence of a relatively strong ν(C=O) is perhaps slightly surprising for a $^1n\pi^*$ excited state but is consistent with the excited state being localized mainly on one of the carbonyls and this assignment was supported by DFT calculations (see ESI). The bands of $^1n\pi^*$ excited state decays at the same rate (τ= 15 (± 2) ps) as the parent partially reforms and a new band grows in at 1645 cm^{-1} assigned to formation of the $^3\pi\pi^*$ excited state of 1a which subsequently decays back to the parent with a lifetime of 1.05 (± 0.05) µs, see ESI.